Dynamical modelling of the RAS-RAF-MEK-ERK pathway in the hepatocellular cells exposed to sorafenib

Anne-Sophie Giacobbi

UNIVERSITÉ de Picardie Jules Verne

Thèse de Doctorat

Mention : Mathématiques

présentée à *l'Ecole Doctorale en Sciences, Technologie, Santé (ED 585)*

de l'Université de Picardie Jules Verne

par

Anne-Sophie GIACOBBI

pour obtenir le grade de Docteur de l'Université de Picardie Jules Verne

Modélisation dynamique de la voie RAS-RAF-MEK-ERK dans les cellules du carcinome hépatocellulaire exposées au sorafénib

Soutenue le 1er juillet 2019, après avis des rapporteurs, devant le jury d'examen

M. Mohammed Guedda	Professeur, UPJV	Président du jury
M. Michael Grinfeld	Professor, Univ. de Strathclyde	Rapporteur
M. Sébastien Benzekry	CR HDR, INRIA Bordeaux	Rapporteur
M^{me} Angélique Stéphanou	CR HDR, CNRS Grenoble	Examinatrice
M. Youssef Bennis	MCU-PH, UPJV et CHU Amiens	Examinateur
M. Antoine Galmiche	PU-PH, UPJV et CHU Amiens	Co-directeur de thèse
M. Youcef Mammeri	MCF HDR, UPJV	Co-directeur de thèse

UNION EUROPÉENNE — l'Europe s'engage en Hauts-de-France avec le FEDER — Région Hauts-de-France — LAMFA — CHU AMIENS PICARDIE

Remerciements

Je voudrais tout d'abord adresser à Youcef et Antoine, mes directeurs, toute ma gratitude. Antoine, tu es à l'initiative de cette collaboration entre mathématiciens et biologistes, après avoir frappé à la porte du LAMFA, avec la conviction que les mathématiques pouvaient guider la recherche médicale. Merci pour cette belle démarche ! J'avais l'espoir tout le long de mes études en mathématiques de travailler un jour dans la recherche sur le cancer... je ne pensais pas débuter si tôt ! Merci d'avoir mené, avec un grand intérêt et un grand enthousiasme, les premiers objectifs de ces travaux. Nos échanges m'ont énormément encouragée, malgré les longs couloirs de l'hôpital qu'il a fallu traverser pour arriver à ton bureau. Aborder ce sujet si complexe, n'aurait évidement pas été possible sans Youcef. Aucun sujet mathématique ne te fait peur. Qu'il s'agisse d'un problème de statistiques, d'équations différentielles, de méthodes numériques ou encore de probabilité, tu as réponse à presque tout. Ta capacité d'adaptation en mathématiques m'impressionne. Merci de m'avoir guidée dans ce domaine si complexe qu'est la modélisation des systèmes biologiques, et de m'avoir fait découvrir autant de disciplines mathématiques. Je te remercie pour ta confiance et de m'avoir accompagnée tout au long de cette thèse.

Je tiens à exprimer mes vifs remerciements aux deux rapporteurs de cette thèse, Sébastien Benzekry et Michael Grinfeld. Merci Sébastien pour l'intérêt que tu as eu à lire cette thèse et d'avoir contribué par ton expertise à l'amélioration du manuscrit. Ton regard sur ces travaux m'a beaucoup encouragée. Michael, I am so grateful for having you as my referee. Thank you for your remarks which help me a lot to put my work in perspective and for your writing advices. The manuscript is already written but I will keep them in mind !

Je suis également très reconnaissante envers Angélique Stéphanou, Mohammed Guedda et Youcef Bennis, qui ont accepté de faire partie de mon jury de thèse.

Je voudrais remercier les biologistes du CHU d'Amiens qui ont collaboré à ce projet. Merci Suzana, Corinne, Christophe et Chloé pour votre contribution et pour le recueil des données expérimentales.

Merci à l'équipe Dracula de l'Inria Lyon de m'avoir invitée à leur séminaire. Vos remarques pertinentes lors de ma venue ont aidé à l'avancement de cette thèse.

Merci à tous les membres du LAMFA pour ces quatre années passées à vos côtés. Je suis particulièrement reconnaissante envers toute l'équipe d'analyse A^3 qui a bien voulu supporter mes exposés, souvent plus biologiques que mathématiques, avec des noms terribles, comme RAF, RAS, MEK ou encore ERK. Je tiens également à remercier Isabelle et Christelle, qui ont rendu les tâches administratives bien plus simples qu'elles ne l'étaient.

Un immense merci à tous les doctorants pour avoir entretenu un véritable esprit de famille au sein des bureaux. Un merci spécial à Aktham et Valérie pour leur bienveillance et leur chaleureux accueil lors de mes premiers pas au bureau et merci au trio infernal de première année.

Merci à tous ceux qui ont croisé mon chemin pendant cette aventure mathématique et notamment lors des nombreuses conférences auxquelles j'ai participé. Océane, je te remercie tout particulièrement pour ton amitié depuis ma toute première conférence à Obernai. Je te souhaite tout le meilleur pour tes derniers mois de thèse ! J'ai également une profonde pensée pour Clara, avec qui j'ai partagé des moments formidables à Madère. Merci pour ta grande générosité, ta force et ton amitié.

Merci à mes chers amis mathématiciens de Paris 6 : Idaline, Vincent et Cambyse. Que je me sois retrouvée avec toi, Cambyse, sur une photo datant de 2012 prise à Jussieu, dans un article en ligne en 2015 sur la situation des doctorants en France, est une coïncidence qui me touche. Je te souhaite une belle réussite pour ta soutenance à venir. Merci à mes amies de toujours : Claire et Elodie pour leur soutien indéfectible.

À ma famille, mille mercis. Le temps passé à vos côtés m'est si précieux. Merci à Charlotte et Pauline pour avoir été disponibles quand j'en avais besoin et pour ces longues heures passées au téléphone ; à Vincent de croire que l'impossible est réalisable ; à Enora et Lorelei de m'avoir fait oublier les soucis de la vie de nombreuses fois ; à Michèle et Christian d'avoir égayé mes week-ends lors de vos visites et d'avoir découvert avec moi la baie de Somme ; à Halima de n'être presque plus effrayée par les maths et à Patrick de t'atteler à cette dure tâche : la lecture de ma thèse.

À ma mère. Je regrette que Jonas K. n'ait toujours pas montré le bout de son nez à Amiens. Mille mercis pour tout et surtout, merci de nous avoir laissés inventer notre vie.

À Sylvain. Un immense merci de m'avoir supportée ces dernières années.

Merci de m'initier à la topologie algébrique, notamment en me faisant croire que tes études sur les espaces stratifiés ne sont que des problèmes de dessins colorés. Merci de croire que je serai peut-être un jour topologue.

Table des matières

Chapitre 1

Introduction

1.1 Le cancer, une maladie complexe

Le cancer est une maladie complexe, caractérisée par l'occurrence d'anomalies allant du niveau moléculaire au corps entier. L'accumulation des mutations et les altérations touchant la régulation de l'expression de gènes contribuent à la transformation maligne [MC15]. L'issue de la maladie résulte des perturbations des systèmes qui régissent la transduction du signal dans la cellule cancéreuse, de la compétition entre cellules malignes et cellules saines, et de la capacité de la tumeur à coopter l'angiogenèse, à envahir les tissus et à former des métastases, et à échapper aux mécanismes effecteurs de l'immunité antitumorale [ENW10].

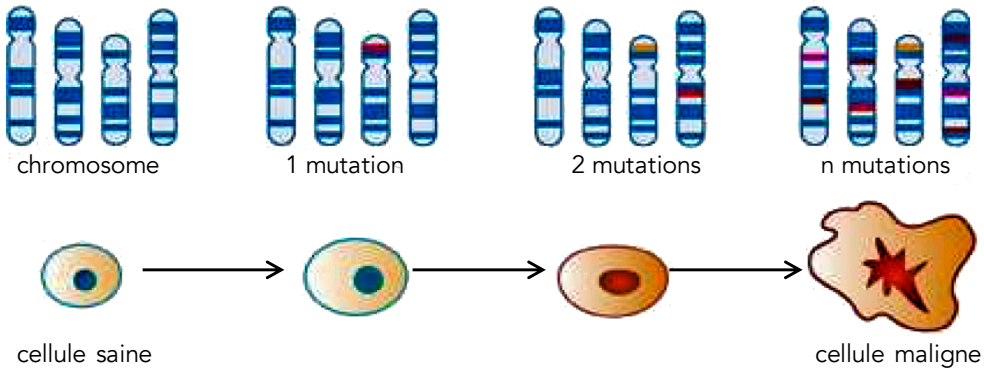

Figure 1.1 – Contribution de l'accumulation de mutations génétiques à la transformation d'une cellule saine en cellule maligne. La majorité de ces mutations n'ont pas d'effet notable, mais certaines peuvent modifier les fonctions cellulaires. L'accumulation progressive de mutations tout au long de la vie peut provoquer le cancer et contribue au vieillissement cellulaire.

A

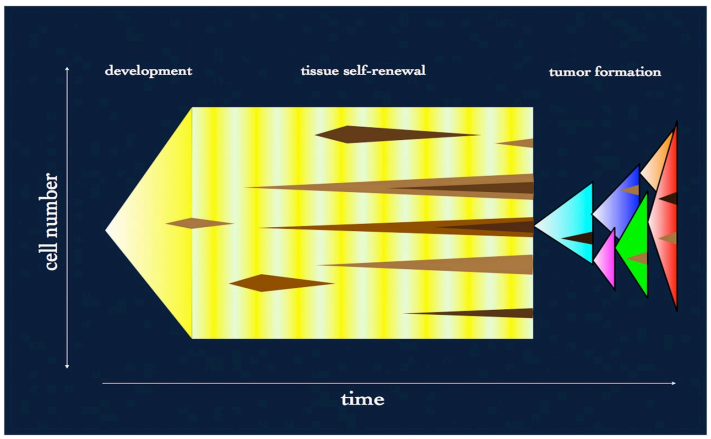

B

Tumor type	25-y-old	Median age at diagnosis	85-y-old
CLL	(10.09 − 5.86)/10.09 = 0.42	(18.53 − 5.86)/18.53 = 0.68	(24.16 − 5.86)/24.16 = 0.76
Uterine cancer	(45.96 − 33.33)/45.96 = 0.27	(77.95 − 33.33)/77.95 = 0.57	(96.48 − 33.33)/96.48 = 0.65
Colorectal cancer	(50.2 − 50.2)/50.2 = 0	(102.4 − 50.2)/102.4 = 0.51	(121.38 − 50.2)/121.38 = 0.59

FIGURE 1.2 – A. Représentation schématique des différentes phases au cours desquelles des mutations somatiques se produisent dans un tissu donnant lieu à un cancer. À partir d'une seule cellule précurseur, un tissu est créé par expansion clonale. Le tissu est soumis à des auto-renouvellements périodiques au cours duquel des mutations se produisent de manière aléatoire et s'éteignent ou se développent au fur et à mesure de l'accumulation de mutations successives. B. Fraction de mutations somatiques apparues avant l'initiation de la tumeur chez des patients de différents âges pour la leucémie lymphocytaire chronique, le cancer de l'utérus et le cancer colorectal d'après I. Matincorena et al. [MC15].

Concernant les cellules du carcinome hépatocellulaire (CHC), le plus commun des cancers du foie, celles-ci présentent peu de mutations. Le diagnostique est d'autant plus difficile que cette forme de cancer est presque toujours précédée d'une cirrhose [SYL10].

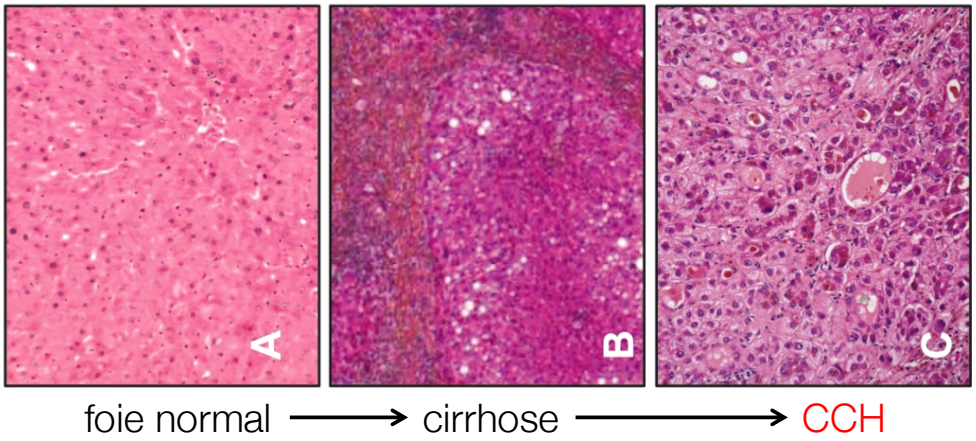

FIGURE 1.3 – Evolution histologique du tissu hépatique aboutissant au carcinome hépatocellulaire chez l'être humain. A un foie sain, succède une cirrhose puis un carcinome hépatocellulaire.

Ces dernières décennies, les avancées de la génomique ont permis d'identifier des acteurs moléculaires essentiels de la cancérogenèse dont certains, comme les composants de la voie oncogénique RTK (receptor tyrosine kinase) - Ras - Raf - MEK (mitogen-activated ERK kinase) - ERK (extracellular signal-regulated kinase), constituent des cibles thérapeutiques potentielles [FMea16]. La conception d'inhibiteurs spécifiques de ces protéines a permis de faire la preuve de principe de l'utilité de ces recherches avec, par exemple, le ciblage thérapeutique de B-Raf1 dans le mélanome malin [CHea11]. Malheureusement, malgré un rationnel biologique établi, ces traitements anticancéreux présentent une efficacité qui se révèle le plus souvent temporaire. Après une période de temps limitée, des adaptations de la machinerie cellulaire peuvent apparaître et, dans certains cas, se traduire par l'inversion de l'effet du médicament, le transformant en un stimulant de la progression tumorale [dTSea13]. Des travaux récents suggèrent que ces remarquables propriétés d'adaptation peuvent découler de l'organisation intrinsèque des réseaux biologiques [JBea16]. Il est donc nécessaire de prendre en compte l'organisation en réseaux et la régulation dynamique des cibles biologiques : c'est un des intérêts du recours à la modélisation mathématique [BCZ09, JL13, KHGK15].

1.2 La voie ERK comme ciblage thérapeutique

La voie Ras-Raf-MEK-ERK est une voie de signalisation intracellulaire. Elle est essentielle dans la transcription du génome et contrôle l'angiogénèse, la survie, la prolifération ainsi que la migration et la différentiation des cellules. Cette voie est souvent dérégulée dans les cancers. A titre d'exemples, la protéine Ras est mutée dans 50% des cancers du colon [TD12] et la protéine Raf l'est dans 60% des mélanomes [LBea10].

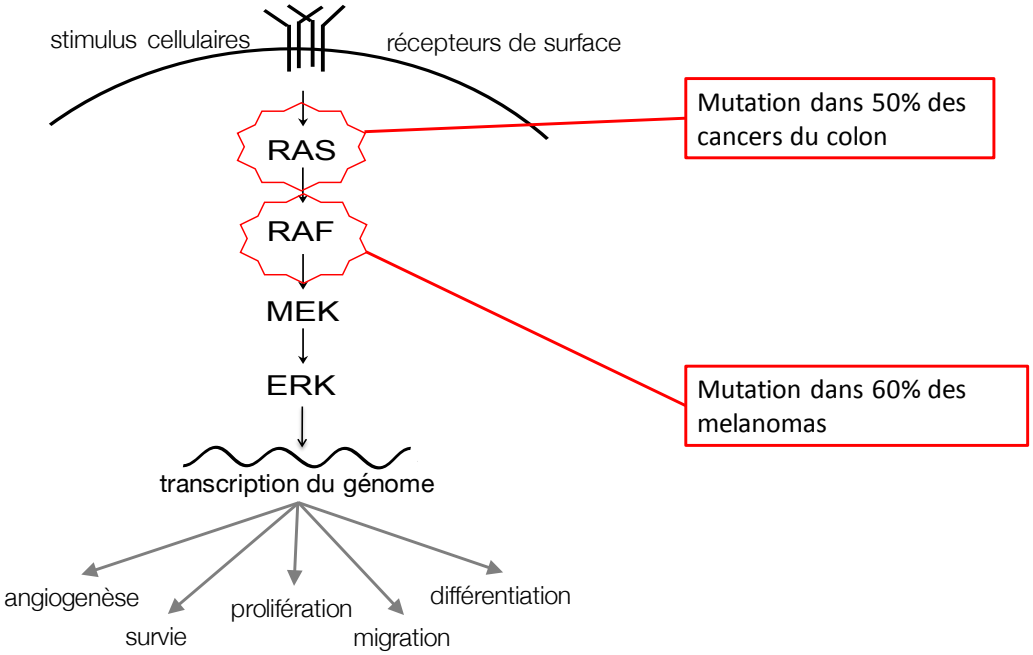

FIGURE 1.4 – Description schématique de la voie de signalisation Ras-Raf-MEK-ERK avec la contribution de la protéine ERK dans les différents mécanismes du développement cellulaire. La protéine Raf mutée est présente dans la moitié des cancers du colon et la protéine Ras est identifiée comme mutée dans 60% mélanomes.

Eteindre cette voie de signalisation fait donc partie des traitements envisagés lors de l'apparition d'un cancer dans lequel elle est suractivée. Inhiber, sans altérer, un ou plusieurs acteurs de la voie devient un axe majeur de la recherche thérapeutique. On cherche alors à réduire la phosphorylation, c'est à dire l'activation de la protéine par l'action d'une protéine kinase ou à accélérer la déphosphorylation, c'est à dire la désactivation de la protéine par l'action de phosphatases.

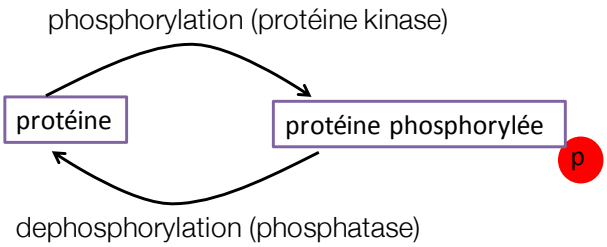

FIGURE 1.5 – Les deux états d'une protéine. Elle est activée par un processus de phosphorylation qui lui ajoute un groupe phosphate et qui est catalysé par une protéine kinase. La désactivation de la protéine consiste en la déphosphorylation qui au contraire élimine son groupe phosphate.

Dans les cas avancés de CHC, le sorafénib était, depuis 2007 (et jusqu'en 2017 avec le régorafénib), le seul traitement ayant montré une efficacité. Le sorafénib est vendu comme un inhibiteur des protéines kinases Raf. Cependant son efficacité reste mineure, prolongeant la vie de quelques mois dans les cas où il agit. Rappelons que près de 80% des patients sont diagnostiqués tardivement et sont donc dans un état de développement avancé de la maladie.

L'objectif du présent travail de thèse à l'interface entre mathématique, biochimie et médecine, consiste à :

— améliorer la connaissance de la voie de signalisation Ras-Raf-MEK-ERK,

— comprendre le mode de fonctionnement du sorafénib,

— identifier et contrôler la régulation de la voie.

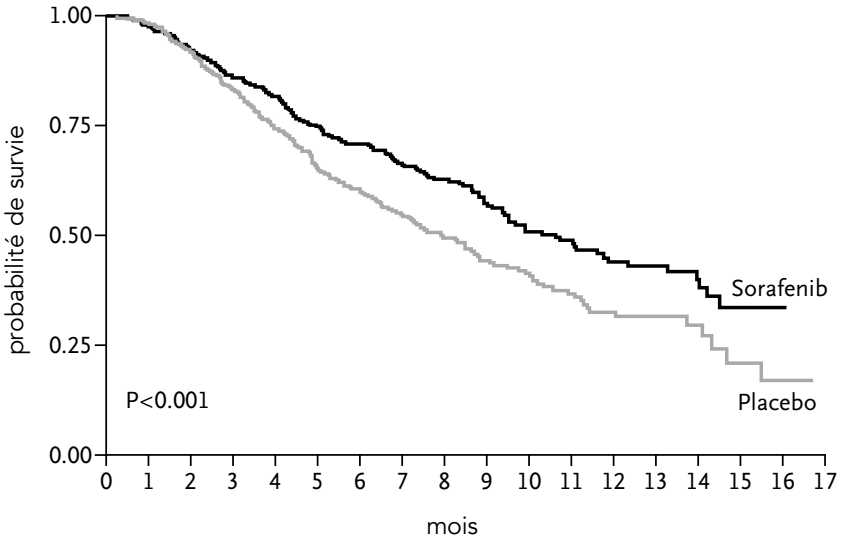

FIGURE 1.6 – Evolution de la probabilité de survie des patients sur 17 mois après administration du sorafénib ou d'un placebo. Sur 602 patients (dont 299 sous sorafénib et 303 sous placebo), la survie globale médiane était de 10.7 mois dans le groupe sorafénib, contre 7.9 mois dans le groupe placebo d'après J.M. Llovet et al. [LRea08].

1.3 Modélisation déterministe des voies de signalisation

Les approches utilisées pour étudier les voies de signalisation intracellulaires reposent souvent sur l'application d'équations différentielles ordinaires (EDO) qui permettent d'en étudier la dynamique. Ces équations peuvent, par exemple, être construites à partir de la loi d'action de masse, ou de la cinétique de Michaelis-Menten, quand les interactions entre composants de ces voies sont de nature enzymatique [OSea05]. La voie Raf-MEK-ERK est l'un des exemples de transduction oncogénique les plus étudiés sous le prisme mathématique, en raison de son implication fréquente dans le cancer [FMea16, KHGK15]. La première modélisation mathématique de cette voie oncogénique, centrée sur l'étude dynamique des composants Raf, MEK, et ERK, a été rapportée en 1996 [HJ96]. Ce travail et plusieurs autres réalisés depuis, ont permis d'explorer des aspects importants de la régulation dynamique de cette cascade de transduction dans les cellules eucaryotes [OSea05]. Parmi les contributions les plus notables, il a été possible d'expliquer (1) la cinétique d'activation hypersensible, en « tout ou rien », de ERK observée à l'échelle de la cellule unique [JM98], (2) d'explorer l'effet des protéines d'« échafaudage » [LBS00], (3) d'expliquer les cinétiques distinctes d'activation de ERK selon les contextes de prolifération/différenciation cellulaire [SOFK04], ou encore (4) de mieux comprendre comment l'activation de ERK est convertie en régulation transcriptionnelle [NBea10]. Nous avons étudié la voie Raf-MEK-ERK dans les cellules de carcinome hépatocellulaire (CHC) exposées au sorafénib [SGea17]. Des EDO non-linéaires traduisant une cinétique enzymatique ont été utilisées pour modéliser les interactions, dans plusieurs lignées de CHC, entre les principaux acteurs de la voie Raf : B-Raf, C-Raf, MEK et ERK. Notre approche associant biologie et mathématiques a identifié deux points importants : (1) la grande hétérogénéité, selon les lignées de cellules, des modes de régulation de la signalisation en aval de Raf : l'analyse de sensibilité révèle, en effet, le rôle de régulateurs essentiels de la voie Raf, différents dans chacune des lignées ; (2) l'importance d'une étape insoupçonnée : l'étape de déphosphorylation des kinases ERK par les phosphatases. En l'absence de phosphatases spécifiques de MEK et de ERK, le sorafénib perd sa capacité de bloquer ERK dans des cellules pourtant sensibles à ce médicament [SGea17]. Cette observation, quoique surprenante, le sorafénib ayant été conçu et développé comme inhibiteur de kinases, a pu être validée expérimentalement. Les approches de modélisation permettent donc de comprendre comment est régulée une voie oncogénique, comme la voie ERK, dans un contexte thérapeutique [SGea17]. Ce type d'études per-

met secondairement, de guider la recherche de biomarqueurs originaux. Elles pourraient être utiles pour prédire l'efficacité du traitement et personnaliser la prescription du sorafénib. La modélisation mathématique révèle donc les détails de l'architecture en réseau des kinases Raf-MEK-ERK. Ces informations cruciales dans le contexte thérapeutique peuvent être obtenues par modélisation, même lorsque le réseau étudié est constitué d'un petit nombre d'acteurs (ici, les kinases Raf, MEK et ERK) [SGea17, JMJ16]. Pour les réseaux complexes, qui peuvent inclure des milliers d'acteurs, il est nécessaire d'appliquer des stratégies de réduction de la complexité, comme l'analyse modulaire (modular response analysis, ou MRA). La première étape de ce type d'analyse repose sur l'identification des noeuds, c'est-à-dire des composants du système qui sont fortement connectés. Cette identification peut être fondée sur des connaissances antérieures du système, ou découler d'études statistiques (par exemple, par regroupement hiérarchique). La dynamique entre les noeuds peut ensuite être analysée à l'aide d'EDO. Pour chaque paramètre, un coefficient de réponse locale, qui reflète l'impact d'un noeud sur l'autre, est défini [KSea13, HKKS16]. Ce type d'analyse a été appliqué, par exemple, à la modélisation des interactions entre les voies oncogéniques Raf-MEK-ERK et AKT (ou protéine kinase B)-mTOR (mammalian target of rapamycin), dans des cellules de cancer colorectal. Elles ont permis de proposer un ciblage thérapeutique amélioré, en associant l'inhibition de MEK et de l'EGFR (epidermal growth factor receptor) [KSea13]. Ce type d'approche permet donc d'étudier l'impact des multiples boucles de rétrocontrôle au sein de larges réseaux de transduction.

D'un point de vue mathématique, il s'agit de décrire un ensemble de réactions biochimiques. Pour une réaction de la forme

$$\mathrm{aA} + \mathrm{bB} \underset{k_d}{\overset{k_p}{\rightleftharpoons}} \mathrm{cC},$$

où A, B, C sont des réactifs chimiques, a, b, c, les coefficients stoechiométriques, k_p le taux de production et k_d le taux de dégradation, pour laquelle on définit une vitesse de réaction

$$v = -\frac{1}{a}\frac{d[A]}{dt} = -\frac{1}{b}\frac{d[B]}{dt} = \frac{1}{c}\frac{d[C]}{dt}.$$

Ici $[X]$ désigne la concentration de l'espèce chimique X exprimée en mol/L. La loi d'action de masse stipule que le taux d'une réaction chimique élémentaire est proportionnel au produit des concentrations des réactifs. Cette loi, qui décrit l'évolution temporelle de la concentration d'une espèce chimique,

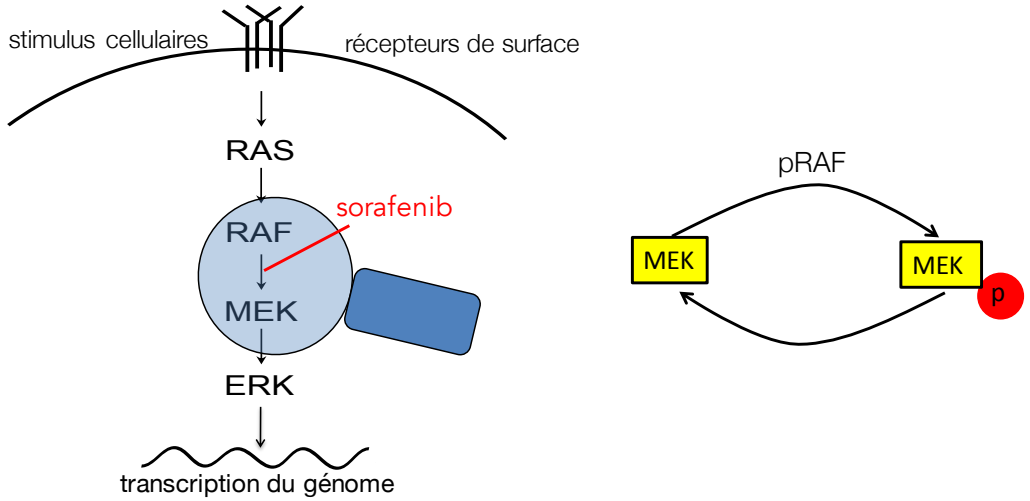

FIGURE 1.7 – Action du sorafénib sur la voie de signalisation Ras-Raf-MEK-ERK. Il est prescrit comme un inhibiteur des kinases impliquées dans la phosphorylation des protéines Raf, bloquant ainsi la propagation du signal au sein de la cellule. On note pRAF la protéine Raf sous forme phosphorylée (qui correspond à sa forme active).

est gouvernée par le système d'équations différentielles non-linéaires suivant

$$\begin{aligned} \frac{d[A]}{dt} &= k_p[C]^c - k_d[A]^a[B]^b \\ &= \text{production - dégradation.} \end{aligned}$$

De nombreuses réactions chimiques ont une énergie d'activation beaucoup trop élevée pour se produire spontanément. Un moyen courant pour y parvenir est une réaction enzymatique, dans laquelle une molécule auxiliaire facilite la réaction. Cette molécule auxiliaire n'est pas utilisée dans la réaction elle-même. Si on note E un enzyme servant de molécule auxiliaire et A le substrat chimique, ils se lient d'abord et forment un complexe AE, puis l'enzyme laisse le substrat se transformer en un produit activé A*. Autrement dit, les réactions sont

$$\mathrm{A} + \mathrm{E} \underset{k_2}{\overset{k_1}{\rightleftharpoons}} \mathrm{AE} \xrightarrow{k_3} \mathrm{A}^* + \mathrm{E},$$

et la loi d'action de masse implique

$$\begin{aligned}
\frac{d[A]}{dt} &= -k_1[A][E] + k_2[AE] \\
\frac{d[E]}{dt} &= -k_1[A][E] + k_2[AE] + k_3[AE] \\
\frac{d[AE]}{dt} &= k_1[A][E] - k_2[AE] - k_3[AE] \\
\frac{d[A^*]}{dt} &= k_3[AE].
\end{aligned}$$

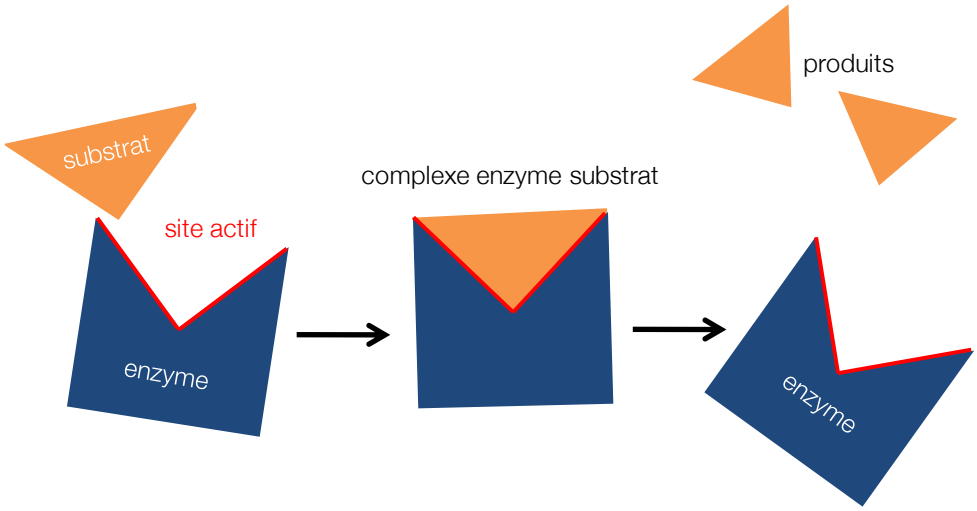

FIGURE 1.8 – Représentation schématique des étapes d'une réaction enzymatique. L'enzyme et le substrat se lient via des sites actifs spécifiques puis forment un complexe. Après dissociation de ce complexe, les produits de cette réaction sont obtenus libérant ainsi l'enzyme qui est disponible pour répéter la catalyse.

Une hypothèse de quasi-stationnarité, consistant à supposer que la première réaction est rapide par rapport aux autres et que les concentrations de l'enzyme et du complexe sont constantes ($\frac{d[E]}{dt} = 0, \frac{d[AE]}{dt} = 0$), permet d'obtenir les équations de Michaelis-Menten notées

$$\mathrm{A} \underset{V_2 E, K_2}{\overset{V_1 E, K_1}{\rightleftharpoons}} \mathrm{A}^*,$$

et écrites

$$\frac{d[A^*]}{dt} = \frac{V_1[E]\left([A_{total}] - [A^*]\right)}{K_1 + \left([A_{total}] - [A^*]\right)} - \frac{V_2[A^*]}{K_2 + [A^*]} \text{ avec } A_{total} = A + A^*.$$

où V_1, K_1, V_2, et K_2 sont les constantes de Michaelis-Menten, qui dépendent des constantes de réactions et des concentrations des enzymes assurant l'activation et la désactivation de A^*. Leur expression respective est donnée dans la section 2.1.2 suivante.

Un inhibiteur enzymatique I va se lier à l'enzyme et en modifier l'activité. Un inhibiteur non compétitif va se fixer sur l'enzyme elle-même ou bien sur le complexe enzyme-substrat, et le substrat peut se fixer sur l'enzyme ou sur le complexe enzyme-inhibiteur :

$$\begin{aligned}
\mathrm{A} + \mathrm{E} + \mathrm{I} &\underset{k_2}{\overset{k_1}{\rightleftharpoons}} \mathrm{AE} + \mathrm{I} \quad \xrightarrow{k_3} \mathrm{pA} + \mathrm{E} + \mathrm{I} \\
\mathrm{A} + \mathrm{E} + \mathrm{I} &\underset{k_2}{\overset{k_1}{\rightleftharpoons}} \mathrm{AE} + \mathrm{I} \quad \underset{k_{-I}}{\overset{k_I}{\rightleftharpoons}} \mathrm{AIE} \\
\mathrm{A} + \mathrm{E} + \mathrm{I} &\underset{k_{-I}}{\overset{k_I}{\rightleftharpoons}} \mathrm{IE} + \mathrm{A} \quad \underset{k_2}{\overset{k_1}{\rightleftharpoons}} \mathrm{AIE}
\end{aligned}$$

En résumé, l'activation et la désactivation d'une protéine A s'écrit

$$\mathrm{A} \underset{v_2 E, k_2, k_I I}{\overset{v_1 E, k_1}{\rightleftharpoons}} \mathrm{A}^*,$$

et est gouvernée par l'équation différentielle non-linéaire

$$\begin{aligned}
\frac{d[A^*]}{dt} &= \frac{v_1[E]\left([A_{total}] - [A^*]\right)}{k_1 + \left([A_{total}] - [A^*]\right)} \left(1 + \frac{[I]}{k_I}\right)^{\alpha_I} - \frac{v_2[A^*]}{k_2 + [A^*]} \\
A_{total} &= A + A^*,
\end{aligned}$$

avec $\alpha_I > 0$ si l'inhibiteur participe à un rétrocontrôle positif et $\alpha_I < 0$ si l'inhibiteur contribue à un rétrocontrôle négatif sur A^*.

La signalisation de la voie Ras-Raf-MEK-ERK repose sur des réactions chimiques issues de la loi d'action de masse et des réactions enzymatiques données par la loi de Michaelis-Menten.

1.4 D'autres approches pour la modélisation de voies oncogéniques

Les exemples de modélisation des niveaux d'activation des kinases oncogéniques que nous avons présentés reposent sur des analyses de populations cellulaires. Ils font donc abstraction du comportement individuel des cellules. A l'échelle de la cellule, les voies oncogéniques, comme ERK, sont activées

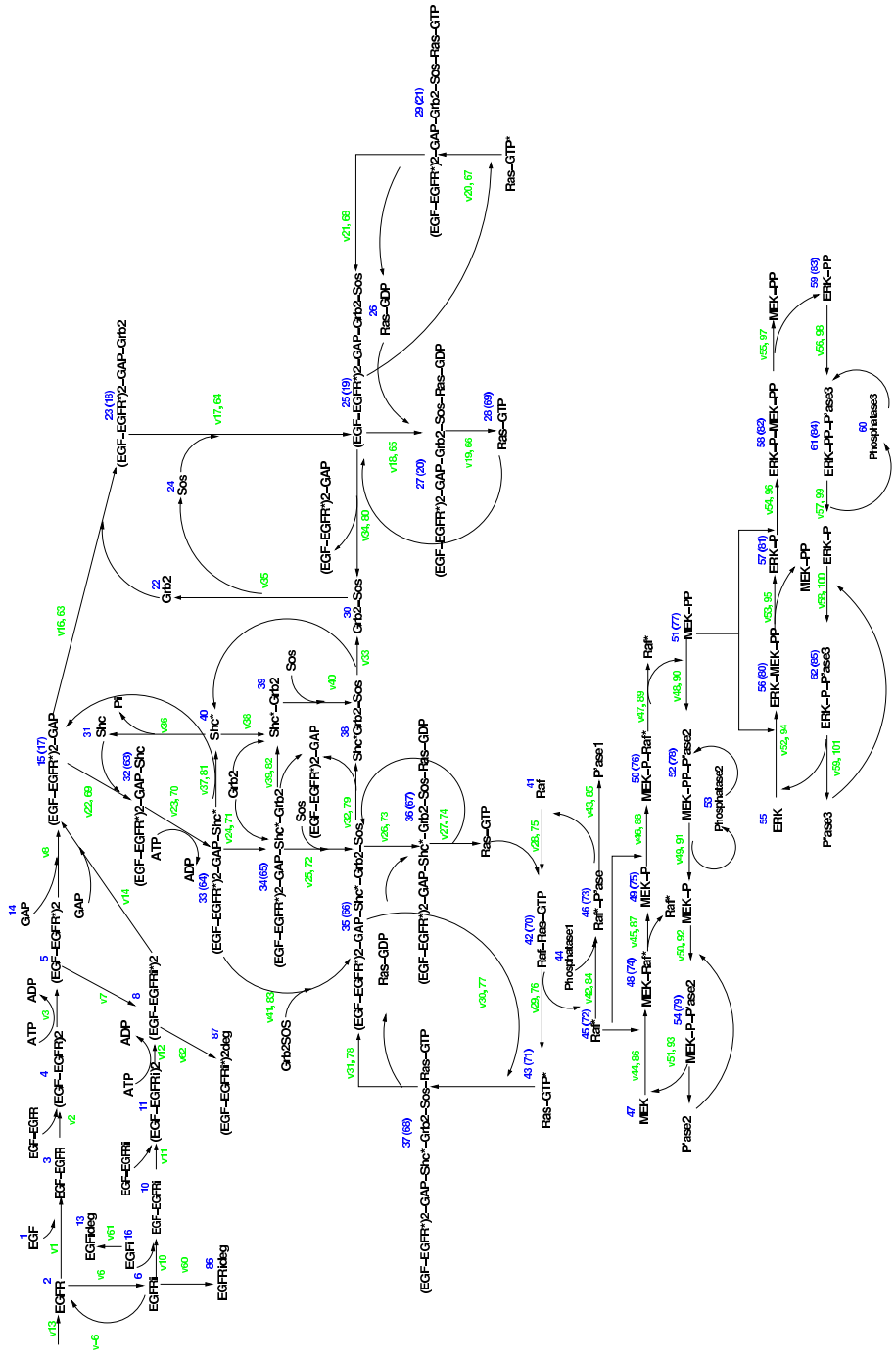

FIGURE 1.9 – Schéma de la cascade de signalisation Ras-Raf-MEK-ERK induite ici par l'EGFR, le récepteur du facteur de croissance épidermique d'après B. Schoeberl et al. [SEJGM02].

préférentiellement sous la forme de pics [AMB13, VPea14], apparaissant de façon partiellement stochastique, avec une fréquence qui conditionne les réponses des cellules, comme la mitogenèse [AMB13, VPea14]. L'état d'activation des composants d'amont (le « bruit », qui est une caractéristique des réseaux biologiques), mais aussi les différentes concentrations des acteurs de la cascade de signalisation, rendent impossible une modélisation mathématique entièrement déterministe. La modélisation de cette composante stochastique permet d'explorer les différences de régulation dynamique de Ras-Raf-MEK-ERK entre cellules, et d'en trouver l'origine. On peut ainsi montrer l'importance des différences qui existent entre cellules, de génomes identiques, et qui s'exercent en amont du module MEK-ERK [RCea15, FBea16]. Cette notion d'hétérogénéité cellulaire intra-tumorale est importante. Elle conditionne en effet de nombreux aspects de la progression tumorale et la réponse des tumeurs aux traitements médicaux [MM13]. Les travaux de modélisation des voies oncogéniques à l'échelle des cellules uniques révèlent l'existence d'une hétérogénéité phénotypique d'origine non-génétique, inhérente à l'organisation des réseaux de transduction au sein des cellules cancéreuses [RCea15, FBea16]. Les modèles qui incorporent une composante stochastique permettent donc de décrire, et de comprendre en partie, cette hétérogénéité phénotypique qui caractérise les tumeurs.

Des approches utilisant la logique booléenne, permettent également d'étudier les réseaux de transduction dans les cellules cancéreuses [AJOK09, vdH-Bea14, AJTea16]. Sur le principe, l'analyse quantitative est, dans ce type de modèle, remplacée par des variables binaires qui décrivent la fonctionnalité de chaque élément : l'activation de chaque acteur d'un réseau est soumise à différentes conditions logiques, et la stabilité des réseaux booléens dépend des connections qu'établissent les noeuds qui les constituent. Ce type de modèle présente l'avantage de permettre l'étude de nombreux acteurs, généralement choisis à partir de connaissances préexistantes dans le domaine. L'un des objectifs de ce type de modélisation est d'identifier les états attracteurs, présumés représenter les états stables du système modélisé. Ces états stables peuvent, par exemple, correspondre aux différents statuts du réseau oncogénique dans un contexte de ciblage thérapeutique. L'étude de la régulation de la protéine p53, un des déterminants de l'efficacité des chimiothérapies anti-tumorales, offre un bon exemple d'application de la modélisation logique de la régulation de p53 en oncologie [AJOK09] (Figures 1.10-1.11). Les modèles booléens peuvent également permettre d'appréhender certains mécanismes à l'origine de la plasticité phénotypique observée dans les cellules cancéreuses. En définissant les états attracteurs dans un système booléen, il est possible d'aborder l'existence de plusieurs états métastables au sein d'un système biologique [AJTea16]. Une étude menée sur les cancers du poumon à

petites cellules, montre un exemple récent d'utilisation d'un modèle booléen fondé sur l'état d'activation de 33 facteurs de transcription. Il a en effet été possible dans ce cas de mettre en évidence plusieurs états du réseau transcriptionnel et de les relier à l'émergence d'une hétérogénéité phénotypique dans le contexte thérapeutique [UWea17]. Des approches pratiques permettent de contourner une limitation essentielle des modèles booléens qui tendent à refléter grossièrement la réalité biologique. Une étude récente rapporte ainsi l'intérêt d'un formalisme à l'interface entre logique booléenne et EDO afin de modéliser la dynamique des réseaux [EDMea17]. Cette étude, qui revèle l'existence de différences individuelles entre des lignées cellulaires cancéreuses coliques, montre également que l'information contenue dans l'organisation en réseau prédit la sensibilité des cellules à un panel de médicaments de ciblage thérapeutique, indépendamment de l'analyse génomique [EDMea17]. Ce type de modélisation apporte donc une information utile à la compréhension des mécanismes qui rendent les cellules cancéreuses sensibles ou résistantes au ciblage thérapeutique.

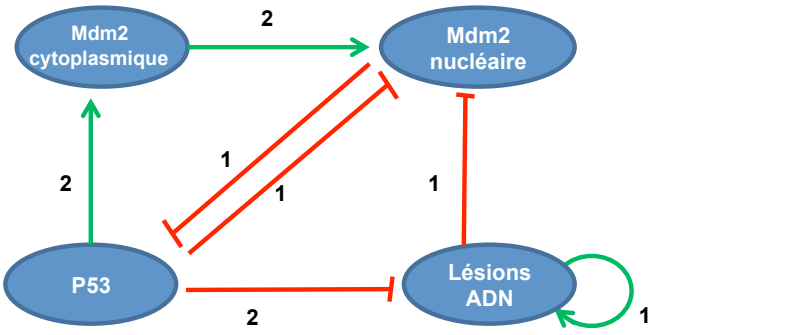

Composant	Niveau	Règles logiques
p53	2	!Mdm2nucléaire
Mdm2cytoplasmique	2	p53
	1	!p53
Mdm2nucléaire	1	Mdm2cytoplasmique:2 | (Mdm2cytoplasmique:1 & !p53 & !LésionsADN)
LésionsADN	1	LésionsADN & !p53

FIGURE 1.10 – Composants du système et leurs interactions. Les niveaux de p53 (ou TP53, tumor protein 53) sont régulés par l'ubiquitine ligase Mdm2 (mouse double minute 2 homolog) qui catalyse la dégradation continue de p53. Inversement, p53 diminue les niveaux de Mdm2 nucléaire en inhibant sa translocation vers le noyau. Dans le même temps, p53 active la transcription du gène MDM2. Les règles logiques qui sont appliquées entre les différentes variables sont montrées dans le panneau, avec les symboles Booléens et leur signification : $! = NOT; \& = AND; | = OR$. Dans la forme la plus simple de logique, les variables prennent une valeur de 1 (= présent) ou 0 (= absent). L'état actuel du système est décrit par un vecteur d'état, par exemple 0101 (c'est à dire : p53 = absent, Mdm2 cytoplasmique = présent, Mdm2 nucléaire = absent, lésions de l'ADN = présent). En appliquant des fonctions logiques, il est possible de déterminer l'évolution de l'état du système d'après W. Abou-Jaoudé et al. [AJOK09].

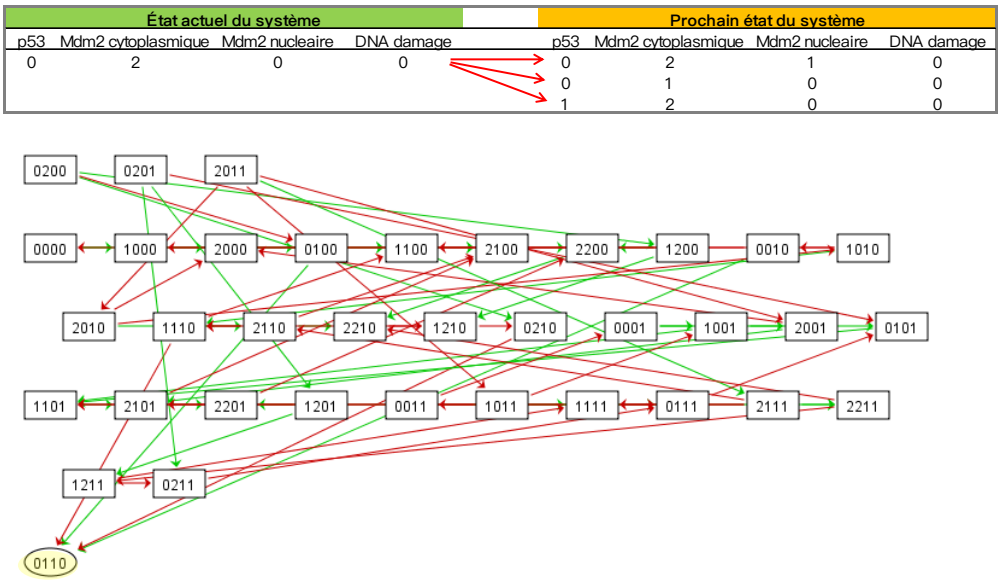

FIGURE 1.11 – Evolution de l'état 0200, où trois évolutions sont possibles. On peut identifier l'état 0110 (p53 = absent, Mdm2 cytoplasmique = présent, Mdm2 nucléaire = présent, lésions de l'ADN = absent, souligné ici en jaune) comme un état stable. Il est aussi possible d'appliquer des perturbations afin d'explorer la robustesse du système, et son évolution dans différentes conditions initiales W. Abou-Jaoudé et al. [AJOK09].

1.5 Organisation de la thèse

Le chapitre 2 fait l'object de l'article *Z. Saidak, A.S. Giacobbi C. Louandre, C. Sauzay, Y. Mammeri, A. Galmiche, Mathematical modelling unveils the essential role of cellular phosphatases in the inhibition of RAF-MEK-ERK signalling by sorafenib in hepatocellular carcinoma cells, Cancer letters 392, (2017), 1-8.*

La cascade Ras-Raf-MEK-ERK est une voie clé du signal oncogénique de transduction activée dans de nombreux types de tumeurs chez l'homme. Le sorafénib, le traitement médical de référence contre le carcinome hépatocellulaire à un stade avancé, inhibe la cascade Raf-MEK-ERK dans les cellules CHC. Sur la base d'études antérieures suggérant que cette cascade est une cible importante du sorafénib dans les cellules CHC, nous avons exploré sa régulation à travers la modélisation en utilisant des équations différentielles ordinaires non-linéaires. On cherche en particulier à comprendre la régulation du taux de la protéine ERK sous sa forme active (pERK) au sein de la voie. **Nos différents travaux portent donc sur l'étude du comportement de pERK en temps long**.

On s'intéresse dans ce premier chapitre au coeur de la voie prenant en compte les principales interactions chimiques. Ces interactions sont établies à partir d'une étude statistique de la variance des données expérimentales et sont représentées dans la figure 1.12. Elles sont décrites par le système d'équations différentielles non-linéaires

$$
\begin{aligned}
\frac{d[pBRAF]}{dt} &= \frac{V_{B,1}([BRAF_{tot}]-[pBRAF])}{K_{B,1}+([BRAF_{tot}]-[pBRAF])}\left(1+\frac{[pERK]}{K_{B,E}}\right)^{-\alpha} \\
&\quad - \frac{V_{B,2}[pBRAF]}{K_{B,2}+[pBRAF]} \\
\frac{d[pCRAF]}{dt} &= \frac{V_{C,1}([CRAF_{tot}]-[pCRAF])}{K_{C,1}+([CRAF_{tot}]-[pCRAF])}\left(1+\frac{[pERK]}{K_{C,E}}\right)^{-\beta} \\
&\quad - \frac{V_{C,2}[pCRAF]}{K_{C,2}+[pCRAF]} \\
\frac{d[pMEK]}{dt} &= \frac{(V_{M,1}+V_{M,2}[pBRAF]+\widetilde{V}_{M,2}[pCRAF])([MEK_{tot}]-[pMEK])}{K_{M,1}+([MEK_{tot}]-[pMEK])} \\
&\quad - \frac{V_{M,3}[pMEK]}{K_{M,2}+[pMEK]} \\
\frac{d[pERK]}{dt} &= \frac{(V_{E,1}+V_{E,2}[pMEK])([ERK_{tot}]-[pERK])}{K_{E,1}+([ERK_{tot}]-[pERK])} \\
&\quad - \frac{V_{E,3}[pERK]}{K_{E,2}+[pERK]}
\end{aligned}
$$

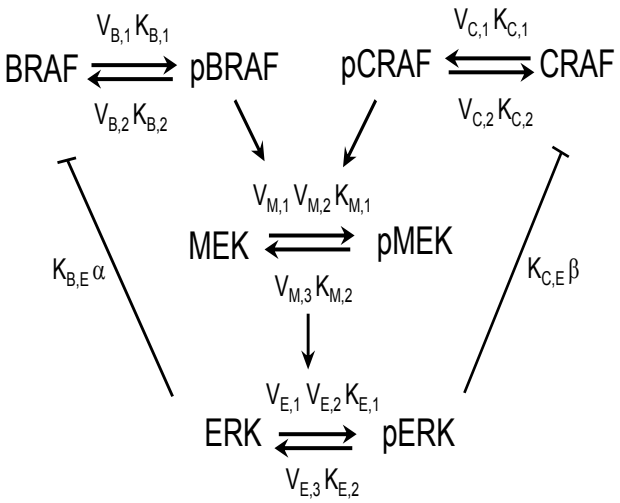

FIGURE 1.12 – Schéma représentant les étapes de phosphorylation, déphosphorylation entre les protéines B-Raf, C-Raf, MEK et ERK et les paramètres cinétiques associés.

L'étude du modèle mathématique met en évidence **la déphosphorylation de ERK et non l'inhibition des protéines Raf dans l'action**

anti-cancéreuse du sorafénib.

Les résultats obtenus au cours des dernières décennies confirment le rôle essentiel de cette cascade dans l'efficacité contre le CHC. Cependant des mécanisme de résistances font obstacles à l'efficacité thérapeutique du sorafénib. Entre autres, le récepteur activé du facteur de croissance épidermique (EGFR) est capable de promouvoir la résistance des lignées cellulaires et des tumeurs au sorafénib [ELea12, GDea13]. D'autres RTKs tels que le récepteur de l'insuline (IR) suggèrent la nécessité de contrôler de manière robuste les kinases oncogènes pour obtenir une efficacité thérapeutique. Bien que cibler la cascade RTK-ERK dans le CHC puisse sembler une tâche simple, l'existence d'un câblage complexe dans les voies de transduction oncogéniques, avec de multiples boucles de rétroaction et des redondances, constitue un obstacle majeur à l'efficacité thérapeutique. Comprendre comment les cellules résistent au traitement est alors un challenge majeur. Le troisième chapitre se concentre sur l'exploration des résistances du CHC au sorafénib en prenant en compte les principaux RTKs impliqués dans les cellules du CHC. Les interactions entre l'EGFR et la famille des récepteurs de l'insuline, ainsi qu'entre l'IR et l'IGF1-R (insulin-like growth factor 1 receptor), sont inclus dans la dynamique de la voie Ras-Raf-MEK-ERK qui en devient enrichie de quatre nouvelles équations différentielles ordinaires non-linéaires :

$$
\begin{aligned}
\frac{d[EGFR]}{dt} &= [EGFR]\left(p_{e,1}[ERK] + p_{e,2}\right) \\
&\quad - [EGFR]\left(c_{e,1}[IR] + c_{e,2}[IGF1R]\right) - \left(b_{e,1}[IR] + b_{e,2}[IGF1R]\right), \\
\frac{d[IR]}{dt} &= p_{i,1}[IR] - [IR]\left(c_{i,1}[EGFR] + c_{i,2}[IGF1R]\right) \\
&\quad - \left(b_{i,1}[EGFR] + b_{i,2}[IGF1R]\right), \\
\frac{d[IGF1R]}{dt} &= p_{j,1}[IGF1R] - [IGF1R]\left(c_{j,1}[EGFR] + c_{j,2}[IR]\right) \\
&\quad - \left(b_{j,1}[EGFR] + b_{j,2}[IR]\right) \\
\frac{d[RAS_{GTP}]}{dt} &= \left(r_1[EGFR]^{r_2} + r_3[IR]^{r_4} + r_5[IGF1R]^{r_6} + r_7\right) \\
&\quad \left([RAS_{tot} - [RAS_{GTP}]\right)\left(1 + \frac{[pERK]}{r_8}\right)^{r_9} \\
&\quad - r_{10}[RAS_{GTP}]
\end{aligned}
$$

Notre étude met en évidence la complexité et la versatilité de la régulation de la voie de transduction. L'EGFR apparaît activé via le modèle mathématique et comme observé par Ezzoukhry et al. et Niu et al. [NLea17, ELea12]. D'autres synergies se mettent en place dues à différentes actions qui ont lieu à différents niveaux de la cascade. Pour la lignée résiliente Hep3b, on observe

que les protéines kinases B-Raf et MEK induisent une résistance au traitement, et MEK est particulièrement actif dans la lignée résistante PLC/PRF5. Un protocole thérapeutique est alors envisagé pour empêcher ces résistances. Le contrôle optimal a permis de déterminer **la meilleur stratégie thérapeutique qui repose sur le tramétinib, un inhibiteur de MEK**.

Dans le quatrième chapitre, nous nous concentrons sur l'étude théorique du comportement spatiotemporel des solutions. Pour simplifier, on considère le système de deux équations suivant :

$$\begin{aligned}\frac{\partial u}{\partial t} &= D_1\Delta u + \frac{V_{u,1}(\overline{u}-u)}{K_{u,1}+\overline{u}-u}\left(1+\frac{v}{K_{u,3}}\right)^{-\alpha} - \frac{V_{u,2}u}{K_{u,2}+u}\\ \frac{\partial v}{\partial t} &= D_2\Delta v + \frac{V_{v,1}u(\overline{v}-v)}{K_{v,1}+\overline{v}-v} - \frac{V_{v,2}v}{K_{v,2}+v}\end{aligned}$$

La dimension spatiale est prise en compte via le terme de diffusion. Ainsi, chaque lignée cellulaire exhibe une dynamique bien particulière de solutions. Les solutions correspondant à la lignée sensible sont décroissantes et convergent vers un état d'équilibre proche de 0. Concernant la lignée résistante, les solutions sont croissantes et convergent vers un point stationnaire loin de 0. Les autres solutions, relatives à la lignée résiliente, sont quant à elles décroissantes puis croissantes avant d'atteindre un état d'équilibre. Nous montrons que **la dynamique en temps long des solutions spatiotemporelles coïncide avec celle sans diffusion**. Ce comportement est illustré par des simulations numériques du modèle en 2D, puis sur des morphologies 2D et 3D, constituant un cadre plus proche de la réalité biologique quant à la géométrie des cellules. Une méthode d'éléments finis a été utilisée pour réaliser ces simulations.

Financement

Ce travail a été financé par La Ligue contre le Cancer, le Comité de la Somme et Conseil Régional de Picardie. La thèse est elle payée par le Fond Européen de Développement Régional (FEDER) et le Conseil Régional de Picardie.

Références

[AJOK09] W. Abou-Jaoudé, D.A. Ouattara, and M. Kaufman, *From structure to dynamics : frequency tuning in the p53-Mdm2 network I. Logical approach*, J Theor Biol **258** (2009), 561–77.

[AJTea16] W. Abou-Jaoudé, P. Traynard, and P.T. Monteiro et al., *Logical modeling and dynamical analysis of cellular networks*, Front Genet **7** (2016), 94.

[AMB13] J.G. Albeck, G.B. Mills, and J.S. Brugge, *Frequency-modulated pulses of ERK activity transmit quantitative proliferation signals*, Mol Cell **49** (2013), 249–61.

[BCZ09] E. Barillot, L. Calzone, and A. Zinovyev, *Biologie des systèmes appliquée aux cancers*, Med Sci (Paris) **25** (2009), 601–7.

[CHea11] P.B. Chapman, A. Hauschild, and C. Robert et al., *Improved survival with vemurafenib in melanoma with BRAF v600e mutation*, N Engl J Med **364** (2011), 2507–16.

[dTSea13] M. das Thakur, F. Salangsang, and A.S. Landman et al., *Modelling vemurafenib resistance in melanoma reveals a strategy to forestall drug resistance*, Nature **494** (2013), 251–5.

[EDMea17] F. Eduati, V. Doldàn-Martelli, and B. Klinger et al., *Drug resistance mechanisms in colorectal cancer dissected with cell type-specific dynamic logic models*, Cancer Res **3364-75** (2017), 77.

[ELea12] Z. Ezzoukhry, C. Louandre, and E. Trécherel et al., *EGFR activation is a potential determinant of primary resistance of hepatocellular carcinoma cells to sorafenib*, International Journal of Cancer **131** (2012), 2961–2969.

[ENW10] M. Egeblad, E.S. Nakasone, and Z. Werb, *Tumors as organs : complex tissues that interface with the entire organism*, Dev Cell **18** (2010), 884–901.

[FBea16] S. Filippi, C.P. Barnes, and P.D. Kirk et al., *Robustness of MEK-ERK dynamics and origins of cell-to-cell variability in MAPK signaling*, Cell Rep **15** (2016), 2524–35.

[FMea16] D. Fey, D. Matallanas, and J. Rauch et al., *The complexities and versatility of the RAS-to-ERK signalling system in normal and cancer cells*, Semin Cell Dev Biol **58** (2016), 96–107.

[GDea13] C. Godin, S. Dupont, and Z. Ezzoukhry et al., *Heterogeneous sensitivity of hepatocellular carcinoma to sorafenib revealed by the short-term culture of tumor fragments*, Anticancer Research **33** (2013), 1415–1420.

[HJ96] C.Y. Huang and J.E. Ferrell Jr, *Ultrasensitivity in the mitogen-activated protein kinase cascade*, Proc Natl Acad Sci USA **93** (1996), 10078–83.

[HKKS16] M. Halasz, B.N. Kholodenko, W. Kolch, and T. Santra, *Integrating network reconstruction with mechanistic modeling to predict cancer therapies*, Sci Signal **9** (2016), ra114.

[JBea16] N.V. Jordan, A. Bardia, and B.S. Wittner et al., *HER2 expression identifies dynamic functional states within circulating breast cancer cells*, Nature **537** (2016), 102–6.

[JL13] K.A. Janes and D.A. Lauffenburger, *Models of signalling networks : what cell biologists can gain from them and give to them.*, J Cell Sci **126** (2013), 1913–21.

[JM98] J.E. Ferrell Jr and E.M. Machleder, *The biochemical basis of an all-or-none cell fate switch in Xenopus oocytes*, Science **280** (1998), 895–8.

[JMJ16] K.J. Jensen, C.B. Moyer, and K.A. Janes, *Network architecture predisposes an enzyme to either pharmacologic or genetic targeting*, Cell Syst **2** (2016), 112–21.

[KHGK15] W. Kolch, M. Halasz, M. Granovskaya, and B.N. Kholodenko, *The dynamic control of signal transduction networks in cancer cells*, Nat Rev Cancer **15** (2015), 515–27.

[KSea13] B. Klinger, A. Sieber, and R. Fritsche-Guenther et al., *Network quantification of EGFR signaling unveils potential for targeted combination therapy*, Mol Syst Biol **673** (2013), 9.

[LBea10] K. Lin, S. Baritaki, and L. Militello et al., *The role of B-RAF mutations in melanoma and the induction of EMT via dysregulation of the NF−κB/Snail/RKIP/PTEN circuit*, Genes Cancer **1** (2010), 409–420.

[LBS00] A. Levchenko, J. Bruck, and P.W. Sternberg, *Scaffold proteins may biphasically affect the levels of mitogen-activated protein kinase signaling and reduce its threshold properties*, Proc Natl Acad Sci USA **97** (2000), 5818–23.

[LRea08] J.M. Llovet, S. Ricci, and V. Mazzaferro et al., *Sorafenib in advanced hepatocellular carcinoma*, N. Engl. J. Med. **359** (2008), 378–90.

[MC15] I. Martincorena and P.J. Campbell, *Somatic mutation in cancer and normal cells*, Science **349** (2015), 1483–9.

[MM13] C.E. Meacham and S.J. Morrison, *Tumour heterogeneity and cancer cell plasticity*, Nature **501** (2013), 328–37.

[MTea14] A. Marusyk, D.P. Tabassum, and P.M Altrock et al., *Non-cell-autonomous driving of tumour growth supports sub-clonal heterogeneity*, Nature **514** (2014), 54–8.

[NBea10] T. Nakakuki, M.R. Birtwistle, and Y. Saeki et al., *Ligand-specific c-Fos expression emerges from the spatiotemporal control of ErbB network dynamics*, Cell **141** (2010), 884–96.

[NLea17] Leilei Niu, Liping Liu, and Shengli Yang et al., *New insights into sorafenib resistance in hepatocellular carcinoma : responsible mechanisms and promising strategies*, Biochim Biophys Acta Rev Cancer **1868** (2017), 564–570.

[OSea05] R.J. Orton, O.E. Sturm, and V. Vyshemirsky et al., *Computational modelling of the receptor-tyrosine-kinase-activated MAPK pathway*, Biochem J **392** (2005), 249–61.

[RCea15] H. Ryu, M. Chung, and M. Dobrzynski et al., *Frequency modulation of ERK activation dynamics rewires cell fate*, Mol Syst Biol **11** (2015), 838.

[SEJGM02] B. Schoeberl, C. Eichler-Jonsson, E.D. Gilles, and G. Muller, *Computational modeling of the dynamics of the MAP kinase cascade activated by surface and internalized EGF receptors*, Nat. Biotechnol. **20** (2002), 370–375.

[SGea17] Z. Saidak, A.S. Giacobbi, and C. Louandre et al., *Mathematical modelling unveils the essential role played by cellular phosphatases in the inhibition of RAF-MEK-ERK signalling by sorafenib in hepatocellular carcinoma cells*, Cancer Lett **392** (2017), 1–8.

[SOFK04] S. Sasagawa, Y. Ozaki, K. Fujita, and S. Kuroda, *Prediction and validation of the distinct dynamics of transient and sustained ERK activation*, Nat Cell Biol **7** (20200504), 365–73.

[SYL10] A.J. Sanyala, S.K. Yoonb, and R. Lencionic, *The etiology of Hepatocellular Carcinoma and Consequences for Treatment*, The Oncologist **15** (2010), 14–22.

[TD12] C. Tan and X. Du, *KRAS mutation testing in metastatic colorectal cancer*, World J. Gastroenterol. **18** (2012), 5171–5180.

[UWea17] A.R. Udyavar, D.J. Wooten, and M. Hoeksema et al., *Novel hybrid phenotype revealed in small cell lung cancer by a transcription factor network model that can explain tumor heterogeneity*, Cancer Res **77** (2017), 1063–74.

[vdHBea14] S. von der Heyde, C. Bender, and F. Henjes et al., *Boolean ErbB network reconstructions and perturbation simulations reveal individual drug response in different breast cancer cell lines*, BMC Syst Biol **8** (2014), 75.

[VPea14] M. Voliotis, R.M. Perrett, and C. McWilliams et al., *Information transfer by leaky, heterogeneous, protein kinase signaling systems*, Proc Natl Acad Sci USA **111** (2014), 326–33.

Chapitre 2

Methods and material

2.1 Derivation of equations

The derivation of each equation that occurs in the RAS-RAF-MEK-ERK pathway is explained in this section. The general concept can be found in the books [KS09, Alo06]. To simplify the readings, we consider the pathway described by Figure 2.1.

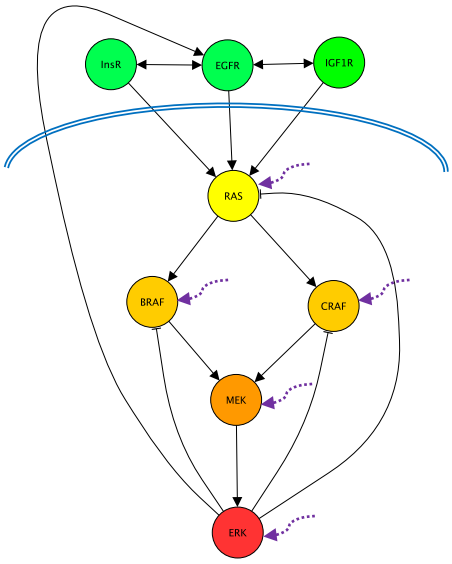

Figure 2.1 – The full RAS-RAF-MEK-ERK pathway studied in this work. The black arrows represent the contribution of a molecule in the activation of the other one by activating its degradation or its production, or by inhibiting its production. The dashed arrows describe the biological processes which occur out of the pathway and which contribute to a molecule activation.

We can split the chemical reactions in two groups for the modelling. A first one, including the receptors (EGFR, IR and IGF1-R) and the RAS protein, is modeled from the mass action law as their activation are dependent on many

types of chemical processes. The other reactions related to BRAF, CRAF, MEK and ERK are enzymatic. We present here the general concept of the mass action law and the enzymatic reaction model.

2.1.1 Mass action Law

We consider the simple reaction in which two reactants A and B give a product C

$$\mathrm{aA} + \mathrm{bB} \underset{k_2}{\overset{k_1}{\rightleftharpoons}} \mathrm{cC},$$

where a, b and c are the stoichiometric coefficients. The production rate k_1 and the degradation rate k_2 are respectively proportional to the product of the reactants concentrations and to the concentration of the species C. The temporal evolution of the specie A is represented by the nonlinear ordinary differential equation

$$\begin{aligned} \frac{d[A]}{dt} &= k_2[C]^c - k_1[A]^a[B]^b \\ &= \text{production - degradation,} \end{aligned}$$

where $[X]$ denotes the concentration of the specie X in mol/L.

2.1.1.1 Dynamics of the tyrosine kinases receptors

We selected three receptors of interest for our modelling : EGFR, IR and IGF1-R which are tyrosine kinase receptors (RTK). A lot of complexe biological processes are involved in the production and the degradation of these receptors. For a receptor R, its concentration $[R]$ is described by

$$\frac{d[R]}{dt} = \text{production - degradation - competition - regulation.}$$

Here, three receptors are of importance, namely $EGFR, IR$ and $IGF1R$. Autocrine loops, proportional to ERK phosphorylation, with positive feedback encourage the $EGFR$ production [ELea12, SHea02] , while competition between insulin receptors and epidermal growth factor receptors may occur [DMBea09, RPM+00]. Thus, the temporal evolution of $EGFR$ is provided by

$$\begin{aligned} \frac{d[EGFR]}{dt} &= [EGFR]\,(p_1[ERK] + p_2) - d_0[EGFR] \\ &\quad - [EGFR]\,(c_1[IR] + c_2[IGF1R]) - (b_1[IR] + b_2[IGF1R])\,. \end{aligned}$$

Here the parameters are nonnegative. This equation is rewritten

$$\begin{aligned}\frac{d[EGFR]}{dt} &= [EGFR]\,(p_{e,1}[ERK] + p_{e,2}) \\ &\quad - [EGFR]\,(c_{e,1}[IR] + c_{e,2}[IGF1R]) - (b_{e,1}[IR] + b_{e,2}[IGF1R])\,,\end{aligned}$$

where $p_{e,2} \in \mathbb{R}$. Similarly, we find

$$\begin{aligned}\frac{d[IR]}{dt} &= p_{i,1}[IR] - [IR]\,(c_{i,1}[EGFR] + c_{i,2}[IGF1R]) \\ &\quad - (b_{i,1}[EGFR] + b_{i,2}[IGF1R])\,,\end{aligned}$$

and

$$\begin{aligned}\frac{d[IGF1R]}{dt} &= p_{j,1}[IGF1R] - [IGF1R]\,(c_{j,1}[EGFR] + c_{j,2}[IR]) \\ &\quad - (b_{j,1}[EGFR] + b_{j,2}[IR])\,.\end{aligned}$$

2.1.1.2 RAS activation

The RAS activation is provided by a guanosine triphosphate (GTP) binding after receiving a signal from the growth factors using the RTK receptors. The activated RAS returns to its inactivated form by splitting the GTP bound into a GDP bound (guanosine diphosphate). Considering the partial contributions of EGFR, IR and IGF1-R in the RAS activation, the reactions are

$$\begin{aligned}\mathrm{RAS_{GDP}} + \mathrm{r_2EGFR} &\underset{s_1}{\overset{r_1}{\rightleftharpoons}} \mathrm{RAS_{GTP}} \\ \mathrm{RAS_{GDP}} + \mathrm{r_4IGF_1{-}R} &\underset{s_2}{\overset{r_3}{\rightleftharpoons}} \mathrm{RAS_{GTP}} \\ \mathrm{RAS_{GDP}} + \mathrm{r_6IR} &\underset{s_3}{\overset{r_5}{\rightleftharpoons}} \mathrm{RAS_{GTP}}.\end{aligned}$$

Moreover, a feedback loop from pERK to RAS occurs in the pathway [KHGK15, SRea09], in which pERK inhibits the RAS activation such that

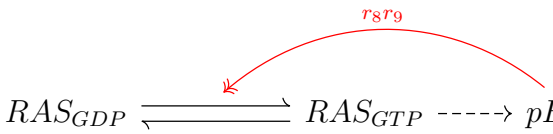

The term of the RAS activation depends then on $\left(1 + \frac{[pERK]}{r_8}\right)^{r_9}$. More details about this writing is given in the next section 1.2.1 above. The parameter r_9 is strictly positive if pERK contributes to an increase of the pathway activation or strictly negative if pERK contributes to a decrease of the pathway activation. The RAS_{GTP} evolution is given by

$$\begin{aligned}\frac{d[RAS_{GTP}]}{dt} &= (r_1[EGFR]^{r_2} + r_3[IR]^{r_4} + r_5[IGF1R]^{r_6} + r_7) \\ &\quad - ([RAS_{GDP}]) \left(1 + \frac{[pERK]}{r_8}\right)^{r_9} \\ &\quad - r_{10}[RAS_{GTP}].\end{aligned}$$

Since the RAS protein is an enzyme, its total amount RAS_{tot}, is driven by the enzyme conservation law that gives

$$[RAS_{tot}] = [RAS_{GDP}] + [RAS_{GTP}].$$

Finally, we get

$$\begin{aligned}\frac{d[RAS_{GTP}]}{dt} &= (r_1[EGFR]^{r_2} + r_3[IR]]^{r_4} + r_5[IGF1R]^{r_6} + r_7) \\ &\quad - ([RAS_{tot}] - [RAS_{GTP}]) \left(1 + \frac{[pERK]}{r_8}\right)^{r_9} \\ &\quad - r_{10}[RAS_{GTP}],\end{aligned}$$

where $r_{10} = s_1 + s_2 + s_3$ and r_7 is the contribution part out of the pathway.

2.1.2 Enzymatic reactions

The chemical reactions associated to BRAF, CRAF, MEK and ERK are enzymatic, in which an enzyme facilitates the reaction by increasing its speed. Such reaction enable to activate a substrat A into its activated form pA (p for phosphorylated) after binding the enzyme E. This reaction can be represented as follow

$$\mathrm{A} + \mathrm{E} \underset{k_2}{\overset{k_1}{\rightleftharpoons}} \mathrm{AE} \xrightarrow{k_3} \mathrm{pA} + \mathrm{E},$$

where AE is the enzyme-substrate complex. Note that the enzyme E is not modified at the end of the reaction.

The mass action law implies

$$\begin{aligned}\frac{d[A]}{dt} &= -k_1[A][E] + k_2[AE] \\ \frac{d[E]}{dt} &= -k_1[A][E] + k_2[AE] + k_3[AE] \\ \frac{d[AE]}{dt} &= k_1[A][E] - k_2[AE] - k_3[AE] \\ \frac{d[pA]}{dt} &= k_3[AE].\end{aligned}$$

We assume that the first reaction is fast and the concentration of the complex is constant. We deduce from the enzyme conservation law $[E] = [E_0] - [AE]$, with E_0 a constant,

$$\begin{aligned} \frac{d[AE]}{dt} = 0 &= k_1[A][E] - k_2[AE] - k_3[AE] \\ &= k_1[E_0][A] - (k_1[A] + k_2 + k_3)[AE], \end{aligned}$$

which implies

$$[AE] = \frac{k_1[E_0][A]}{(k_2 + k_3 + k_1[A])}.$$

Finally, the concentration of the activated product is given by

$$\frac{d[pA]}{dt} = \frac{k_3 k_1[E_0][A]}{(k_2 + k_3 + k_1[A])}.$$

In the same way, we consider the desactivation of the product pA by a phosphatase P, providing back the initial substrat A according to the chemical reactions

$$\mathrm{pA} + \mathrm{P} \underset{\widetilde{k_3}}{\overset{\widetilde{k_1}}{\rightleftharpoons}} \mathrm{pAP} \xrightarrow{\widetilde{k_3}} \mathrm{A} + \mathrm{P}.$$

It comes the differential equation

$$\frac{d[pA]}{dt} = -\frac{\widetilde{k_3}\widetilde{k_1}[P_0][pA]}{(\widetilde{k_2} + \widetilde{k_3} + \widetilde{k_1}[pA])}.$$

Combining the activation and the desactivation, the enzyme reaction is

$$\mathrm{A} \underset{V_2, K_2}{\overset{V_1 E, K_1}{\rightleftharpoons}} \mathrm{pA},$$

The Michaelis-Menten equations are found and we get

$$\begin{aligned} \frac{d[pA]}{dt} &= \frac{V_1[E][A]}{K_1 + [A]} - \frac{V_2[pA]}{K_2 + [pA]} \\ A_{total} &= A + pA. \end{aligned}$$

where $K_1 = \frac{k_2 + k_3}{k_1}$, $V_2 = \widetilde{k_3}[P_0]$ and $K_2 = \frac{\widetilde{k_2} + \widetilde{k_3}}{\widetilde{k_1}}$. The term $V_1[E]$ is provided by the constant term $k_3[E_0]$ which is dependent on the enzyme concentration $[E]$ through $[E_0]$.

Remark 2.1 *If a substrate M can be activated by two enzymes, E_1, E_2 and the complex E_1E_2 , the reactions are*

$$\begin{aligned} E_1 + M &\longrightarrow E_1 + pM, \\ E_2 + M &\longrightarrow E_2 + pM, \\ E_1E_2 + M &\longrightarrow E_1E_2 + pM, \\ E_1 + E_2 &\longrightarrow E_1E_2. \end{aligned}$$

The concentration of pM is then given by

$$\begin{aligned} \frac{d[pM]}{dt} &= \frac{(V_1[E_1E_2] + V_2[E_1] + \widetilde{V}_2[E_2])[M]}{K + [M]} \\ &= \frac{(-\widetilde{V}_1[E_1][E_2] + V_2[E_1] + \widetilde{V}_2[E_2])[M]}{K + [M]}. \end{aligned}$$

If $V[E] := (-\widetilde{V}_1[E_1][E_2] + V_2[E_1] + \widetilde{V}_2[E_2])$, the previous equation is of type Michaelis-Menten if $V \geq 0$ and $K \geq 0$, in other words

$$(V_1[E_1E_2] + V_2[E_1] + \widetilde{V}_2[E_2]) \geq 0.$$

By conservation of mass, one can write

$$[E_1] + [E_2] + [E_1E_2] = [E_0]$$

and we get

$$V_1[E_1E_2] = V_1[E_0] - V_1[E_1] - V_1[E_2].$$

Finally, the nonlinear ordinary differential equation becomes

$$\frac{d[pM]}{dt} = \frac{(V_1[E_0] + (V_2 - V_1)[E_1] + (\widetilde{V}_2 - V_1)[E_2])[M]}{K + [M]}.$$

Remark 2.2 *In vitro experimental conditions allow to justify the quasi-steady state approximation made in the enzymatic reactions. Indeed, the substrate concentrations are much greater than the total enzyme concentrations. We are talking about Michaelis condition.*

2.1.2.1 Enzymatic inhibitions

An enzymatic inhibitor I may modify the enzyme capacity. The inhibitor can bind to the enzyme, and prevent the primary substrate to react. The

inhibitor is said competitive if it binds to the active site and prevents binding of the substrate. The reactions read as

$$\begin{aligned} \mathrm{A} + \mathrm{E} &\underset{k_2}{\overset{k_1}{\rightleftharpoons}} \mathrm{AE} \qquad \xrightarrow{k_3} \mathrm{pA} + \mathrm{E} \\ \mathrm{E} + \mathrm{I} &\underset{k_{-I}}{\overset{k_1}{\rightleftharpoons}} \mathrm{IE}. \end{aligned}$$

Now, the concentrations $[E] = [E_0] - [AE] - [IE]$ and $[I] = [I_0] - [IE]$ from the mass conservation law, and according to the quasi-state approximation, one finds

$$\begin{aligned} \frac{d[IE]}{dt} = 0 &= k_I[E][I] - k_{-I}[IE] \\ &= k_I([E_0] - [AE] - [IE])([I_0] - [IE]) - k_{-I}[IE] \\ \frac{d[AE]}{dt} = 0 &= k_1[A][E] - k_2[AE] - k_3[AE] \\ &= (k_1[E_0] - k_1[IE])[A] - (k_1[A] + k_2 + k_3)[AE], \end{aligned}$$

Then, the complex are

$$\begin{aligned} [AE] &= \frac{k_1 k_{-I}[E_0][A]}{(k_3 + k_2 + k_1[A])k_{-I} + (k_3 + k_2)k_I[I]} \\ [IE] &= \frac{(k_3 + k_2)k_I[E_0][I]}{(k_3 + k_2 + k_1[A])k_{-I} + (k_3 + k_2)k_I[I]}. \end{aligned}$$

The dynamics of the product pA is thus governed by

$$\begin{aligned} \frac{d[pA]}{dt} &= \frac{k_3 k_1 k_{-I}[E_0][A]}{(k_3 + k_2 + k_1[A])k_{-I} + (k_3 + k_2)k_I[I]} \\ &= \frac{V_1[E_0][A]}{K_1 + [A] + K_2[I]}. \end{aligned}$$

The inhibitor is said uncompetitive if it binds to the AE complex and prevents conversion to product, and the chemical reactions are

$$\begin{aligned} \mathrm{A} + \mathrm{E} &\underset{k_2}{\overset{k_1}{\rightleftharpoons}} \mathrm{AE} \qquad \xrightarrow{k_3} \mathrm{pA} + \mathrm{E} \\ \mathrm{AE} + \mathrm{I} &\underset{k_{-I}}{\overset{k_I}{\rightleftharpoons}} \mathrm{AIE}. \end{aligned}$$

The concentration conservation is $[E] = [E_0] - [AE] - [AIE]$ that implies

$$\begin{aligned} [AE] &= \frac{k_1 k_{-I}[E_0][A]}{k_I(k_{-I}[I] + k_1[A][I]) + k_3 k_{-I} + k_2 k_{-I} + k_1 k_{-I}[A]} \\ [AIE] &= \frac{k_1 k_I[E_0][A][I]}{k_I(k_{-I}[I] + k_1[A][I]) + k_3 k_{-I} + k_2 k_{-I} + k_1 k_{-I}[A]}. \end{aligned}$$

We deal with similarly to get the dynamics of the product pA as the nonlinear differential equation

$$\begin{aligned}\frac{d[pA]}{dt} &= \frac{k_3 k_1 k_{-I}[E_0][A]}{k_I(k_{-I}[I] + k_1[A][I]) + k_3 k_{-I} + k_2 k_{-I} + k_1 k_{-I}[A]} \\ &= \frac{V_1[E_0][A]}{K_1 + [A]\left(1 + \frac{[I]}{K_2}\right)}.\end{aligned}$$

The inhibitor is said noncompetitive (or allosteric) if it can bind to either enzyme or enzyme-substrate complex, and the substrate can bind to enzyme or the enzyme-inhibitor complex. In case of negative feedback, the reactions read as

$$\begin{aligned}\mathrm{A} + \mathrm{E} + \mathrm{I} &\underset{k_2}{\overset{k_1}{\rightleftharpoons}} \mathrm{AE} + \mathrm{I} \qquad \xrightarrow{k_3} \mathrm{pA} + \mathrm{E} + \mathrm{I} \\ \mathrm{A} + \mathrm{E} + \mathrm{I} &\underset{k_2}{\overset{k_1}{\rightleftharpoons}} \mathrm{AE} + \mathrm{I} \qquad \underset{k_{-I}}{\overset{k_I}{\rightleftharpoons}} \mathrm{AIE} \\ \mathrm{A} + \mathrm{E} + \mathrm{I} &\underset{k_{-I}}{\overset{k_I}{\rightleftharpoons}} \mathrm{IE} + \mathrm{A} \qquad \underset{k_2}{\overset{k_1}{\rightleftharpoons}} \mathrm{AIE}\end{aligned}$$

Similar computations with the mass balance is $[E] = [E_0] - [AE] - [IE] - [AIE]$ and the complexes $[AE], [IE]$ and $[AIE]$ provide the dynamics of the product pA according noncompetitive inhibition as follows

$$\begin{aligned}\frac{d[pA]}{dt} &= \frac{k_3 k_1 k_{-I}[E_0][A]}{(k_3 + k_2 + k_1[A])k_{-I} + (k_3 + k_2)k_I[I]} \\ &= \frac{V_1[E_0][A]}{K_1 + [A]}\left(\frac{1}{1 + \frac{[I]}{K_3}}\right).\end{aligned}$$

In case of positive feedback, the dynamics becomes

$$\frac{d[pA]}{dt} = \frac{V_1[E_0][A]}{K_1 + [A]}\left(1 + \frac{[I]}{K_3}\right).$$

Note that if n molecules of inhibitor has to fit together with the enzyme in order for the reaction to take place, we replace $[I]$ by $[I]^n$.

To sum up, the activation by a phosphorylated enzyme via general noncompetitive inhibition and the desactivation by phosphatases of the protein A are written

$$\mathrm{A} \underset{v_2 E, k_2, k_I I}{\overset{v_1 E, k_1}{\rightleftharpoons}} \mathrm{pA},$$

and are governed by the nonlinear ordinary differential equation

$$\begin{aligned} \frac{d[pA]}{dt} &= \frac{v_1[E][A]}{k_1+[A]}\left(1+\frac{[I]}{k_I}\right)^{\alpha_I} - \frac{v_2[pA]}{k_2+[pA]} \\ A_{total} &= A + pA \end{aligned}$$

where $\alpha_I > 0$ if the feedback is positive and $\alpha_I < 0$ if the feedback is negative.

2.1.2.2 BRAF, CRAF

The activation of the RAF family proteins is dependent on the RAS protein which acts like an enzyme. Moreover, positive or negative feedback from $pERK$ may occur and are modeled by noncompetitive inhibition [KHGK15, SRea09]. The chemical reactions related to BRAF and CRAF are

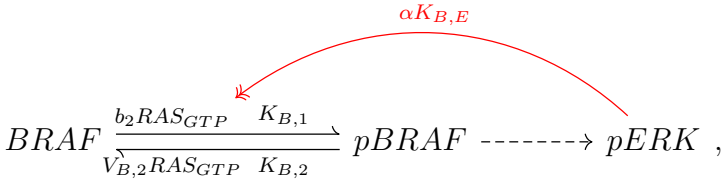

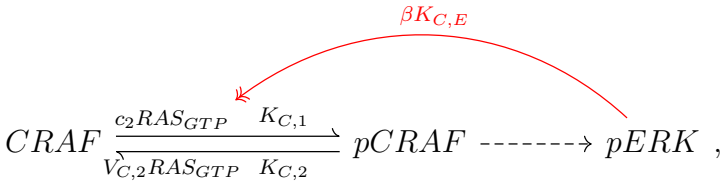

where $\alpha > 0$ and $\beta > 0$ if pERK leads to an increase of the pathway activation or $\alpha < 0$ and $\beta < 0$ if pERK leads to a decrease of the pathway activation at the RAF level. To take into account the biological processes involved in the BRAF and CRAF productions, which are not dependent on the ERK pathway, a parameter has been also added for each RAF production (b_1 for BRAF and c_1 for CRAF).

$$\begin{aligned} \frac{d[pBRAF]}{dt} &= \frac{(b_1+b_2[RAS_{GTP}])([BRAF_{tot}]-[pBRAF])}{K_{B,1}+([BRAF_{tot}]-[pBRAF])}\left(1+\frac{[pERK]}{K_{B,E}}\right)^{\alpha} \\ &\quad - \frac{V_{B,2}[pBRAF]}{K_{B,2}+[pBRAF]} \\ \frac{d[pCRAF]}{dt} &= \frac{(c_1+c_2[RAS_{GTP}])([CRAF_{tot}]-[pCRAF])}{K_{C,1}+([CRAF_{tot}]-[pCRAF])}\left(1+\frac{[pERK]}{K_{C,E}}\right)^{\beta} \\ &\quad - \frac{V_{C,2}[pCRAF]}{K_{C,2}+[pCRAF]}. \end{aligned}$$

Remark 2.3 *In Chapter 3, we take* $V_{B,1} = b_1 + b_2[RAS_{GTP}]$ *and* $V_{C,1} = c_1 + c_2[RAS_{GTP}]$ *for the RAF-MEK-ERK model as the different sources of the RAF production were not distinguish.*

2.1.2.3 MEK

The MEK protein is activated in turn such that

$$\text{MEK} \underset{V_{M,3}E_2, K_{M,2}}{\overset{V_M E_2, K_{M,1}}{\rightleftharpoons}} \text{pMEK},$$

where E_2 is the contribution of the two upstream enzymes in the pathway, pBRAF and pCRAF [KHGK15, SEJGM02]. The evolution of the pMERK amount is given by

$$\begin{aligned}\frac{d[pMEK]}{dt} &= \frac{(V_{M,1} + V_{M,2}[pBRAF] + \tilde{V}_{M,2}[pCRAF])([MEK_{tot}] - [pMEK])}{K_{M,1} + ([MEK_{tot}] - [pMEK])} \\ &\quad - \frac{V_{M,3}[pMEK]}{K_{M,2} + [pMEK]}.\end{aligned}$$

As previously, the first parameter $V_{M,1}$ represents the effect of biological processes out of the pathway.

$$\begin{aligned}\frac{d[pMEK]}{dt} &= \frac{(V_{M,1} + V_{M,2}[pBRAF] + \tilde{V}_{M,2}[pCRAF])([MEK_{tot}] - [pMEK])}{K_{M,1} + ([MEK_{tot}] - [pMEK])} \\ &\quad - \frac{V_{M,3}[pMEK]}{K_{M,2} + [pMEK]}.\end{aligned}$$

2.1.2.4 ERK

The activation of ERK is induced by the phosphorylated MEK as an enzyme [KHGK15, SEJGM02] such that

$$\text{ERK} \underset{V_{E,3}pMEK, K_{E,2}}{\overset{V_{E,2}pMEK, K_{E,1}}{\rightleftharpoons}} \text{pERK}.$$

Adding a parameter $V_{E,1}$, describing the exterior contribution in the ERK activation, we get

$$\begin{aligned}\frac{d[pERK]}{dt} &= \frac{(V_{E,1} + V_{E,2}[pMEK])([ERK_{tot}] - [pERK])}{K_{E,1} + ([ERK_{tot}] - [pERK])} \\ &\quad - \frac{V_{E,3}[pERK]}{K_{E,2} + [pERK]}.\end{aligned}$$

Remark 2.4 *Since we are dealing with sorafenib at constant dose in vitro experiments, the model does not include the pharmacokinetics of sorafenib.*

2.2 Parameters estimation

After defining the model, a main issue concerns the parameters estimation to relevant values for our biological context. Here we discuss the identifiability, the identification and the sensitivity analysis [WP97].

2.2.1 Identifiability

To simplify the writings, let us consider the model $\mathcal{M}(\theta)$ defined as

$$u'(t) = \frac{V_{u,1}(\overline{u}-u(t))}{K_{u,1}+\overline{u}-u(t)}\left(1+\frac{v(t)}{K_{u,3}}\right)^{-\alpha} - \frac{V_{u,2}u(t)}{K_{u,2}+u(t)} \tag{2.1}$$

$$v'(t) = \frac{V_{v,1}u(t)(\overline{v}-v(t))}{K_{v,1}+\overline{v}-v(t)} - \frac{V_{v,2}v(t)}{K_{v,2}+v(t)} \tag{2.2}$$

with the parameter $\theta = (V_{u,1}, V_{u,2}, K_{u,1}, K_{u,2}, K_{u,3}, \alpha, V_{v,1}, V_{v,2}, K_{v,1}, K_{v,2})$.

Definition 2.5 *The model $\mathcal{M}$ is identifiable if*

$$\mathcal{M}(\theta) = \mathcal{M}(\widetilde{\theta}),$$

then $\theta = \widetilde{\theta}$.

A direct computation provides the system identifiability. Indeed, the second equation (2.2)

$$\frac{V_1 u(\overline{v}-v))}{K_1+\overline{v}-v} - \frac{V_2 v(t)}{K_2+v} = \frac{\widetilde{V}_1 u(\overline{v}-v)}{\widetilde{K}_1+\overline{v}-v} - \frac{\widetilde{V}_2 v}{\widetilde{K}_2+v}$$

can be rewritten as

$$\begin{aligned}
&(K_1K_2\widetilde{K}_2\widetilde{V}_1\overline{v} + K_2\widetilde{K}_2\widetilde{V}_1\overline{v}^2)u + v + v^2 \\
&+ \left(\left(-2\widetilde{V}_1u + 2\widetilde{V}_2\right)\overline{v} + \left(\widetilde{K}_2 + K_2 - K_1\right)\widetilde{V}_1u + \left(\widetilde{K}_1 - K_2 + K_1\right)\widetilde{V}_2\right)v^3 \\
&+ \left(\widetilde{V}_1u - \widetilde{V}_2\right)v^4 \\
&= \\
&(K_2\,\widetilde{K}_1\,\widetilde{K}_2\,V_1\overline{v} + K_2\,\widetilde{K}_2\,V1u\,\overline{v}^2)u + v + v^2 \\
&+ \left((-2V_1u + 2V_2)\,\overline{v} + \left(\widetilde{K}_2 - \widetilde{K}_1 + K_2\right)\,V_1u + \left(-\widetilde{K}_2 + \widetilde{K}_1 + K_1\right)\,V_2\right)\,v^3 \\
&+ (V_1u - V_2)\,v^4.
\end{aligned}$$

Then assuming that (u_0, v_0) is not an equilibrium point of the system and comparing the power uv^4, v^4, uv^3, v^3, u provide the result [DVJb00].

We deal similarly with the first equation (2.1)

$$\frac{V_1(\overline{u}-u)}{K_1+\overline{u}-u}\left(1+\frac{v}{K_3}\right)^{-\alpha}-\frac{V_2 u}{K_2+u} = \frac{\widetilde{V}_1(\overline{u}-u)}{\widetilde{K}_1+\overline{u}-u}\left(1+\frac{v}{\widetilde{K}_3}\right)^{-\widetilde{\alpha}}-\frac{\widetilde{V}_2 u}{\widetilde{K}_2+u}$$

that is rewritten as

$$\begin{aligned}
&\left(K_2\,\widetilde{K}_2\,V_1\,\overline{u}^2+K_2\,\widetilde{K}_1\,\widetilde{K}_2\,V_1\,\overline{u}\right)\left(\frac{v}{K_3}+1\right)^{-\alpha}+u+u^2\\
&+\left(\left(-2V_1\,\overline{u}+\left(\widetilde{K}_2-\widetilde{K}_1+K_2\right)V_1\right)\left(\frac{v}{K_3}+1\right)^{-\alpha}+2V_2\,\overline{u}+\left(-\widetilde{K}_2+\widetilde{K}_1+K_1\right)V_2\right)u^3\\
&+\left(V_1\left(\frac{v}{K_3}+1\right)^{-\alpha}-V_2\right)u^4\\
&=\\
&\left(K_2\,\widetilde{K}_2\,\widetilde{V}_1\,\overline{u}^2+K_1\,K_2\,\widetilde{K}_2\,\widetilde{V}_1\,\overline{u}\right)\left(\frac{v}{\widetilde{K}_3}+1\right)^{-\widetilde{\alpha}}+u+u^2\\
&+\left(\left(-2\widetilde{V}_1\,\overline{u}+\left(\widetilde{K}_2+K_2-K_1\right)\widetilde{V}_1\right)\left(\frac{v}{\widetilde{K}_3}+1\right)^{-\widetilde{\alpha}}+2\widetilde{V}_2\,\overline{u}+\left(\widetilde{K}_1-K_2+K_1\right)\widetilde{V}_2\right)u^3\\
&+\left(\widetilde{V}_1\left(\frac{v}{\widetilde{K}_3}+1\right)^{-\widetilde{\alpha}}-\widetilde{V}_2\right)u^4
\end{aligned}$$

One combines with the series expansion

$$1-\frac{\alpha v}{K_3}+\frac{\left(\alpha^2+\alpha\right)v^2}{2{K_3}^2}-\frac{\left(\alpha^3+3\alpha^2+2\alpha\right)v^3}{6{K_3}^3}+\frac{\left(\alpha^4+6\alpha^3+11\alpha^2+6\alpha\right)v^4}{24{K_3}^4}+\ldots$$

2.2.2 Identification

Since our system of nonlinear differential equations is not analytically solvable, one has to define the cost function running simulations of the model with respect to parameters. The cost function, which is chosen stricly convex and coercive to ensure the existence and uniqueness of the minimizer, is the mean-square error between our available experimental data and the solution of the model. Given the concentration of

$$y_{\text{exp}} = (EGFR, IR, IGF1R, RAS_{GTP}, pBRAF, pCRAF, pMEK, pERK)$$

measured at time $4, 8$, and 18 hours, a mean square error can be defined as

$$J(p) = \sum_{i=1}^{M}\sum_{j=1}^{N}\frac{\left(y^j_{\text{exp}}(t_i) - y^j(t_i,p)\right)^2}{\sigma_{j,i}}$$

is minimized. Here $y^j(t_i, p)$ denotes the output of the mathematical model at time t_i of the jth molecule computed with the parameter p, and $y^j_{\text{exp}}(t_i)$ is the mean of the repeated experimental measures of the jth protein rate at the time t_i done with a standard deviation $\sigma_{j,i}$.

To ensure the convergence, our strategy consists in 3 steps.

1. We choose a set of random initial parameters.
2. The cost function is minimized using several algorithms.
3. The obtained optimal parameters is modified by random perturbations, and the second step is redone.

Deterministic methods are used to minimize this cost function. We give the principles below.

2.2.2.1 Simplex methods

Simplex methods are derivative-free algorithms which are widely used for solving unconstrained nonlinear optimization problem. A simplex is the generalization of the triangle in n dimensions, which is formed by the convex hull of $n + 1$ points. Those methods are based on a simplex building, which after several iterations, will contain the best vertices minimizing the cost objective function.
We explain here the main idea of the Nelder-Mead algorithm [NM65]. Let S be the simplex with the vertices $x_1, x_2, ..., x_{n+1}$. At each iteration, the vertices are ordered with respect to the objection function value

$$J(x_1) < J(x_2) < \ldots < J(x_{n+1}) \tag{2.3}$$

where x_1 the best vertex and x_{n+1} is the worst vertex. The simplex is then modified using operations (reflection, expansion, contraction and shrink) in order to get a new simplex with a better objective function value. The point x_{n+1} is replaced by its reflection through the centroid of the remaining n points. If the new cost function value is better than the other points, S is expanded in that direction. If the new point is better than the best vertex but worse than the second best point of the vertices, we keep this point and we start again. Otherwise, the local profile of the function is a valley and a contraction of S is maded. If the new point obtained is not better, a shrink of S occurs through a homothety with center x_1, which is the best vertex of S and a ratio σ. The NM algorithm steps is given in with the standard values $(\alpha, \beta, \gamma, \sigma) = (1, 2, \frac{1}{2}, \frac{1}{2})$.

Algorithm 1 Nelder-Mead algorithm

1. **Initialization**. Choice of $n+1$ points to generate the simplex.
2. Calculate f at the value of the $n+1$ vertices and sort the vertices such that 2.3 holds.
3. **Reflection**. Compute $x_r = \widetilde{x} + \alpha(\widetilde{x} - x_{n+1})$. Evaluate $J(x_r)$. **If** $J(x_1) < J(x_r) \leq J(x_n)$ **then** $x_{n+1} = x_r$ and go to step 2.
4. **Expansion**. **If** $J(x_r) < J(x_1)$ **then** compute the expansion point

$$x_e = \widetilde{x} + \beta(x_r - \widetilde{x}).$$

Evaluate $J(x_e)$. **If** $J(x_e) < J(x_r)$ **then** $x_{n+1} = x_e$. Otherweise, $x_{n+1} = x_r$ and go back to step 2.
5. **Outside contraction**. **If** $J(x_n) \leq J(x_r) < J(x_{n+1})$ **then** compute the outside contraction point

$$x_{oc} = \widetilde{x} + \gamma(x_r - \widetilde{x}).$$

Evaluate $J(x_{oc})$. **If** $J(x_{oc}) \leq J(x_r)$ **then** $x_{n+1} = x_{oc}$. Otherwise, go back to step 7.
6. **Inside contraction**. **If** $J(x_r) \geq J(x_{n+1})$ **then** compute the inside contraction point

$$x_{ic} = \widetilde{x} - \gamma(x_r - \widetilde{x}).$$

Evaluate $J(x_{ic})$. **If** $J(x_{ic}) < J(x_{n+1})$ **then** $x_{n+1} = x_{ic}$. Otherwise, go back to step 7.
7. **Shrink**. **For** $2 \leq i \leq n+1$, compute $x_i = x_1 + \sigma(x_i - x_1)$.

The COBYLA algorithm (Constrained Optimization By Linear Approximations) was implemented by Powell [Pow94]. It is based on linear approximations of the objective function and constraints using a simplex of $n+1$ vertices. Here, the constraints inequalities are given by the parameters x_k satisfying

$$x_k \geq 0,$$

where $0 \leq k \leq n$ with the parameters set $\mathcal{P} = (x_0, x_1, \ldots, x_n)$.

2.2.2.2 Methods based on the Newton algorithm

The quasi-Newton methods are used to solve unconstrained minimization problems [BGLS06]. Considering the minimization of the convexe function $J : \mathbb{R}^n \mapsto \mathbb{R}$, the optimization problem becomes looking for a vector $x \in \mathbb{R}^n$ such that

$$\nabla J(x) = 0. \tag{2.4}$$

This idea is based on the Newton method where a points sequence is generated from a initial point x_0 such that

$$x_{k+1} = x_k - \mathcal{H}(J(x_k))^{-1}.\nabla J(x_k),$$

such that x_{k+1} get closer to the solution of (2.4) at each iteration. However, the computation of the Hessian matrix inverse can be time-consuming with large dimension. The quasi-newton methods provide an approximation of $\mathcal{H}(f(x_k))^{-1}$ by considering a matrix B_k which satisfies

$$x_{k+1} - x_k = B_k(\nabla J(x_{k+1}) - \nabla J(x_k)),$$

which called is the quasi-newton relation. At each iteration, the current point is computed by

$$x_{k+1} = x_k - B_k \nabla J(x_k).$$

The matrix B_k is updated at each iteration and its expression depend on the method used.

In the Broyden-Fletcher-Goldfarb-Shanno (BFGS) method, the steps to approximate the solution of (2.4) are described in Algorithm 2.

Algorithm 2 BFGS

Initialization. Given x_0, B_0. B_0 can be the identity matrix.
At each iteration k :
Calculate $d_k = -B_k \nabla f(x_k)$.
Determinate ρ_k by a line-search with respect to the descent direction d_k such that

$$\nabla f(x_k + \rho_k d_k) < \nabla f(x_k).$$

Compute $x_{k+1} = x_k + \rho_k d_k$.
Calculate

$$B_{k+1} = B_k + \frac{y_k y_k^T}{y_k^T l_k} - \frac{B_k y_k y_k^T B_k}{l_k^T B_k l_k},$$

where $y_k = \nabla f(x_{k+1}) - \nabla f(x_k)$ and $l_k = \rho_k d_k = x_{k+1} - x_k$.
k=k+1.

The Sequential Quadratic Programming (SQP) method is a constrained optimization method where the initial minimization problem with constraints are replaced by an approximation sequence of quadratic problems with linear constraints. This method was used to compute the optimal control (see section 4.1.5). Considering the minimization of $J : \mathbb{R}^n \mapsto \mathbb{R}$ and the constraints function $C : \mathbb{R}^n \mapsto \mathbb{R}^s$, the initial problem is

$$\begin{cases} \min\limits_{x \in \mathbb{R}^n} J(x) \\ \\ C_i(x) \geq 0, i = 1, \ldots, s \end{cases}$$

In our work, the constraints are on some parameters x_i such that $x_i \geq 0$. Replacing C_i by $-C_i$, the Lagrangian associated to this problem is written

$$L(x; \lambda) = J(x) + \lambda^T C(x),$$

where $\lambda = (\lambda_1, \ldots, \lambda_s)$ is the Lagrange multiplier with $\lambda_i \in \mathbb{R}$ for all $i = 1, \ldots, s$. If J and C are differentiable at x, and under some assumptions on C, the optimal conditions for a such minimum x^* of J read as

$$\nabla L(x^*; \lambda^*) = 0,$$

with λ^* associated to x^*. It follows that (x^*, λ^*) must satisfy

$$\begin{cases} \nabla L(x^*; \lambda^*) = 0 \\ \\ \lambda_i C_i(x^*) = 0, i = 0, 1, \ldots, s \end{cases}$$

Using the Newton method to approximate a such (x^*, λ^*), those conditions can be replaced at the iteration k by

$$\begin{cases} \mathcal{H}_x L(x^k;\lambda^k)d + \sum_{i=1}^{s}(\alpha_i - \lambda_i)\nabla C_i(x^k) = -\nabla_x L(x^k;\lambda^k) \\ \\ \nabla C_i(x^k)^T d + C_i(x^k) = 0, i = 0, 1, \ldots, s \end{cases}$$

where $d = x_{k+1} - x_k$ and $\mathcal{H}_x L(x^k;\lambda^k)$ is the Hessian matrix of the Lagrangian in x. The Hessian matrix $\mathcal{H}$ of L is supposed to be inversible. These new conditions are the Lagrange optimal conditions of the following quadratic problem (QP)

$$\begin{cases} \min\limits_{d\in\mathbb{R}^n} J(x_k)^T d + \frac{1}{2} d^T \mathcal{H}_x L(x^k;\lambda^k)d \\ \\ C_i(x^k)^T d + \nabla C_i(x^k)^T d = 0, i = 0, 1, \ldots, s \end{cases}$$

The problem (QP) can be seen as a minimization of the Lagrangian quadratic approximation of the initial problem with linear approximation of constraints. The SQP method is presented in Algorithm 3.

Algorithm 3 SQP with constraints inequalities

Initialization. Given J, C, x_0 an initial point, $\lambda_0 \in \mathbb{R}^s$ an initial multiplier and $\epsilon > 0$.
$k = 0$.
While $|| \nabla L(x^k;\lambda^k) ||> \epsilon$ do
(i) Solve the quadratic problem (QP)

$$\begin{cases} \min\limits_{d\in\mathbb{R}^n} J(x_k)^T d + \frac{1}{2} d^T \mathcal{H}_x L(x^k;\lambda^k)d \\ C_i(x^k)^T d + \nabla C_i(x^k)^T d = 0, i = 0, 1, \ldots, s \end{cases}$$

to obtain the solution d_k and the multiplier λ' associated to the constraints inequalities.
(ii) $x_{k+1} = x_k + d_k$ and $\lambda_{k+1} = \lambda'$.
Return x_k.

An approximation of the Hessian matrix $\mathcal{H}$ is usually made to get a positive-definite matrix which gives the uniqueness of the solution with the SQP algorithm. A BFGS algorithm can be used to do this approximation.

Parameters identification was performed thanks to these methods with the *optimize* solvers of the Scipy library.

2.2.3 Sensitivity analysis

Sensitivity analysis is used to point the most influent reactions and parameters of the model. A measure for sensitivity consists in determining the relative change of a system feature due to a change in a parameter. In this work, our tests are performed thanks to ANOVA, Morris and Sobol methods. in agreement with Figure 2.2 from [IL15].

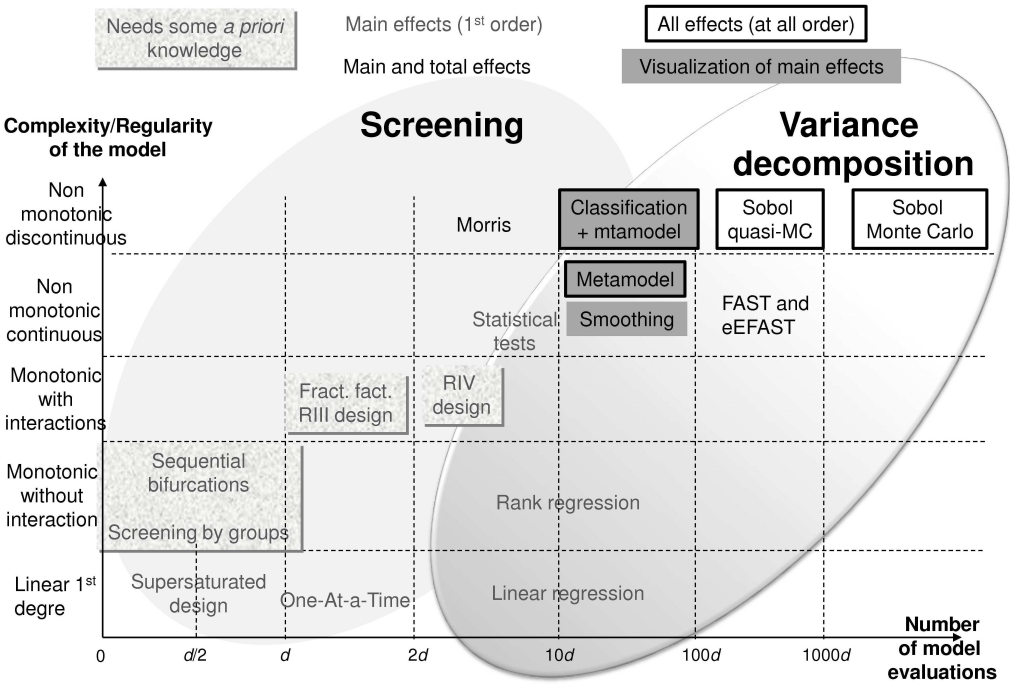

FIGURE 2.2 – Synthesis of sensitivity analysis method with respect to the number of parameters d [IL15].

2.2.3.1 ANOVA

The analysis of variance, or ANOVA, is based on a statistic model to analyze the group means in a sample and to provide estimations of the importance of groups on the variance of the model output [CM06]. In order to select the experimental data to calibrate our model, an ANOVA was performed. Let be $x_{i,j,n}$ the experimental measure of a protein X of the cell line i at the time j. Each measure was repeated n times. In our context, the goal of the variance analysis is to study the significant effects of the cell line i and the time j on the measure x in order to select or not this measure for the model calibration. We assume that the variable $x_{i,j,n}$ follows a normal distribution with mean $\mu_{i,j}$ and variance σ^2. One notes that the variance is the same for each measure which ensures homoscedasticity. We consider the linear model of 2-factor ANOVA with interactions

$$x_{i,j,n} = \mu + \alpha_i + \beta_j + \gamma_{i,j} + \epsilon_{i,j,n} \tag{2.5}$$

with $i = 1, \ldots, r$, $j = 1, \ldots, t$, $n = 1, \ldots, s$, $\mu + \alpha_i + \beta_j = \mu_{i,j}$ and $\epsilon_{i,j,n}$ i.i.d random variables $N(0, \sigma)$ for all i, j, n. The contribution of each factor, the cell line i and the time j, is represented respectively by the variables α_i and β_j. The interactions effect of both factors is described by the parameter $\gamma_{i,j}$. We define the following variables

$$\begin{aligned}
\overline{x} &= \frac{1}{rts} \sum_{i,j,n} x_{i,j,n}, \\
\overline{x}_{i,j,.} &= \frac{1}{s} \sum_{n} x_{i,j,n}, \\
\overline{x}_{i,.,.} &= \frac{1}{ts} \sum_{j,n} x_{i,j,n}, \\
\overline{x}_{.,j,.} &= \frac{1}{rs} \sum_{i,n} x_{i,j,n},
\end{aligned}$$

which are the different means over the different combinaisons of indices. Using the variance decomposition and the model 2.5, the total variation of all the measures $SS - t$ can be explained by the variation related to the the i (SS_1) and the factor j (SS_2), the variation of the interaction between the factors i and j ($SS_{1,2}$), and the unexplained variation (SS_u) such that

$$SS_t = SS_1 + SS_2 + SS_{1,2} + SS_u$$

with

$$\begin{aligned} SS_t &= \sum_{i,j,n}(x_{i,t,n} - \overline{x})^2, \\ SS_1 &= \sum_{i,j,n}(\overline{x}_{i,.,.} - \overline{x})^2, \\ SS_2 &= \sum_{i,j,n}(\overline{x}_{.,j,.} - \overline{x})^2, \\ SS_{1,2} &= \sum_{i,j,n}(\overline{x}_{i,j,.} - \overline{x}_{i,.,.} - \overline{x}_{.,j,.} + \overline{x})^2, \\ SS_u &= \sum_{i,j,n}(x_{i,t,n} - \overline{x}_{i,j,.})^2. \end{aligned}$$

The three following statistical hypothesis are then tested

$$\begin{cases} H_0 : \forall i, \alpha_i = 0 \\ H_1 : \exists i, \alpha_i \neq 0 \end{cases} \qquad \begin{cases} H_0 : \forall_j, \beta_j = 0 \\ H_1 : \exists \beta_j, \beta_j \neq 0 \end{cases} \qquad \begin{cases} H_0 : \forall (i,j), \gamma_{i,j} = 0 \\ H_1 : \exists (i,j), \gamma_{i,j} \neq 0 \end{cases}$$

Each test evaluates the dependence mean $\mu_{i,j}$ respectively on the index i, the index j and the interactions with respect to the following test variables

$$\begin{aligned} F_1 &= \frac{SS_1 rt(s-1)}{(r-1)SS_u}, \\ F_2 &= \frac{SS_2 rt(s-1)}{(t-1)SS_u}, \\ F_3 &= \frac{SS_{1,2} rt(s-1)}{(t-1)(r-1)SS_u}. \end{aligned}$$

If F_i is not in agreement with the Fisher law, then the H_0 hypothesis is rejected with $i = 1, 2, 3$. In this case, F_i is greater than a threshold, calculated from a significant level $\alpha \in [0\,,1]$ and the two associated degrees of freedom.

2.2.3.2 Morris analysis

The Morris method [Mor91] provides a parameters ranking in three groups with respect to their effect on the model output : negligible effects, linear effects without interaction and effects with interactions or nonlinear effects. This method was used to identify the importance of biological processes at different level of the ERK pathway on the pERK activity.

Let $x_1, x_2, ..., x_d$ be the model parameters with $x_i \in [0\,,1]$. The first step

of the Morris method is to repeat r times an one-at-a-time (OAT) design from the optimal parameters set. A regular grid is then generated by discretizing each parameter according to q-levels. A first trajectory point $P^1 = ({x_1}^1, {x_2}^1, \ldots, x_i^1, \ldots, {x_d}^1)$ is randomly chosen in the OAT design and the model output is evaluated at this point. The second trajectory point will differ from the first one in only one parameter. If the change of the parameter x_i is considered, we denote this point by

$$P^2 = ({x_1}^2, ..., {x_d}^2) = (x_1^1, x_2^1, ..., x_i^1 \pm \Delta, ..., x_d^1),$$

where $\Delta = \frac{n}{q-1}$ with $n \in [\![0, q-1]\!]$. Computing iteratively this method by changing at each iteration one parameter, a first trajectory with $d+1$ points is obtained. Repeating r times this design, we get r trajectories for which the output model is evaluated at each point of the trajectory. A number of $r(d+1)$ running is then required. For each trajectory, the output variation is computed with respect to the variation of the parameter x_i. It defines the elementary effect, E_k^i, of the parameter x_i associated to the k-th trajectory such that

$$E_k^i = \frac{Y(\ldots, x_i \pm \Delta, \ldots) - Y(\ldots, x_i, \ldots)}{\pm\Delta}.$$

The mean effect of the parameter x_i is then represented by

$$\mu_i = \frac{1}{r} \sum_{k=1}^{r} E_k^i,$$

where r is the number of trajectory. Two sensitivity indices are estimated for each parameter : the absolute mean tendency μ_i^*, and the elementary effect deviation σ_i, which are define by

$$\mu_i^* = \frac{1}{r} \sum_{k=1}^{r} \mid E_k^i \mid$$

and

$$\sigma_i = \sqrt{\frac{1}{r-1} \sum_{k=1}^{r} \left(E_k^i - \mu_i\right)^2}.$$

The indices values give the parameters ranking : if $\mu_i^* \simeq 0$, then the parameter x_i has no impact on the output Y (negligible effect). If $\mu_i^* \gg 0$ and $\sigma_i \simeq 0$, x_i has a linear effect without interaction on Y and if $\mu_i^* \gg 0$ and $\sigma_i \gg 0$, x_i has nonlinear effect on Y or is in interaction with Y.

2.2.3.3 Sobol analysis

The Sobol method provides global sensitivity indices for nonlinear models [Sob01]. As before, the first step of this sensitivity method is to generate a sample design, here using a Monte-Carlo method, in order to represent the uncertainties of the parameters through the model. From this design, an estimation of the importance of each parameter on the output variance is given using the decomposition of the variance. To evaluate the effect of the parameter x_i on the output variance, x_i can be fixed at the value x and the following quantity is considered

$$V_{X_{-i}}(Y|x_i = x),$$

where X_{-i} is the space containing all the parameters except x_i. Since the exact value of x_i is not known, we look at the average of all the possible values of x_i

$$E_{X_i}(V_{X_{-i}}(Y|x_i)).$$

If this quantity is low, then fixing x_i reduces the output variance, which means that x_i is of importance. Using the total variance formula, we get

$$V(Y) = V_{X_i}(E_{X_{-i}}(Y|x_i)) + E_{X_i}(V_{X_{-i}}(Y|x_i)).$$

Now, if the first term is of the sum is high, x_i is of importance. To simplify the notation, the variance indices will be omitted. The fist-order index is define by

$$S_i = \frac{V(E(Y|x_i))}{V(Y)},$$

where S_i represents the main contribution of the parameter x_i on the output variance. To compute this index, we assume that the parameters are mutually independent. Then, I.M. Sobol shows that there is an unique decomposition of the output (result reported in the section 4.3 of [SRAea08]) such that

$$Y = f(x_1, \ldots, x_d) = f_0 + \sum_{i=1}^{d} f_i(x_i) + \sum_{1 \geq i,j \geq d} f_{i,j}(x_i, x_j) + \ldots + f_{i,\ldots,d}(x_i, \ldots, x_d),$$

where

$$\begin{aligned} f_0 &= E(Y) \\ f_i &= E(Y|x_i) - E(Y) \\ f_{i,j} &= E(Y|x_i, x_j) - f_i - f_j - E(Y) \\ &\ldots \end{aligned}$$

Assuming that f is square integrable over the existence domain Ω, each term of the decomposition of Y is in $L^2(\Omega)$. Thus, the output variance $V(Y)$ is written

$$V(Y) = \sum_{i=1}^{d} V(f_i) + \sum_{i \neq j} V(f_{i,j}) + \ldots + V(f_{1,\ldots,d}). \tag{2.6}$$

Considering the first p terms, the first-order index related to the parameter x_i is then

$$S_i = \frac{V(E(Y|x_i))}{V(Y)} = 1 - \frac{E(V(Y|x_i))}{V(Y)}.$$

The next order index $S_{i,j}$ describes the main effect of x_i and the interaction effects of x_i with x_j on the output variance such that

$$S_{i,j} = \frac{V(f_{i,j})}{V(Y)}.$$

The total sum of indices including the parameter x_i satisfies

$$\sum_{i} + \sum_{i \neq j} S_{i,j} + \ldots + S_{1,\ldots,d} = 1.$$

Using the total variance formula, we consider the total index of x_i

$$S_{T_i} = \frac{E(V(Y|X_{-i}))}{V(Y)} = 1 - \frac{V(E(Y|X_{-i}))}{V(Y)},$$

where X_{-i} is the space of all parameters except x_i. This quantity represents the indices sum with respect to the main effect of x_i and the effects of all the interactions including x_i. To estimate these indices, two N-samples were generated by Monte-Carlo. Let A and B be two N-samples that read as

$$A = \begin{bmatrix} x_{1,1}^A & \ldots & x_{1,d}^A \\ \ldots & \ldots & \ldots \\ x_{N,1}^A & \ldots & x_{N,d}^A \end{bmatrix}, \quad B = \begin{bmatrix} x_{1,1}^B & \ldots & x_{1,d}^B \\ \ldots & \ldots & \ldots \\ x_{N,1}^B & \ldots & x_{N,d}^B \end{bmatrix}.$$

Each column of A and B corresponds to a set of N values for each parameter by applying an uniform distribution on $[x^*(1-0.1), x^*(1+0.1)]$, were x^* is the optimal value of the parameter. $2N$ values are then generated for each parameter. A combinaison C_i is then considered for all $i = 1, \ldots, d$ such that

$$C_i = \begin{bmatrix} x_{1,1}^A & x_{1,i}^B & x_{1,d}^A \\ \ldots & \ldots & \ldots \\ x_{N,1}^A & x_{N,i}^B & x_{N,d}^A \end{bmatrix},$$

where the column i of A is replaced by the column i of B. Running $N(d+2)$ times the model is required to compute the outputs vectors for each sample. Let Y_A, Y_B and C_i be these N-dimensional vectors. The Sobol indices can be then estimated and are given by

$$\widehat{S}_i = \frac{\widehat{V}_i}{\widehat{V}} \quad \text{and} \quad \widehat{S_{T_i}} = \frac{\widehat{V_{-i}}}{\widehat{V}},$$

with

$$\widehat{V}_i = \frac{1}{N}\sum_{k=1}^{N} Y_{B,k}(Y_{C_i,k} - Y_{A,k}) \text{ and } \widehat{V_{-i}} = \frac{1}{N}\sum_{k=1}^{N} Y_{A,k}(Y_{A,k} - Y_{C_i,k}).$$

Here, 22 millions of samples were generated to estimate the first-order index S_i and the total index S_{T_i}.

All of the sensitivity methods, ANOVA, Morris and Sobol, were performed using R software and the *sensitivity* package.

2.3 Material

To study the regulation of the RAS-RAF-MEK-ERK pathway after sorafenib treatment, and particularly the pERK regulation, the model needs to be calibrated on realistic data. Thus, three human cell lines (Huh7, Hep3b and PLC/PFR5) with a specific sensitivity profil to sorafenib, are prepared for a western blot analysis to get such data.This method provides a detection and an identification of specific proteins in a biological sample. The cell lines are treated by sorafenib with a constant dose (Fig. 2.3). For each cell line, four cellular samples are blocked respectively at 0 hour, 4 hours, 8 hours and 18 hours after sorafenib input. Then, each cells sample corresponding to a mix of proteins is submitted to an electrophoresis to split the proteins with respect to the molecular weight on a gel matrix. This step is called the migration samples. A transfer from the gel matrix to a membrane support is made and the proteins are detected by specific anti-bodies. To reveal the protein detection, the membrane is then incubated with a chemiluminescent reagent in a dark room in order to provide the footprint of each protein on a film. The film scan result is shown in Figure 2.4.

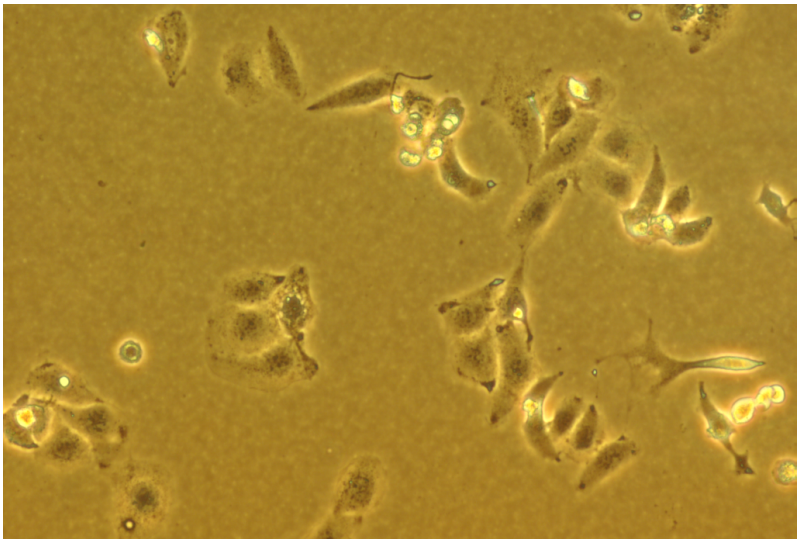

FIGURE 2.3 – The Huh7 cell line after sorafenib treatment.

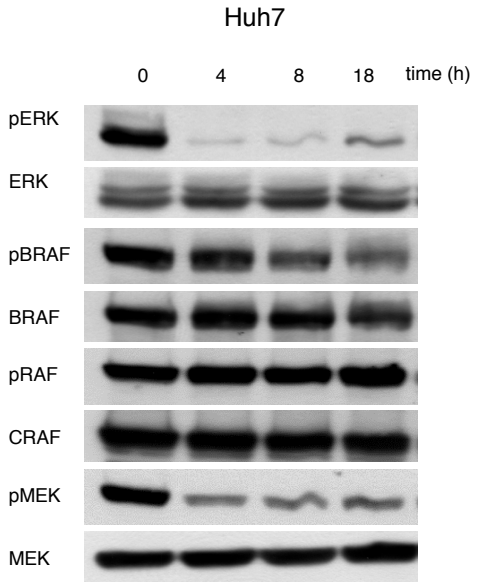

FIGURE 2.4 – Proteins detection using Western blot analysis for the Huh7 cell line.

From this scan, a quantification of each protein is made using ImageJ software. The ratio r_t of a protein activity at the time t is given by

$$r_t = \frac{N_t^X}{m_C}$$

where N_t^X is the pixels number of the detection band of the protein X at the time t and m_C is the loading controls mean in pixels number, which have been subtracted from the pixels number of the background to reduce the image contrast errors. Loading controls are made to distinguish the bands between the proteins. The molecule selected for these controls is expressed at high-level and its amount is supposed to be constant trough the biological experiments. Each protein ratio is then normalized with respect to the initial ratio at $t = 0$. Thus, the available data used for our modelling are rates of the protein activity without unit and not a concentration expressed in $mol.L^{-1}$.

References

[Alo06] U. Alon, *An introduction to systems biology : Design principles of biological circuits*, Chapman & Hall, 2006.

[BGLS06] J.F. Bonnans, J.C. Gilbert, C. Lemaréchal, and C.A. Sagastizábal, *Numerical Optimization - Theoretical and Practical Aspects*, Berlin : Springer-Verlag, 2006.

[CM06] P.A Cornillon and E. Matzner, *Régression, théorie et applications*, Statistique et probabilités appliquées, Springer, 2006.

[DMBea09] C. Desbois-Mouthon, A. Baron, and M.J. Blivet-Van Eggelpoël et al., *Insulin-like growth factor-1 receptor inhibition induces a resistance mechanism via the epidermal growth factor receptor/HER3/AKT signaling pathway : rational basis for cotargeting insulin-like growth factor-1 receptor and epidermal growth factor receptor in hepatocellular carcinoma*, Clinical Cancer Research **15** (2009), 5445–5456.

[DVJb00] L. Denis-Vidal and G. Joly-blanchard, *An easy to check criterion for(un)identifiability of uncontrolled systems and its applications*, IEEE Transactions on Automatic Control **45** (2000), 768–771.

[ELea12] Z. Ezzoukhry, C. Louandre, and E. Trécherel et al., *EGFR activation is a potential determinant of primary resistance of hepatocellular carcinoma cells to sorafenib*, International Journal of Cancer **131** (2012), 2961–2969.

[IL15] B. Iooss and P. Lemaître, *A review on global sensitivity analysis methods*, C. Meloni and G. Dellino. Uncertainty management in Simulation-Optimization of Complex Systems : Algorithms and Applications, Springer, 2015.

[KHGK15] W. Kolch, M. Halasz, M. Granovskaya, and B.N. Kholodenko, *The dynamic control of signal transduction networks in cancer cells*, Nature Reviews Cancer **15** (2015), 515–527.

[KS09] J. Keener and J. Sneyd, *Mathematical physiology I : Cellular physiology. Second edition*, New-York : Springer-Verlag, 2009.

[Mor91] M.D. Morris, *Factorial sampling plans for preliminary computational experiments*, Technometrics **33** (1991), 161–174.

[NM65] J.A. Nelder and R. Mead, *A simplex method for function minimization*, The computer Journal **8** (1965), 308–313.

[Pow94] M.J.D. Powell, *A direct search optimization method that models the objective and constraint functions by linear interpolation*, In Advances in Optimization and Numerical Analysis. Mathematics and Its Applications. Dordrecht : Springer Netherlands. (1994), 51–67.

[RPM+00] F.L. Roudabush, K.L. Pierce, S. Maudsley, K.D. Khan, and L.M. Luttrell, *Transactivation of the EGF receptor mediates IGF-1-stimulated shc phosphorylation and ERK1/2 activation in COS-7 cells*, Journal of Biological Chemistry **275** (2000), 22583–22589.

[SEJGM02] B. Schoeberl, C. Eichler-Jonsson, E.D. Gilles, and G. Müller, *Computational modeling of the dynamics of the MAP kinase cascade activated by surface and internalized EGF receptors*, Nature Biotechnology **20** (2002), 370–375.

[SHea02] S.Y. Shvartsman, M. P. Hagan, and A. Yacoub et al., *Autocrine loops with positive feedback enable context-dependent cell signaling*, American Journal of Physiology-Cell Physiology **282** (2002), 545–559.

[Sob01] I.M Sobol, *Global sensitivity indices for nonlinear mathematical models and their Monte Carlo estimates*, Mathematics and Computers in Simulation **55** (2001), 271–280.

[SRAea08] A. Saltelli, M. Ratto, T. Andres, and F. Campolongo et al., *Global sensitivity analysis. The primer*, vol. 304, Wiley, 2008.

[SRea09] S.Y. Shin, O. Rath, and S.M. Choo et al., *Positive- and negative-feedback regulations coordinate the dynamic behavior of the Ras-*

Raf-MEK-ERK signal transduction pathway, Journal of Cell Science **122** (2009), 425–435.

[WP97] E. Walter and L. Pronzato, *Identification of parametric models from experimental data*, Masson, 1997.

Chapitre 3

Le rôle essentiel des phosphatases révélé par la modélisation du coeur de la voie de signalisation RAF-MEK-ERK

Mathematical modelling unveils the essential role of cellular phosphatases in the inhibition of RAF-MEK-ERK signalling by sorafenib in hepatocellular carcinoma cells

Ce chapitre fait l'object de l'article *Z. Saidak, A.S. Giacobbi, C. Louandre, C. Sauzay, Y. Mammeri, A. Galmiche, Mathematical modelling unveils the essential role of cellular phosphatases in the inhibition of RAF-MEK-ERK signalling by sorafenib in hepatocellular carcinoma cells, Cancer letters 392, (2017), 1-8.*

The RAF-MEK-ERK cascade is a key signal transduction pathway that plays an essential role in the response of eukaryotic cells to various trophic stimuli and growth factors, and it is activated in many human tumours [WKM04, DHRK07]. Upon interaction with their cognate ligands, Receptors with Tyrosine Kinase activity (RTK) activate small GTPases of the RAS family leading to the activation of the kinases of the RAF family (CRAF/Raf-1, BRAF, and ARAF), followed by MEK1/2 and ERK1/2, the final effectors of the cascade [WKM04, DHRK07, LT15]. Missense mutations that constitutively activate the RAS and RAF proteins are present in various solid tumours, and have proved instrumental in establishing the role of the RAF-MEK-ERK cascade as a driver in human carcinogenesis [WKM04, DHRK07, LT15]. The recent development of chemical inhibitors of the RAF kinases that are clinically efficacious has established that the RAF-MEK-ERK cascade is a valid target for the medical treatment of solid tumours [LT15, MBS16]. Recently, progress has been made in our understanding of the molecular alterations that drive the appearance of Hepatocellular carcinoma (HCC), the

most frequent form of primary liver cancer [ZRVNL15]. Despite this progress, analysis of the activation status and the regulation of the RAF-MEK-ERK cascade in individual HCC remains difficult. HCC cells do not carry somatic mutations in the genes encoding the RAF kinases, but express reduced levels of negative regulators of the RAF-MEK-ERK cascade, such as the RAS GTPase activating proteins (RAS GAP), or the Raf-1 kinase inhibitor protein (RKIP) [DS15]. In addition, autocrine production of growth factors, such as the Vascular endothelial growth factor (VEGF) and amphiregulin often leads to the activation of the corresponding RTKs and the RAF-MEK-ERK cascade in HCC cells [CEP+06, PWP+14]. The multiplicity of the actors that potentially regulate the RAF-MEK-ERK cascade and the coexistence of multiple alterations constitute major obstacles in the exploration of the regulation of the RAF-MEK-ERK cascade in HCC. Sorafenib, a clinically-approved kinase inhibitor, is currently the treatment of reference for patients with advanced HCC [GCB14]. Sorafenib was initially developed on the basis of its ability to inhibit RAF kinases and the RAF-MEK-ERK cascade in HCC cells [WCT+04]. Cellular studies exploring the resistance of HCC to sorafenib have identified the RAF-MEK-ERK cascade as an important target for this drug [ELT+12, TCM+15, BMU+14]. In HCC cells that are resistant to clinically-relevant concentrations of sorafenib, sorafenib fails to inhibit the phosphorylation of ERK, for example as a consequence of the activation of the Epidermal Growth Factor Receptor (EGFR) or other RTKs [ELT+12, TCM+15]. These studies suggest that perturbations introduced in the intrinsic regulation of the RAF-MEK-ERK cascade are a potential source of resistance of HCC to sorafenib, a finding that highlights the crucial importance of this cascade as a target of sorafenib in HCC. Interestingly, clinical studies exploring the expression of phosphorylated ERK in tumour explants and in circulating tumour cells isolated from the blood of HCC patients confirm the importance of the RAF-MEK-ERK cascade as a target of sorafenib [GDE+13, LSZ+16]. Nevertheless, it remains unclear how sorafenib achieves efficient control over this transduction cascade. Besides its inhibitory activity directed against RAF kinases, sorafenib possesses multiple therapeutic targets that could contribute to its anti-ERK activity. Among these targets are the RTKs, such as the VEGF Receptor [DHH+11]. Part of sorafenib anti-ERK efficacy might come from its ability to induce a broad-range reprogramming of the kinome of cancer cells. Crosstalk between different MAPK signalling pathways, involving stress pathways and phosphatases that are active against components of the RAF-MEK-ERK cascade, may also contribute to the anti-ERK efficacy of sorafenib in HCC cells [RDL+14, AB15, JLW08]. Finally, sorafenib's effect on the protein secretory pathway of HCC cells might interrupt cellular autocrine loops, further contributing to the inhibition of the

RAF-MEK-ERK cascade in this context [YHT+12, HGB+16]. It is currently not clear which of these mechanisms account for the ability of sorafenib to potently inhibit the RAF-MEK-ERK cascade in HCC cells. Mathematical modelling is a useful strategy for addressing the biological behaviour of complex pathways and transduction networks [KHGK15]. Models based on ordinary differential equations (ODE) enable the study of cellular pathways, such as the RAF-MEK-ERK cascade, in a non-reductionist fashion, as well as the exploration of their responses to drugs and a variety of perturbagens at the system level [BF00, SEJGM02, OSV+05, SRC+09, SOG+10]. Based on previous data that have indicated the importance of the RAF-MEK-ERK cascade as a target of sorafenib, we decided to apply mathematical modelling to explore the regulation of this signalling cascade in HCC cells in the therapeutic context.

3.1 Materials and methods

3.1.1 Cell culture and reagents

The three HCC cell lines used in this study (Huh7, Hep3B and PLC/PRF5) were obtained from Dr. Wychowski (Institut de Biologie de Lille, France) and were authenticated using profiling of short tandem repeats at 16 loci (LGC Standards, Strasbourg, France). The cells were cultured in Dulbecco Modified Eagle's Medium (DMEM) (Sigma) supplemented with 10% fetal calf serum (Jacques Boy), 2 mM glutamine, penicillin and streptomycin. Sorafenib was purchased from Selleck chemicals and kept as 10 mM stock in DMSO at 20 C. All other compounds were purchased from Sigma.

3.1.2 Western blots

Complete cell extracts were prepared in RIPA buffer. Proteins were precipitated, loaded on SDS-PAGE and transferred to nitrocellulose membranes using standard procedures [GFS+08]. The primary antibodies raised against the core components of the RAF-MEK-ERK cascade were rabbit antibodies from Cell Signalling Technology (anti-pERK : reference 9101, ERK : 4695, pMEK : 9154, MEK : 8727, pBRAF : 2696, BRAF : 9433, pCRAF : 9427, and CRAF : 9422). The antibody directed against b-actin was a mouse monoclonal from Sigma (A5441). All primary antibodies were used at a dilution of 1 :2000 and incubated overnight. Secondary antibodies coupled to horseradish peroxidase were from GE healthcare. The ECL reaction was used for revelation. Western blots were scanned and quantified using the software

ImageJ (NIH).

3.1.3 Variance analysis

Experimental data were analysed using ANOVA, comparing the three different cell lines and the three experimental replicas for each cell line. We used the Varpart function in R [PNLDB06] to identify the relationships between the different proteins of our model that exert the greatest influence on the downstream components of the cascade.

3.1.4 Mathematical modelling of the RAF-MEK-ERK cascade

We focused our study on the core components of the RAF cascade, i.e. BRAF, CRAF, MEK and ERK. Based on the previous analysis of variance, the model was restricted to five connections with the greatest importance in the activation of ERK. To build the mathematical model, we followed the standard strategy developed in the literature concerning the ERK pathway [BF00, SEJGM02, OSV+05, SRC+09, SOG+10]. We assumed that only two possible states can be reached by each kinase : active (phosphorylated) and inactive (non-phosphorylated). Since we were dealing with enzymatic reactions, the dynamics were described by Michaelis-Menten kinetics and the governing equations were written as a system of four ordinary differential equations (ODE) as follows :

$$
\begin{aligned}
\frac{d[pBRAF]}{dt} &= \frac{V_{B,1}([BRAF_{tot}]-[pBRAF])}{K_{B,1}+([BRAF_{tot}]-[pBRAF])}\left(1+\frac{[pERK]}{K_{B,E}}\right)^{-\alpha} \\
&\quad - \frac{V_{B,2}[pBRAF]}{K_{B,2}+[pBRAF]} \\
\frac{d[pCRAF]}{dt} &= \frac{V_{C,1}([CRAF_{tot}]-[pCRAF])}{K_{C,1}+([CRAF_{tot}]-[pCRAF])}\left(1+\frac{[pERK]}{K_{C,E}}\right)^{-\beta} \\
&\quad - \frac{V_{C,2}[pCRAF]}{K_{C,2}+[pCRAF]} \\
\frac{d[pMEK]}{dt} &= \frac{(V_{M,1}+V_{M,2}[pBRAF]+\widetilde{V}_{M,2}[pCRAF])([MEK_{tot}]-[pMEK])}{K_{M,1}+([MEK_{tot}]-[pMEK])} \\
&\quad - \frac{V_{M,3}[pMEK]}{K_{M,2}+[pMEK]} \\
\frac{d[pERK]}{dt} &= \frac{(V_{E,1}+V_{E,2}[pMEK])([ERK_{tot}]-[pERK])}{K_{E,1}+([ERK_{tot}]-[pERK])} \\
&\quad - \frac{V_{E,3}[pERK]}{K_{E,2}+[pERK]}
\end{aligned}
$$

where $[pX]$ denotes the phosphorylated and $[X_{tot}]$ represents the total amount of X. The parameter $K_{.,.}$ describes the saturated maximal rate of the production or the disappearance of a protein. The parameter $V_{M,1}$ also accounts for the activation by the dimer pBRAFpCRAF (see Remark 3.1). The parameters $V_{B,1}$ and $V_{C,1}$ represent the activation parts of the upstream components that were omitted in our model. Two terms, $V_{M,1}$ and $V_{E,1}$, represent the activation of MEK and ERK that can occur independently of the RAF kinases. The parameters, $-\alpha$ and $-\beta$, can be positive or negative corresponding to a positive or a negative feedback loop from pERK to each RAF kinase.

Remark 3.1 *Similarly to page 31, MEK can be activated by two enzymes, pBRAF, pCRAF and the dimer pBRAFpCRAF [CHMea16]. It provides*

$$\begin{aligned}\frac{d[pMEK]}{dt} &= (V_1[pBRAFpCRAF] + V_{M,2}[pBRAF] + \widetilde{V}_{M,2}[pCRAF]) \\ &\quad \frac{([MEK_{tot}] - [pMEK])}{K_{M,1} + ([MEK_{tot}] - [pMEK])} - \frac{V_{M,3}[pMEK]}{K_{M,2} + [pMEK]}\end{aligned}$$

Since no experimental measure of the dimer activity is available, we assume that

$$V_1[pBRAFpCRAF] = V_{M,1} = constant.$$

3.1.5 Parameter estimation

The model is made up of 22 parameters that need to be determined. Given $\left(y^j_{\text{exp}}(t_i)\right), 1 \leq i \leq M, 1 \leq j \leq N$, N experimental data at M hours, the nonlinear least squares objective function

$$J(p) = \sum_{i=1}^{M} \sum_{j=1}^{N} \frac{\left(y^j_{\text{exp}}(t_i) - y^j(t_i, p)\right)^2}{\sigma_{j,i}}$$

is minimized. Here $y^j(t_i, p)$ denotes the output of the mathematical model at time t_i computed with the parameter p, and $y^j_{\text{exp}}(t_i)$ is the mean of the repeated experimental measures of $y^j_{\text{exp}}(t_i)$ done with a standard deviation $\sigma_{j,i}$. The optimization problem was solved using the Constrained Optimization BY Linear Approximation (Cobyla) [Pow94].

3.1.6 Sensitivity analysis

Morris global sensitivity analysis, a randomised one-at-a-time design, was carried out to identify which of the 22 parameters produced the most significant effects. This method, recommended for large numbers of input and time

consuming models, is useful for studying specific behaviours of a biological system under perturbation, allowing us to improve our understanding of a biological process, adjust the model parameter values or confirm the model robustness [CCS07]. This statistical method involves ranking the parameters into three groups, according to their effects on the model output : negligible effects, linear effects without interactions and nonlinear effects with interactions. By applying perturbations of the magnitude of 10% and 30% of the calibrated parameter values, the Morris sensitivity analysis produced prediction metrics enabling us to compare the simulated population after 18 h of sorafenib treatment. For p parameters, the elementary effects were taken into account by their sequential displacement on l level grid with r trajectories (here $p = 22, l = 10, r = 1000$) to identify the absolute mean tendency $\mu*$ and the interaction effect σ [Mor91, WFJ+14].

3.1.7 RNA interference

Silencer select validated siRNA directed against BRAF (reference 507) and CRAF (11749 and 11750), and Silencer negative control (am4635) were purchased from Applied Biosystems. Transfections were performed using the siPORT-neoFX reagent (Applied Biosystems) and Optimem transfection medium (Invitrogen), according to the manufacturer's instructions.

3.2 Results

3.2.1 Biological analysis of the activation status of the core components of the RAF-MEK-ERK cascade

In order to analyse the impact of sorafenib on the RAF-MEK-ERK cascade in HCC cells, three cell lines with different sensitivities to sorafenib were exposed to a clinically-relevant concentration of the drug ($10\mu M$) for 0, 4, 8 or 18 h. The human HCC cell line Huh7 was previously shown to be sensitive to sorafenib, while Hep3B and PLC/PRF5 cells were found to be resistant to sorafenib in terms of clonogenic growth [ELT+12]. For each cell line, complete cellular extracts were prepared and an immunoblot analysis was performed in order to determine the expression levels of the total and phosphorylated, i.e. activated version of each kinase of the cascade (Fig 3.1). The data expressed as a ratio of phosphorylated over total protein revealed that sorafenib was able to inhibit the RAF-MEK-ERK cascade, with differences in the kinetics and intensity between HCC cell lines. At 18 h, sorafenib was the most potent at inhibiting ERK phosphory- lation in Huh7 cells (an

average of 90% inhibition of the initial ratio of pERK/ERK), and the least potent in PLC/PRF5 cells (less than 30% inhibition) (Fig 3.1). Interestingly, differences in activation were noticed between the isoforms of RAF kinases. In all cells examined, the levels of pBRAF decreased upon sorafenib treatment. In contrast, the phosphorylation levels of CRAF increased gradually in all HCC cell lines exposed to sorafenib (Fig 3.1).

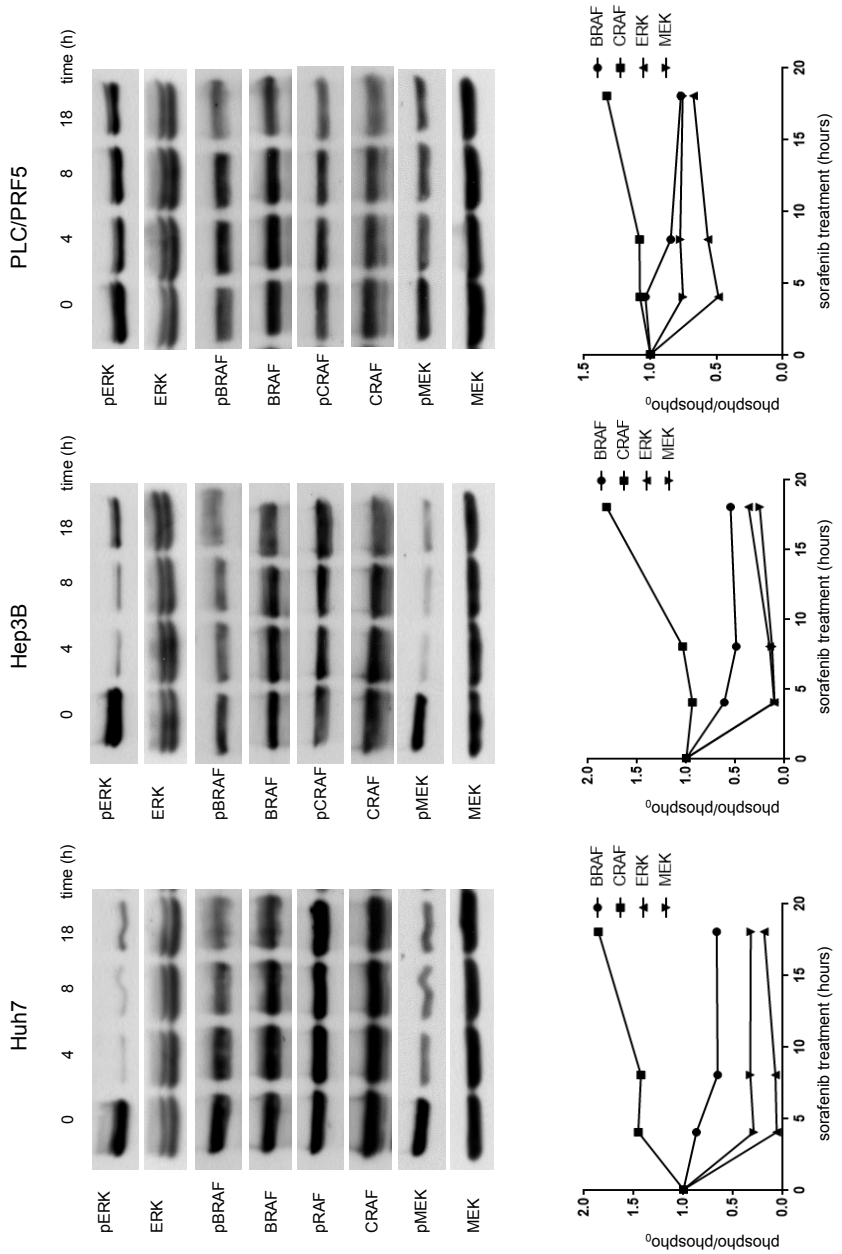

FIGURE 3.1 – Immunoblot analysis of the effect of sorafenib in three human HCC cell lines. Complete cellular extracts were prepared from Huh7, PLC/PRF5 and Hep3B cells exposed to sorafenib at a concentration of 10 mM for 4, 8, and 18 h. The corresponding extracts were analysed by immunoblotting in order to determine the expression levels of the total and phosphorylated (active) forms of BRAF, CRAF, MEK and ERK kinases. In the lower panels, the data are expressed as a ratio of phosphorylated over total protein, taking control conditions as reference.

3.2.2 Model resolution

In order to identify the reactions that were most likely to be biologically important, i.e. the biochemical reactions that best explained the variance of pERK/ERK, we performed a preliminary statistical analysis of the data using ANOVA and variation partitioning (Fig 3.2).

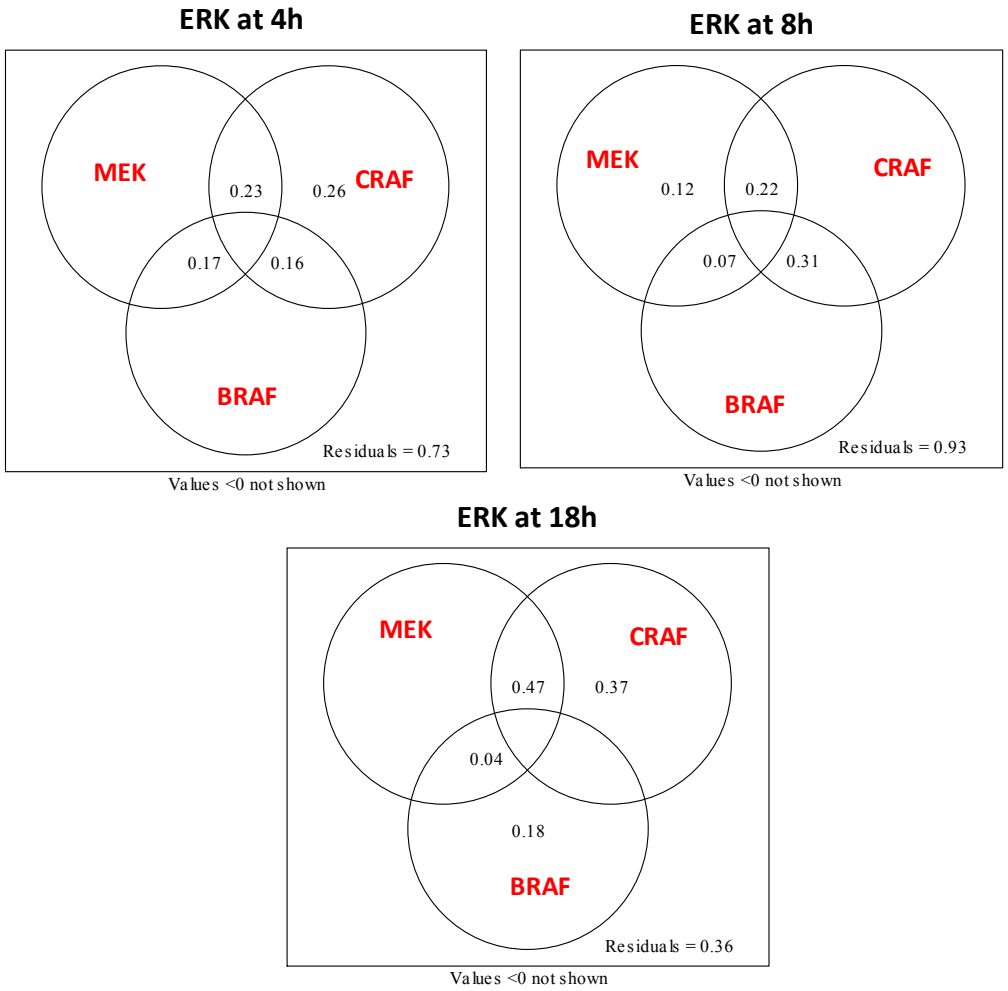

FIGURE 3.2 – The Varpart function in R allowed us to study the relationships between different variables of the RAF kinase system in HCC cells treated with sorafenib. The variables that best explain the variance of ERK were determined after 4 hours, 8 hours and 18 hours of sorafenib treatment.

Based on the ANOVA analysis performed on the pool of HCC cells, we have limited our model to the five relationships that appeared to be of the

greatest importance (Fig 3.3A). A mathematical model of the RAF-MEK-ERK cascade was constructed with four ODE that describe the enzymatic kinetics of each reaction identified as being important by variation partitioning.

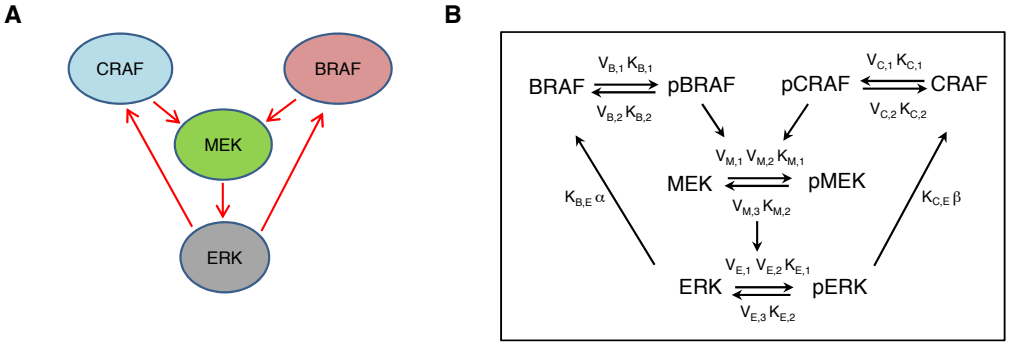

FIGURE 3.3 – Construction of the mathematical model based on ordinary differential equations for *in silico* analysis of RAF-MEK-ERK signalling in HCC cells. A : Schematic representation of the five main connections between the BRAF, CRAF, MEK and ERK variables. B : A summary of the parameters included in the model. The model presented is based on Michaelis-Menten kinetics. For each enzymatic reaction, the parameter $K_{.,.}$ represents the saturated maximal rate of the production or the disappearance of a protein, and the Michaelis constant, $V_{.,.}$ represents the amount of the substrate that produces a half maximal rate.

The model was constructed as described in the materials and methods section, and calibrated for each cell line (Fig 3.4B, Table 3.1). The objective function J computed with the COBYLA algorithm was 0.0122, 0.0646, and 0.0395 for Huh7, Hep3B and PLC/PRF5, respectively. Fig 3.4 shows the evolution of the ratio of phosphorylated vs total expression of BRAF, CRAF, MEK and ERK kinases with respect to time. Note that the values of $-\alpha$ and $-\beta$ are negative, revealing that ERK generates a negative feedback on the pathway. For Hep3b cells, an oscillatory behavior is observed. Such dynamic has been already exhibit by enzymatic systems with Michaelis-Menten kinetics [Gol13].

Parameter	Hep3B	Huh7	PLC/PRF5
Objective function	0.0646	0.0122	0.0395
VB,1	1.6359	1.8305	2.1129
KB,1	1.9986	0.0003	0.0000
KB,E	0.9041	0.5119	1.1427
α	3.993	2.7735	1.6772
VB,2	0.9934	1.7369	3.8387
KB,2	1.0285	0.4570	2.4085
VC,1	1.1444	0.9749	3.9179
KC,1	1.6678	0.0000	0.0112
KC,E	0.7108	0.7633	2.3959
β	4.0724	2.6917	7.8857
VC,2	0.5433	0.9961	0.3329
KC,2	1.7492	0.8771	0.0000
VM,1	0.3428	0.8056	2.9910
VM,2	4.6631	0.2087	0.9539
ṼM,2	-3.6631	0.7913	0.0461
KM,1	0.0012	5.1693	0.0137
VM,3	0.7719	3.0186	10.2080
KM,2	1.1731	0.3544	1.3918
VE,1	0	0.0002	0.0001
VE,2	0.9761	0.6542	0.0091
KE,1	4.171	3.7975	0.0029
VE,3	3.0767	0.8302	0.2687
KE,2	1.1768	0.3401	16.8468

TABLE 3.1 – Parameters calibrated for each cell line.

Remark 3.2 *Let us remind that the activation of MEK through the dimer pBRAFpCRAF is taken into account by the constant term* $V_{M,1}$*. Note that* $V_{M,1} = 0.3428$*,* $V_{M,2} = 4.6631$ *and* $\widetilde{V}_{M,2} = -3.6631$ *for the Hep3b cell line, which gives*

$$V_{M,1} + V_{M,2}[pBRAF] + \widetilde{V}_{M,2}[pCRAF] \geq 0.$$

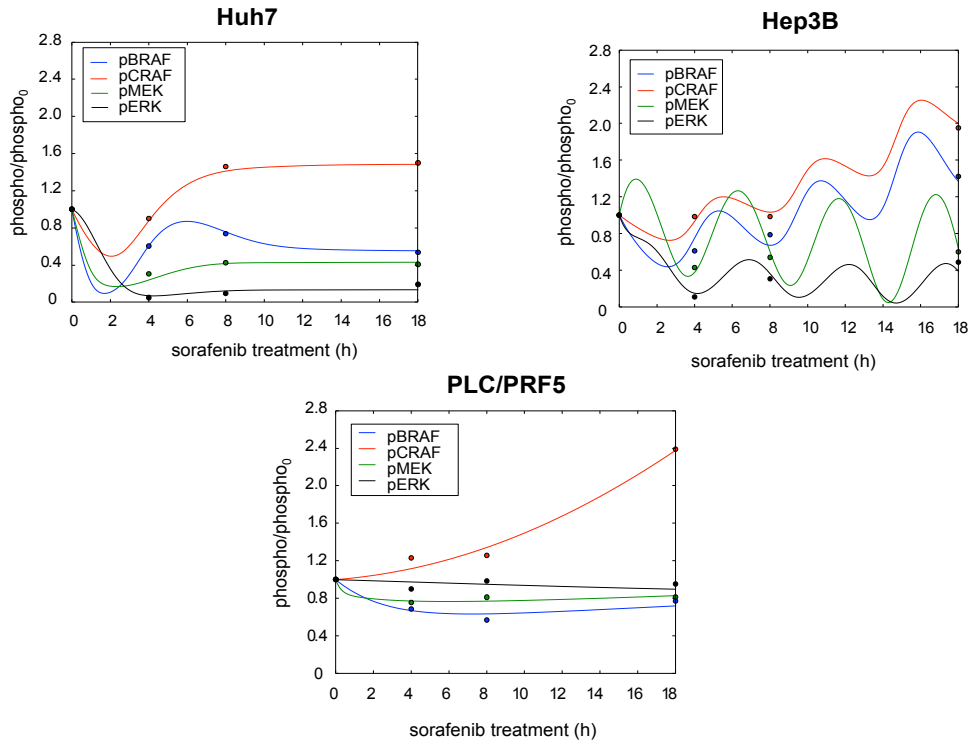

FIGURE 3.4 – Calibration of the mathematical model based on ordinary differential equations for *in silico* analysis of RAF-MEK-ERK signalling in HCC cells. Simulations were performed for the three HCC cell lines. The dots denote the experimental data.

Remark 3.3 *Note that the model of the Hep3b cell line shows enzymatic dynamics with an oscillatory behavior. This type of dynamic has already been observed in enzymatic systems with feedback regulations and in biological systems modeled by the Michaelis-Menten equations [BGLS06].*

3.2.3 Cell heterogeneity underlined by sensitivity analysis

In order to explore the regulation of the RAF-MEK-ERK pathway using our model, we performed a sensitivity analysis. The most influential parameters with respect to the absolute mean tendency μ^* and the standard deviation σ of the elementary effects are shown in Fig 3.5. The uppermost parameters, i.e. those with large σ values, are indicative of nonlinear and interaction effects, while the rightmost parameters, i.e. with large μ^* values, translate into linear and additive effects. All parameters are below the dashed line $\mu^* = 2\sigma/\sqrt{r}$, where $\sigma/\sqrt{r}$ denotes the standard error of the mean and r is the number of trajectories. This translates into a confidence interval of 95% [Mor91, WFJ+14]. The sensitivity analysis was performed taking the pERK/ERK ratio at 18 h as read-out. This analysis revealed great differences between the HCC cell lines in their regulation of the RAF-MEK- ERK cascade, both in terms of dynamics and the parameters involved. When perturbations of 10% were applied, no parameters appeared to have a significant impact in PLC/PRF5 cells. In Huh7 cells, the $V_{E,3}$ parameter that reflects the satured maximal rate of pERK disappearance, was identified as being important for the pERK/ERK output (Fig 3.5). In Hep3B cells, the parameters $V_{B,1}$ and $V_{B,2}$, reflecting the saturated maximal rates of the production and degradation of BRAF, respectively, were predicted to play a leading role in the regulation of ERK activation (Fig 3.5). When larger perturbations were applied, $V_{E,3}$ was identified as being influential in addition to $V_{B,1}$ and $V_{B,2}$ (Fig 3.5).

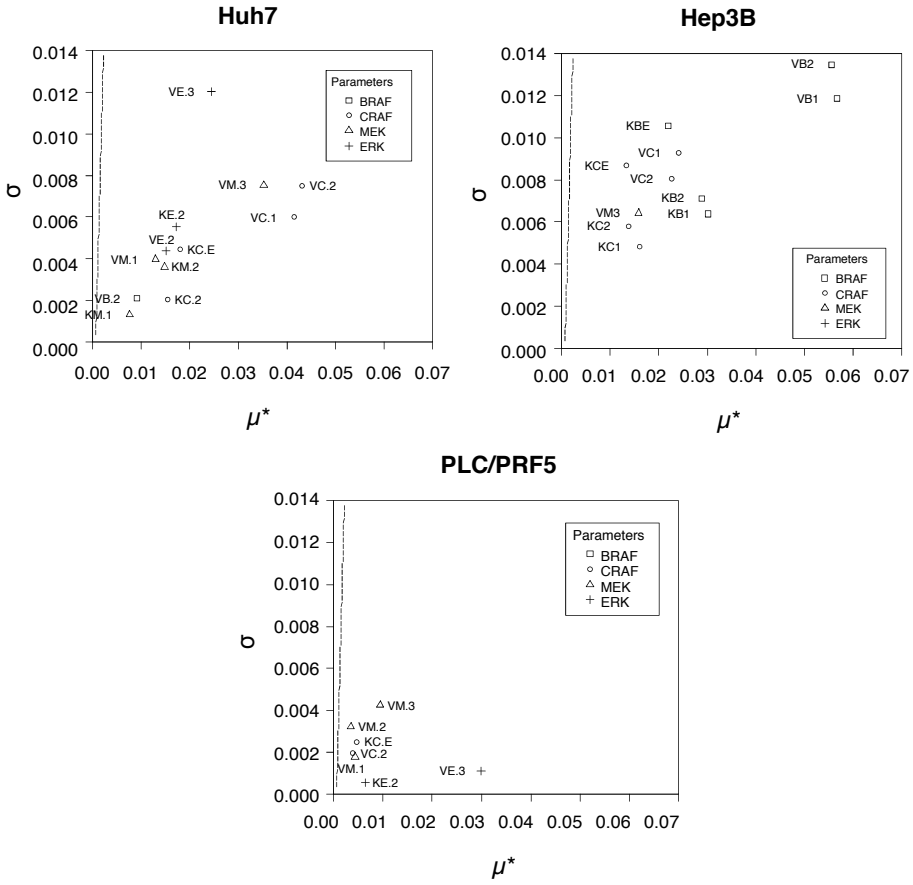

FIGURE 3.5 – Absolute mean value μ^* vs standard deviation σ of elementary effects. The graph presents the relative importance of each parameter used in the model, considering the pERK/ERK ratio at 18 h as read-out. Each parameter is characterized by two Morris indices, σ and μ^*, which represent the nonlinear effects or the interactions and the significance of the effects, respectively. The dashed line $\mu^* = 2\sigma/\sqrt{r}$, where $\sigma/\sqrt{r}$ denotes the standard error of the elementary effects mean, translates into a confidence interval of 95% over the parameter space.

3.2.4 *In silico* prediction of the impact of therapeutic targeting at different levels of the RAF-MEK-ERK cascade

We explored the impact of manipulations applied at each level of the RAF-MEK-ERK cascade in the three cell lines *in silico*. First, in order to address the activity of the RAF kinases, we analysed the effect of varying the parameter $V_{M,2}$, which reflects the kinase activity levels of both BRAF and CRAF toward MEK (Fig 3.6). The model predicted that $V_{M,2}$ has little impact on the ratio of pERK/ERK at 18 h, in all three cell lines (Fig 3.6). On the contrary, the model predicted that the parameters $V_{M,3}$ and $V_{E,3}$, which represent the disappearance rate of pMEK and pERK, respectively, were two key parameters that determine the response of HCC cells to sorafenib. A reduction of $V_{E,3}$ abolished the inhibitory effect of sorafenib on pERK/ERK levels in the two sorafenib-sensitive cell lines (Fig 3.6). This prediction suggested that the direct inhibition of either RAF kinase contributes only weakly to the control of pERK in HCC cells exposed to sorafenib. Instead, the results suggested that pERK disappearance, possibly reflecting its active dephosphorylation, was an essentiel step for the control of ERK signalling in HCC cells in this context.

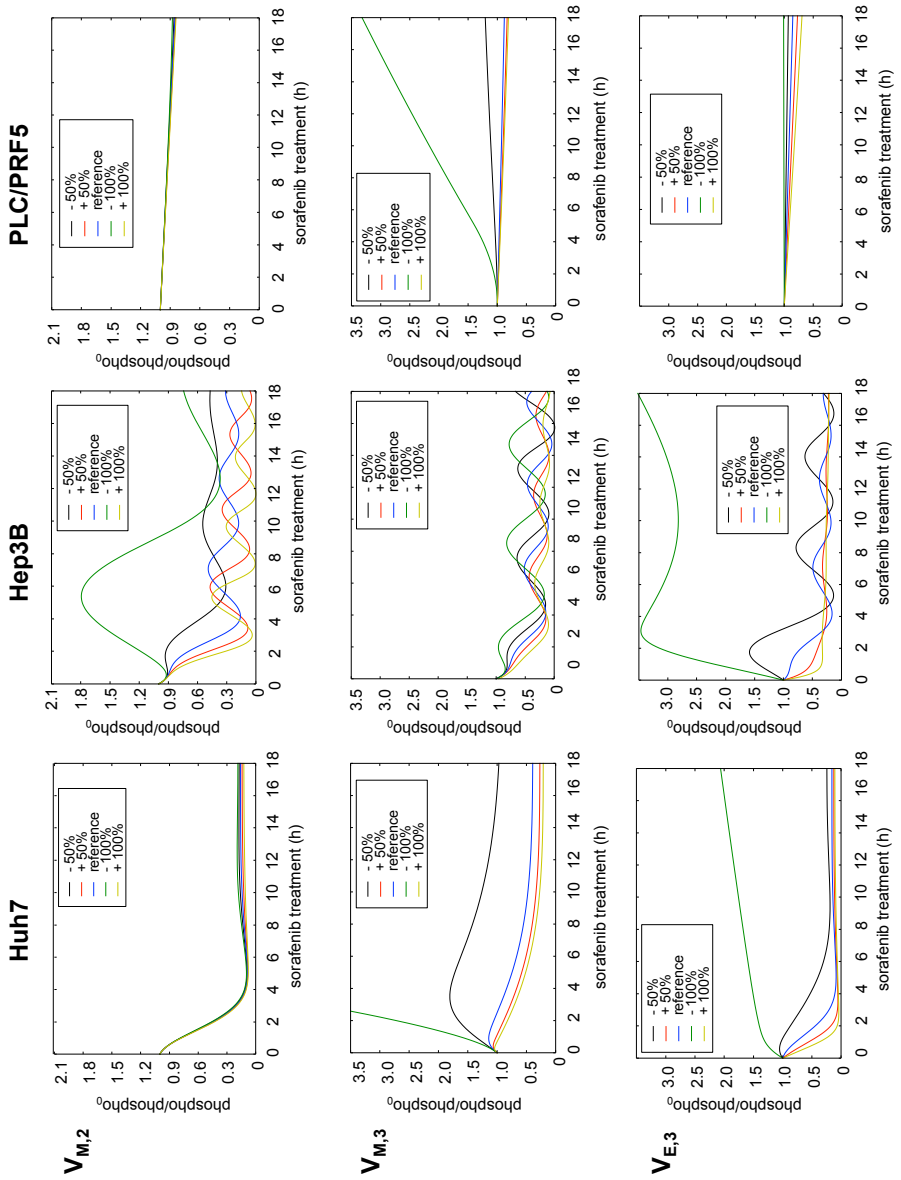

FIGURE 3.6 – Computational simulation of the effects of selected parameter variations on ERK activation. We present the numerical computations obtained by varying the parameters $V_{M,2}$ (representing the kinase activity of BRAF and CRAF toward MEK), $V_{M,3}$ (the rate at which pMEK disappears) and $V_{E,3}$ (the rate at which pERK disappears). In each case, the corresponding parameters were decreased or increased by 50% and 100% relative to the reference calibrated value (in blue).

3.2.5 Essential role of phosphatase activity in the inhibition of the RAF-MEK-ERK cascade by sorafenib in HCC cells

In order to challenge these predictions, we initially performed RNA interference directed against BRAF and CRAF in the Hep3B cell line. In agreement with the *in silico* prediction, a strong reduction in the expression of either RAF kinase isoform did not detectably change the pERK levels in Hep3B cells under basal conditions or upon application of sorafenib (Fig 3.7A and B). In order to address the second prediction, *i.e.* the importance of an active mechanism promoting the loss of pERK in cells exposed to sorafenib, we experimentally analysed the effect of sorafenib under pharmacological inhibition of cellular phosphatases. We used okadaic acid (OA), a cell-permeable, broad spectrum inhibitor of protein phosphatases of the PP2A family [CE04]. We also tested the possible contribution of phosphatases of the DUSP (Dual-specificity phosphatases) family, a family of phosphatases with distinct substrate preferences for specific MAPKs. We used the chemical inhibitor BCI, directed against the two isoforms of DUSP (DUSP1/6) known to be active on pERK [MVB+09]. Huh7 and Hep3B cells were preincubated with pharmacologically-active concentrations of both inhibitors (Fig 3.7C). Both inhibitors induced significant cell toxicity in HCC cells upon long exposure, either alone or in association with sorafenib. In order to minimize possible secondary interferences and the possibility of observing non-specific events, sorafenib was applied to HCC cells for up to 8 h, and an immunoblot analysis was performed in order to examine the levels of pMEK and pERK. In striking agreement with the *in silico* predictions, we observed that both phosphatase inhibitors abolished the ability of sorafenib to control ERK phosphorylation in Huh7 and Hep3B cells (Fig 3.7C). Interestingly however, OA was slightly less efficacious than BCI in preventing the disappearance of pERK levels induced by sorafenib, especially at the early time points following sorafenib application. OA prevented the inhibitory effects of sorafenib on pMEK and pERK equally, whereas BCI strictly prevented the effects of sorafenib on pERK (Fig 3.7C). Protein levels of the protein phosphatase DUSP1 remained stable during this window of time. Based on these experimental observations, we concluded that :
i) our mathematical model accurately predicted the effects of therapeutic manoeuvering of the RAF-MEK- ERK cascade ; ii) the activity of MEK and ERK phosphatases is an essential condition for a robust inhibition of the RAF-MEK-ERK cascade by sorafenib in HCC cells.

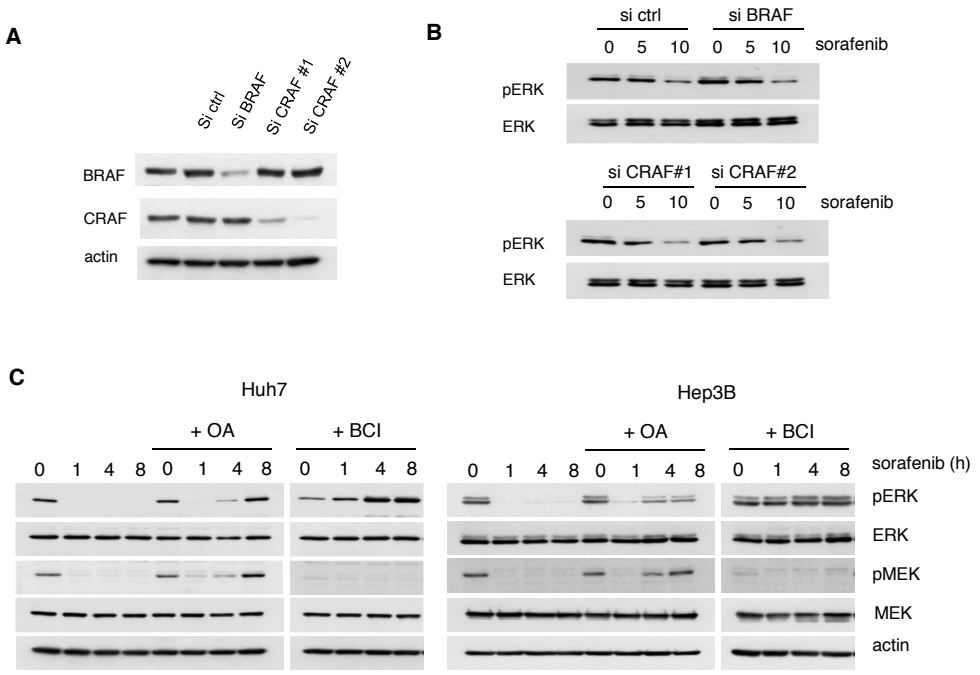

FIGURE 3.7 – Cellular phosphatase activity is essential for the inhibition of pERK by sorafenib in sensitive HCC cells. A : The expression levels of individual isoforms of the RAF kinases were analysed in Hep3B cells transfected with control siRNA vs siRNA directed against BRAF or CRAF. B : An immunoblot analysis of ERK activation in Hep3B cells transfected with siRNA directed against BRAF or CRAF and exposed to the indicated concentrations of sorafenib (5 or 10 μM) for 18 h. C : immunoblot analysis of ERK and MEK activation in Huh7 and Hep3B cells preincubated for 30 min with the phosphatase inhibitors okadaic acid (100 μM) or BCI (10 μM), before the application of sorafenib (10 μM) for the indicated time period.

3.3 Discussion

In the present study, we explored the regulation of the RAF- MEK-ERK cascade in HCC cells upon exposure to sorafenib, the medical treatment of reference for this type of tumour, using a mathematical modelling approach. Mathematical modelling based on ODE is well-suited for exploring the dynamics of oncogenic signalling at the system level, predicting the response of cancer cells to drugs, and ultimately, for the design of rationally improved therapeutic strategies [KHGK15]. Two important predictions made by the model were experimentally validated : i) HCC cells exposed to sorafenib demonstrate marked heterogeneity in terms of regulation of the RAF-MEK-ERK cascade in the therapeutic context ; ii) Cellular phosphatases play an essential role in the inhibition of RAF-MEK- ERK signalling by sorafenib in HCC cells. The observation that HCC cells show marked heterogeneity in their response to sorafenib is not surprising, considering previous reports that found variable effects of sorafenib on pERK expression levels in HCC cells and tissues in culture [ELT+12, TCM+15, BMU+14, GDE+13, LSZ+16]. In the present report, we were able to tie this variability to differences in the intrinsic control of the RAF-MEK-ERK cascade among HCC cells. Our sensitivity analysis revealed that the signalling nodes, i.e. the most important points of control for the regulation of ERK signalling, were different for each HCC cell line. At this stage however, the biological basis for these differences remains unknown. More work is required to understand the distinct regulation that applies to the core components of the RAF-MEK-ERK cascade in different HCC cells exposed to sorafenib. Strikingly, our findings indicate that cellular phosphatases are essential for a robust inhibition of the RAF-MEK-ERK cascade by sorafenib in HCC cells. In the two cell lines, Huh7 and Hep3B, in which sorafenib inhibited pERK signalling, pharmacological inhibition of phosphatases prevented the effects of sorafenib. The present findings might at first appear surprising, considering that sorafenib was initially developed and is presumed to be a kinase inhibitor. However, several recent reports have shown that some cellular effects of sorafenib depend on active cellular phosphatases. Sorafenib was for example found to inhibit the transcription factor STAT3 (Signal Transducer and Activator of Transcription factor 3) in HCC cells via the activity of the phosphatase SHP-1 (SH2 domain- containing phosphatase 1), a member of the family of non-receptor protein tyrosine phosphatases [CLTea09, TSC+14, SSJ+15, WYS+15, FST+15, CTH+16]. More recently sorafenib was also shown to directly activate Protein Tyrosine Phosphatase 1B (PTP1B) in this contex [TCC+16]. Based on these studies and ours, we propose that intracellular phosphatases should be explored further as targets of sorafenib in HCC. Our pharmacological observations suggest

that protein Ser/Thrphosphatases of the PP2A family and phosphatases of the DUSP1/6 family both contribute to the inhibitory effect of sorafenib on ERK signalling. Nevertheless, we observed differences between the effects of these inhibitors in the different HCC cell lines studied. Indeed, OA essentially prevented the disappearance of pMEK, while BCI strictly exerted its inhibitory effect on pERK. This observation is in agreement with the reported ability of PP2A to mainly target pMEK, while the activity of DUSP1/6 is restricted to pERK [JLW08]. Furthermore, we found that OA displayed a somewhat weaker and delayed efficacy compared to BCI. Based on these observations, we suggest that phosphatases of the DUSP1/6 family might contribute first and most importantly to the inhibitory effect of sorafenib on ERK signalling. The precise respective contribution of each phosphatase in this context nevertheless still remains to be determined. Finally, these findings offer new perspectives for clinical developments. Recent studies point to phosphatases as potential regulators of HCC progression and patient prognosis [HCC+16, CPM+08]. The protein phosphatase DUSP1 is of particular importance in the context of human hepatocarcinogenesis, since decreased protein levels of DUSP1 were reported in a subset of HCC with poor prognosis [CPM+08]. The activity of ERK kinases itself regulates the ubiquitin-dependent turn-over of DUSP1 at the protein level, thereby partially accounting for the downregulation of DUSP1 protein levels in this subset of tumours [CPM+08]. Therefore, the phosphatase activity of DUSP1 is a key element in the restriction of the activity of ERK kinases in HCC [CPM+08]. Identification of new biomarkers based on protein phosphatases reflecting the activity of protein phosphatases that would predict the efficacy of sorafenib in individual patients is a promising lead for future developments, considering the need to personalize the medical treatment of individual HCC tumours [GCB14]. Ultimately, a better understanding of protein phosphatase regulation could also assist in the conception of new therapeutic strategies for improved treatment of HCC.

References

[AB15] M. Avila and C. Berasain, *Making sorafenib irresistible : in vivo screening for mechanisms of therapy resistance in hepatocellular carcinoma hits on Mapk14*, Hepatology **61** (2015), 1755–1757.

[BF00] F.A. Brightman and D.A. Fell, *Differential feedback regulation of the MAPK cascade underlies the quantitative differences in EGF and NGF signalling in PC12 cells*, FEBS Lett. **482** (2000), 169–174.

[BMU+14] C. Breunig, B. J. Mueller, L. Umansky, K. Wahl, K. Hoffmann, and F. Lehner et al., *BRaf and MEK inhibitors differentially regulate cell fate and microenvironment in human hepatocellular carcinoma*, Clin. Cancer Res. **20** (2014), 2410–2423.

[CCS07] F. Campolongo, J. Cariboni, and A. Saltelli, *An effective screening design for sensitivity analysis of large models*, Environ. Model Softw. **22** (2007), 1509–1518.

[CE04] K. Chatfield and A. Eastman, *Inhibitors of protein phosphatases 1 and 2A differentially prevent intrinsic and extrinsic apoptosis pathways*, Biochem. Biophys. Res. Commun. **323** (2004), 1313–1320.

[CEP+06] J. Castillo, E. Erroba, M.J. Perugorría, M. Santamaría, D.C. Lee, and J. Prieto et al., *Amphiregulin contributes to the transformed phenotype of human hepatocellular carcinoma cells*, Cancer Res. **66** (2006), 6129–6138.

[CHMea16] C.V. Chatelle, D. Hövermann, A. Müller, and H.J. Wagner et al., *Optogenetically controlled RAF to characterize BRAF and CRAF protein kinase inhibitors*, Scientific Reports **6** (2016), 23713.

[CLTea09] K.F. Chen, T.H. Liu, W.T. Tai, and P.J. Chen et al., *1027 Sorafenib overcomes TRAIL resistance of hepatocellular carcinoma cells through the inhibition of signal transducers and activators of transcription 3*, Ejc Supplements - EJC SUPPL **7** (2009), 95–95.

[CPM+08] D.F. Calvisi, F. Pinna, F. Meloni, S. Ladu, R. Pellegrino, M. Sini, and et al., *Dual-specificity phosphatase 1 ubiquitination in extracellular signal-regulated kinase-mediated control of growth in human hepatocellular carcinoma*, Cancer Res. **68** (2008), 4192–4200.

[CTH+16] T.I. Chao, W.T. Tai, M.H. Hung, M.H. Tsai, M.H. Chen, and M.J. Chang et al., *A combination of sorafenib and SC-43 is a synergistic SHP-1 agonist duo to advance hepatocellular carcinoma therapy*, Cancer Lett. **371** (2016), 205–213.

[DHH+11] M.I. Davis, J.P. Hunt, S. Herrgard, P. Ciceri, L.M. Wodicka, and G. Pallares et al., *Comprehensive analysis of kinase inhibitor selectivity*, Nat. Biotechnol. **29** (2011), 1046–1051.

[DHRK07] A.S. Dhillon, S. Hagan, O. Rath, and W. Kolch, *MAP kinase signalling pathways in cancer*, Oncogene **26** (2007), 3279–3290.

[DS15] B. Delire and P. Stärkel, *The Ras/MAPK pathway and hepatocarcinoma : pathogenesis and therapeutic implications*, Eur. J. Clin. Invest **45** (2015), 609–623.

[ELT+12] Z. Ezzoukhry, C. Louandre, E. Trécherel, C. Godin, B. Chauffert, and S. Dupont et al., *EGFR activation is a potential determinant of primary resistance of hepatocellular carcinoma cells to sorafenib*, Int. J. Cancer **131** (2012), 2961–2969.

[FST+15] L.C. Fan, C.W. Shiau, W.T. Tai, M.H. Hung, P.Y. Chu, and F.S. Hsieh et al., *SHP-1 is a negative regulator of epithelial-mesenchymal transition in hepatocellular carcinoma*, Oncogene **34** (2015), 5252–5263.

[GCB14] A. Galmiche, B. Chauffert, and J.C. Barbare, *New biological perspectives for the improvement of the efficacy of sorafenib in hepatocellular carcinoma*, Cancer Lett. **346** (2014), 159–162.

[GDE+13] C. Godin, S. Dupont, Z. Ezzoukhry, C. Louandre, D. Chatelain, and L. Henaut et al., *Heterogeneous sensitivity of hepatocellular carcinoma to sorafenib revealed by the short-term culture of tumor fragments*, Anticancer Res. **33** (2013), 1415–1420.

[GFS+08] A. Galmiche, J. Fueller, A. Santel, G. Krohne, I. Wittig, and A. Doye et al., *Isoform-specific interaction of C-RAF with mitochondria*, J. Biol. Chem. **283** (2008), 14857–14866.

[Gol13] A. Goldbeter, *Oscillatory enzyme reactions and Michaelis-Menten kinetics*, FEBS letters **587** (2013), 2778–2784.

[HCC+16] M.H. Hung, Y.L. Chen, P.Y. Chu, C.T. Shih, H.C. Yu, and W.T. Tai et al., *Upregulation of the oncoprotein SET determines poor clinical outcomes in hepatocellular carcinoma and shows therapeutic potential*, Oncogene **35** (2016), 4891–4902.

[HGB+16] A. Houessinon, A. Gicquel, F. Bochereau, C. Louandre, R. Nyga, and C. Godin et al., *Alpha-fetoprotein is a biomarker of unfolded protein response and altered proteostasis in hepatocellular carcinoma cells exposed to sorafenib*, Cancer Lett. **370** (2016), 242–249.

[HYBea10] G. Hartzivassiliou, I. Yen, B.J. Brandhuber, and D.J. Anderson et al., *RAF inhibitors prime wild-type RAF to activate the MAPK pathway and enhance growth*, Nature **464** (2010), 431–435.

[JLW08] M.R. Junttila, S.P. Li, and J. Westermarck, *Phosphatase-mediated crosstalk between MAPK signaling pathways in the regulation of cell survival*, FASEB J. **22** (2008), 954–965.

[KHGK15] W. Kolch, M. Halasz, M. Granovskaya, and B.N. Kholodenko, *The dynamic control of signal transduction networks in cancer cells*, Nat. Rev. Cancer **15** (2015), 515–527.

[LSZ+16] J. Li, L. Shi, X. Zhang, B. Sun, Y. Yang, and N. Ge et al., *pERK/pAkt phenotyping in circulating tumor cells as a biomarker for sorafenib efficacy in patients with advanced hepatocellular carcinoma*, Oncotarget **7** (2016), 2646–2659.

[LT15] H. Lavoie and M. Therrien, *Regulation of RAF protein kinases in ERK signalling*, Nat. Rev. Mol. Cell Biol. **16** (2015), 281–298.

[MBS16] R. Mandal, S. Becker, and K. Strebhardt, *Stamping out RAF and MEK1/2 to inhibit the ERK1/2 pathway : an emerging threat to anticancer therapy,*, Oncogene **35** (2016), 2547–2561.

[Mor91] M.D. Morris, *Factorial sampling plans for preliminary computational experiments*, Technometrics **33** (1991), 161–174.

[MVB+09] A. Molina, A. Vogt, A. Bakan, W. Dai, P. Queiroz de Oliveira, and W. Znosko et al., *Zebrafish chemical screening reveals an inhibitor of Dusp6 that expands cardiac cell lineages,*, Nat. Chem. Biol. **5** (2009), 680–687.

[OSV+05] R.J. Orton, O.E. Sturm, V. Vyshemirsky, M. Calder, D.R. Gilbert, and W. Kolch, *Computational modelling of the receptor-tyrosine-kinase-activated MAPK pathway,*, Biochem. J. **392** (2005), 249–261.

[PNLDB06] P.R. Peres-Neto, P. Legendre, S. Dray, and D. Borcard, *Variation partitioning of species data matrices : estimation and comparison of fractions*, Ecology **87** (2006), 2614–2625.

[Pow94] M.J.D. Powell, *A direct search optimization method that models the objective and constrained fractions by linear interpolation*, in : S. Gomez, J.-P. Hennart (Eds.), Advances in Optimization and Numerical Analyses, Kluwer Academic, Dordrecht (1994), 51–67.

[PWP+14] S. Peng, Y. Wang, H. Peng, D. Chen, S. Shen, and B. Peng et al., *Autocrine vascular endothelial growth factor signaling promotes cell proliferation and modulates sorafenib treatment efficacy in hepatocellular carcinoma*, Hepatology **60** (2014), 1264–1277.

[RDL+14] R. Rudalska, D. Dauch, T. Longerich, K. McJunkin, T. Wuestefeld, and T.W. Kang et al., *In vivo RNAi screening identifies a mechanism of sorafenib resistance in liver cancer*, Nat. Med. **20** (2014), 1138–1146.

[SEJGM02] B. Schoeberl, C. Eichler-Jonsson, E.D. Gilles, and G. Muller, *Computational modeling of the dynamics of the MAP kinase cascade activated by surface and internalized EGF receptors*, Nat. Biotechnol. **20** (2002), 370–375.

[SOG+10] O.E. Sturm, R. Orton, J. Grindlay, M. Birtwistle, V. Vyshemirsky, and D. Gilbert et al., *The mammalian MAPK/ERK pathway exhibits properties of a negative feedback amplifier*, Sci. Signal **3** (2010), ra90.

[SRC+09] S.Y. Shin, O. Rath, S.M. Choo, F. Fee, B. McFerran, and W. Kolch et al., *Positive- and negative-feedback regulations coordinate the dynamic behavior of the Ras-Raf-MEK-ERK signal transduction pathway*, J. Cell Sci. **122** (2009), 425–435.

[SSJ+15] T.H. Su, C.W. Shiau, P. Jao, C.H. Liu, C.J. Liu, and W.T. Tai et al., *Sorafenib and its derivative SC-1 exhibit antifibrotic effects through signal transducer and activator of transcription 3 inhibition*, Proc. Natl. Acad. Sci. U. S. A. **112** (2015), 7243–7248.

[TCC+16] W.T. Tai, Y.L. Chen, P.Y. Chu, L.J. Chen, M.H. Hung, and C.W. Shiau et al., *Protein tyrosine phosphatase 1B dephosphorylates PITX1 and regulates p120RasGAP in hepatocellular carcinoma*, Hepatology **63** (2016), 1528–1543.

[TCM+15] V. Tovar, H. Cornella, A. Moeini, S. Vidal, Y. Hoshida, and D. Sia et al., *Tumour initiating cells and IGF/FGF signalling contribute to sorafenib resistance in hepatocellular carcinoma*, Gut (2015), pii : gutjnl–2015–309501. [Epub ahead of print].

[TSC+14] W.T. Tai, C.W. Shiau, P.J. Chen, P.Y. Chu, H.P. Huang, and C.Y. Liu et al., *Discovery of novel src homology region 2 domain-containing phosphatase 1 agonists from sorafenib for the treatment of hepatocellular carcinoma*, Hepatology **59** (2014), 190–201.

[WCT+04] S.M. Wilhelm, C. Carter, L. Tang, D. Wilkie, A. McNabola, and H. Rong et al., *BAY 43-9006 exhibits broad spectrum oral antitumor activity and targets the RAF/MEK/ERK pathway and receptor tyrosine kinase involved in tumor progression and angiogenesis*, Cancer Res. **64** (2004), 7099–7109.

[WFJ+14] H.M. Wainwright, S. Finsterle, Y. Jung, Q. Zhou, and J.T. Birkholzer, *Making sense of global sensitivity analyses*, Comput. Geosci. **65** (2014), 84–94.

[WKM04] C. Wellbrock, M. Kasarides, and R. Marais, *The RAF proteins take centre stage*, Nat. Rev. Mol. Cell Biol. **5** (2004), 875–885.

[WYS+15] S.H. Wang, S.H. Yeh, C.W. Shiau, K.F. Chen, W.H. Lin, and T.F. Tsai et al., *Sorafenib action in hepatitis B virus X-activated oncogenic androgen pathway in liver through SHP-1*, J. Natl. Cancer Inst. 1 **7** (2015), djv190.

[YHT+12] P. Yi, A. Higa, S. Taouji, M.G. Bexiga, E. Marza, and D. Arma et al., *Sorafenib-mediated targeting of the AAA^+ ATPase p97/VCP leads to disruption of the secretory pathway, endoplasmic reticulum stress, and hepatocellular cancer cell death*, Mol. Cancer Ther. **11** (2012), 2610–2620.

[ZRVNL15] J. Zucman-Rossi, A. Villanueva, J.C. Nault, and J.M. Llovet, *Genetic landscape and biomarkers of hepatocellular carcinoma*, Gastroenterology **149** (2015), 1226–1239.

Chapitre 4

La réponse hétérogène au sorafénib vue à travers différents mécanismes de résistance entre lignées

The heterogeneous response to sorafenib seen through different mechanisms of resistance between cell lines

Hepatocellular carcinoma (HCC), the most frequent form of primary liver tumor, is medically challenging. It represents one of the solid tumours for which physicians have the fewest therapeutic options available. Since its introduction and the results of the pivotal SHARP trial published in 2008, sorafenib has remained the cornerstone of the medical treatment of advanced stages of HCC. It is currently proposed as a first line treatment for advanced stages of HCC, due to its proven ability to increase overall survival of HCC patients in this setting. Its efficacy is nevertheless limited, due to the development of resistance [BMea14, ELea12, GDea13, RDea14].

Sorafenib is a broad spectrum kinase inhibitor active on RAF kinases and a handful of Receptor Tyrosine Kinases (RTK). Therefore, much emphasis has been put on exploring the control of the cancer cell kinome as the basis of its anti-oncogenic efficacy. As a consequence of this mode of action, sorafenib is able to inhibit the oncogenic kinase cascade RAF-MEK-ERK [GCB14, WCea04]. Results obtained over the past decades support the essential role of this cascade in the efficacy of HCC. Inter alia, activated Epidermal Growth Factor Receptor (EGFR) is able to promote the resistance of HCC cell lines and tumours to sorafenib [ELea12, GDea13]. Other RTKs such as the Insulin Receptor (IR) suggest the need to robustly control the oncogenic kinases to achieve therapeutic efficacy in HCC. Although targeting the RTK-ERK cascade in HCC may appear as a simple task, the existence of complex wiring in oncogenic transduction pathways, with multiple feedback loops and redundancies constitutes a huge obstacle to therapeutic efficacy.

Mathematical modelling offers the opportunity to address the regulation of the oncogenic signalling [KHGK15, OSea05, SGea17, SEJGM02, SRea09].

We have recently applied mathematical modelling based on nonlinear ordinary differential equations (ODE) to address the regulation of the RAF-MEK-ERK cascade in HCC cells exposed to sorafenib [SGea17]. Based on the principles of Michaelis-Menten enzyme kinetics, it was possible to show the essential role of phosphatases as key regulators of ERK and MEK activation upon HCC exposure to sorafenib. Interestingly, the study pointed to hitherto unsuspected actors involved in ERK regulation under sorafenib in HCC cells. It also unveiled the power of mathematical modelling for the exploration of the regulation of oncogenic signalling in the therapeutic setting. In the present study, we decided extend the mathematical model of the RAF-MEK-ERK kinase cascade in HCC. We focused this time on exploring the resistance of HCC to sorafenib taking into account the main RTKs engaged in HCC cells.

4.1 Materials and methods

4.1.1 Cell culture

The HCC cell lines used in this study (Hep3B, and PLC/PRF5) were obtained from ATCC and were authenticated using profiling of short tandem repeats at 16 loci (LGC Standards, Strasbourg, France). Cells were cultured in Dulbecco Modified Eagle's Medium (DMEM) supplemented with 10% fetal calf serum (Jacques Boy), 2 mM glutamine, 100 g/mL penicillin and streptomycin. Antibodies & reagents. Sorafenib, erlotinib, linsitinib and trametinib were purchased from Selleck chemicals and kept as 10 mM stock in DMSO at -20°C. All primary antibodies were from Cell signalling. The anti-rabbit IgG-HRP was from GE Healthcare. The ECL reaction was used for revelation. Western blots were scanned and quantified using the software ImageJ (NIH).

4.1.2 Variance analysis

The biological data related to the tyrosine kinase receptor (RTK) were analyzed in order to select the most relevant components in the ERK signalling. The activity of 20 tyrosine kinase receptors (RTK) were measured by RTK array as presented in Fig. 4.1A. The undetectable data were not taken into account in the modelling because of no substantial activity. Thanks to a variance analysis in each cell line [PNLDB06], 3 over the remaining 7, namely EGFR, IR and IGF1-R, were identified as the most contributor to the ERK activity. We present in Fig. 4.1B the quantification of the EGFR, IR and

IGF1-R activity, the three RTK selected, for each cell line. The data related to RAS pull-down is also added.

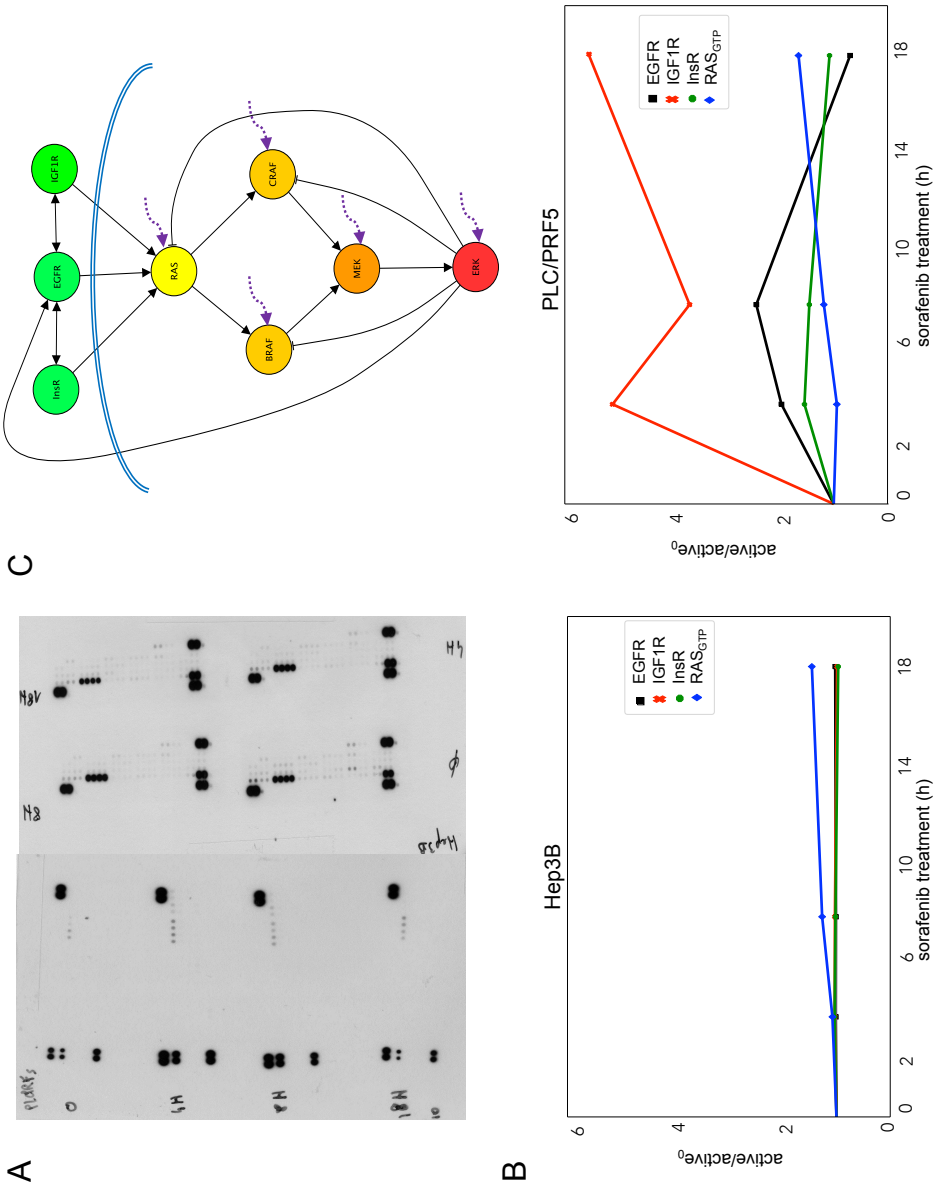

FIGURE 4.1 – A- Detection results of the RTK and RAS activations obtained by RTK array and by pull-down assay respectively. The expression level of 20 receptor tyrosine kinases were revealed at 4, 8 and 18h after sorafenib exposure. B- Quantification of the three selected RTK (EGFR, IGF1R, IR) and the RAS protein after sorafenib treatment for each cell line. C- Schematic representation of the biochemical interactions considered in the RAS-RAF-MEK-ERK pathway model.

4.1.3 Model of the RAS-RAF-MEK-ERK signalling

Based on the previous analysis the three tyrosine kinase receptors, EGFR, IR and IGF1-R are included in the ERK signalling model as well as the RAS protein and the downstream RAS-MEK-ERK pathway. In order to build the mathematical equations, we exhibit the interactions between the components considered in the modelling. An illustration is given in the Fig. 4.1C. The tyrosine kinase receptors activation leads to receptor autophosphorylation, propagation signalling by stimulating proteins and receptor degradation. EGFR is involved in an autocrine loop with positive feedback regulating the ERK pathway activity [SHea02]. To account this process in the model, the EGFR activation is proportional to the ERK phosphorylated concentration. Crosstalks between EGFR and the insulin family receptors, as well as between IGF1-R and IR, have been reported in the literature [DMBea09, RDea14]. The IGF1-R inhibition as a targeted therapy contributes to a resistance mechanism in the HCC by activating EGFR. It suggests that the insulin family receptors activation induces the EGFR degradation. Furthermore, the EGFR degradation by itself and by insulin family receptors arises from distinct processes. Thus, the interactions between IGF1-R, IR and EGFR are translated as competition-mutualism terms. The activate forms of IGF1-R, IR and EGFR are enable to stimulate the RAS protein by changing its binding GDP to GTP. The RAS activation is also controlled by a feedback loop from the phosphorylated form of ERK. Then, RASGTP activates the RAS-MEK-ERK downstream pathway. We refer to our previously a RAS-MEK-ERK pathway modelling for more details [SGea17]. We deal with two states for each component, activate form and inactivate form. The mass action law provides the dynamics of EGFR, IGF1-R, IR and RAS, while Michaelis-Menten kinetics described the enzymatic activity of BRAF, CRAF, MEK and ERK. The dynamic of the RAS-RAF-MEK-ERK pathway is governed by the following system of nonlinear ordinary differential equations :

$$
\begin{aligned}
\frac{d[EGFR]}{dt} &= [EGFR]\left(p_{e,1}[ERK] + p_{e,2}\right) \\
&\quad - [EGFR]\left(c_{e,1}[IR] + c_{e,2}[IGF1R]\right) - \left(b_{e,1}[IR] + b_{e,2}[IGF1R]\right), \\
\frac{d[IR]}{dt} &= p_{i,1}[IR] - [IR]\left(c_{i,1}[EGFR] + c_{i,2}[IGF1R]\right) \\
&\quad - \left(b_{i,1}[EGFR] + b_{i,2}[IGF1R]\right), \\
\frac{d[IGF1R]}{dt} &= p_{j,1}[IGF1R] - [IGF1R]\left(c_{j,1}[EGFR] + c_{j,2}[IR]\right) \\
&\quad - \left(b_{j,1}[EGFR] + b_{j,2}[IR]\right) \\
\frac{d[RAS_{GTP}]}{dt} &= \left(r_1[EGFR]^{r_2} + r_3[IR]^{r_4} + r_5[IGF1R]^{r_6} + r_7\right) \\
&\quad \left([RAS_{tot}] - [RAS_{GTP}]\right)\left(1 + \frac{[pERK]}{r_8}\right)^{r_9} \\
&\quad - r_{10}[RAS_{GTP}] \\
\frac{d[pBRAF]}{dt} &= \frac{\left(b_1 + b_2[RAS_{GTP}]\right)\left([BRAF_{tot}] - [pBRAF]\right)}{K_{B,1} + \left([BRAF_{tot}] - [pBRAF]\right)}\left(1 + \frac{[pERK]}{K_{B,E}}\right)^{-\alpha} \\
&\quad - \frac{V_{B,2}[pBRAF]}{K_{B,2} + [pBRAF]} \\
\frac{d[pCRAF]}{dt} &= \frac{\left(c_1 + c_2[RAS_{GTP}]\right)\left([CRAF_{tot}] - [pCRAF]\right)}{K_{C,1} + \left([CRAF_{tot}] - [pCRAF]\right)}\left(1 + \frac{[pERK]}{K_{C,E}}\right)^{-\beta} \\
&\quad - \frac{V_{C,2}[pCRAF]}{K_{C,2} + [pCRAF]} \\
\frac{d[pMEK]}{dt} &= \frac{\left(V_{M,1} + V_{M,2}[pBRAF] + \widetilde{V}_{M,2}[pCRAF]\right)\left([MEK_{tot}] - [pMEK]\right)}{K_{M,1} + \left([MEK_{tot}] - [pMEK]\right)} \\
&\quad - \frac{V_{M,3}[pMEK]}{K_{M,2} + [pMEK]} \\
\frac{d[pERK]}{dt} &= \frac{\left(V_{E,1} + V_{E,2}[pMEK]\right)\left([ERK_{tot}] - [pERK]\right)}{K_{E,1} + \left([ERK_{tot}] - [pERK]\right)} \\
&\quad - \frac{V_{E,3}[pERK]}{K_{E,2} + [pERK]}
\end{aligned}
$$

Here the amounts of the RTK active forms are denoted $[EGFR]$, $[IR]$, $[IGF1R]$, and the phosphorylated amount of the enzyme X is $[pX]$. The total amount of the enzyme X is denoted by $[Xtot]$. The parameters in blue are known as Michael-Menten kinetics rates and their values have been set from the RAF-MEK-ERK model in [SGea17]. Regarding the red parameters, the degradation of each receptor depends on a competition term and a regulation term involving EGFR, IR and IGF1R. The parameters b_1 and c_1 represent the contribution of external biological processes to the ERK pathway in the RAF kinases production. The part of the active RAS, RAS_{GTP}, in the RAF kinases production are controlled by the parameters b_2 and c_2 . All the red parameters values are unknown, and will be calibrated to identify key features

of the resistance mechanisms to sorafenib.

4.1.4 Parameters estimation and analysis

The general least square method constrained optimization by linear approximation (COBYLA) [Pow94] is performed to calibrate the values of the 22 unknown parameters. The aim is to minimize the difference between the experimental data ($x_{j,i}$) and the mathematical model output ($y_j(t_i, p)$) by considering the following objective function :

$$\sum_{i=1}^{M}\sum_{j=1}^{N}\frac{\left(y^j_{\text{exp}}(t_i) - y^j(t_i,p)\right)^2}{\sigma_{j,i}}$$

where M is the number of experimental data and N is the number of time points of each experimental data assuming that the experimental errors are independent and normally distributed with the standard deviation $\sigma_{i,j}$.
The Morris global sensitivity analysis [Mor91, CCS07, WFJ+12] is applied to adjust the model parameters values and to explore the influence of each parameter with respect to the ERK activity.

4.1.5 Optimization method to control the ERK phosphorylation

An optimization method to control the ERK phosphorylation is proposed in order to investigate the resistance mechanisms to sorafenib in the HCC. To identify the best combination of inhibitors in every steps of the RAS-RAF-MEK-ERK pathway, one aims at finding the therapeutic strategy that mostly reduces the ERK amount. The receptors inhibitors associated to EFGR, IR and IGF1-R, act on the production of these activated receptors, whereas for the remaining components of the pathway, the inhibitors can inhibit the protein phosphorylation and/or promote the protein dephosphorylation. Mathematical speaking, we define the control vector

$$u = (p_{e,1}, p_{i,1}, p_{j,1}, r_7, r_{10}, b_1, V_{B,2}, c_1, V_{C,2}, V_{M,1}, V_{M,3}),$$

which contains every feasible inhibitions with respect to the inhibitors and its action levels (Table 4.1). The optimization problem resides in finding the control u, such that the objective function

$$J = \int_0^T [pERK(t)]^2 dt$$

is minimized. Here $T = 18$ hours is the treatment duration. Positive constraint is required regarding $(r_7, r_{10}, b_1, V_{B,2}, c_1, V_{C,2}, V_{M,1}, V_{M,3})$. Sequential quadratic programming (SQP) [BGLS06] is performed.

Inhibitor	Target	Involved mechanisms	Associated parameters
Sorafenib	RAF	- phosphorylation + dephosphorylation	b_1, c_1 $V_{B,2}$, $V_{C,2}$
Erlotinib	EGFR	- production	$p_{e,1}$
Linsitinib	IGF1-R	- production	$p_{j,1}$
Trametinib	MEK	- phosphorylation + dephosphorylation	$V_{M,1}$ $V_{M,3}$

TABLE 4.1 – Inhibitors used for the pharmacological tests which its target and the associated model parameters.

4.2 Results

4.2.1 Model calibration

The mathematical model of the RAS-RAF-MEK-ERK pathway includes eight equations describing the dynamic evolution of each component amount after sorafenib treatment. The 22 parameters were adjusted on the experiment data. The remaining parameters values were obtained from the RAF-MEK-ERK pathway model in [SGea17] (see Table 4.2). The calibrated solution are presented in Fig. 4.2. The adjustment error was 0.077 and 0.069 for PLC/PFR5 and Hep3b respectively. Each curve depicts the dynamics of one pathway component, normalized as a ratio of activated/phosphorylated over the total protein concentration. The duration of sorafenib treatment efficiency is 18 hours in *in vitro* and *in silico* experiments. Parameter r_9 is positive which means that ERK is involved in a positive feedback loop at RAS level. These mechanisms balance the ERK-negative feedback loop ($-\alpha$ and $-\beta$ negative) at RAF level obtained in our previous modelling.

Parameter	Hep3B	PLC/PRF5	Parameter	Hep3B	PLC/PRF5
Objective function	0.0646	0.0395	b1	1.64E+00	2.11E+00
pe,1	1.73E-04	2.93E+00	b2	2.82E-05	1.43E-02
pe,2	-9.70E-05	-2.73E+00	KB,1	2.00E+00	0.00E+00
ce,1	0.00E+00	0.00E+00	KB,E	9.04E-01	1.14E+00
ce,2	0.00E+00	0.00E+00	α	3.99E+00	1.68E+00
be,1	-8.05E-05	-1.19E-03	KB,2	1.03E+00	2.41E+00
be,2	-6.76E-05	2.20E-03	c1	1.15E+00	3.92E+00
pi,1	1.75E-04	5.02E-02	c2	-2.43E-05	1.33E+00
ci,1	6.49E-05	1.90E-02	KC,1	1.67E+00	1.12E-02
ci,2	0.00E+00	0.00E+00	KC,E	7.11E-01	2.40E+00
bi,1	0.00E+00	0.00E+00	β	4.07E+00	7.89E+00
bi,2	0.00E+00	0.00E+00	KC,2	1.75E+00	0.00E+00
pj,1	-2.28E-03	1.42E+00	VM,1	3.43E-01	2.99E+00
cj,1	7.13E-05	7.11E-01	VM,2	4.66E+00	9.54E-01
cj,2	0.00E+00	0.00E+00	ṼM,2	-3.66E+00	4.61E-02
bj,1	0.00E+00	0.00E+00	KM,1	1.20E-03	1.37E-02
bj,2	0.00E+00	0.00E+00	VM,3	7.72E-01	1.02E+01
r1	-1.93E-03	7.49E-02	KM,2	1.17E+00	1.39E+00
r2	9.02E-05	4.53E-01	VE,1	0.00E+00	1.00E-04
r3	-1.48E-04	5.34E-01	VE,2	9.76E-01	9.10E-03
r4	3.13E-04	3.83E+00	KE,1	4.17E+00	2.90E-03
r5	3.98E-05	4.18E-01	VE,3	3.08E+00	2.69E-01
r6	-3.52E-05	2.79E-05	KE,2	1.18E+00	1.68E+01
r7	1.37E-04	2.68E-05			
r8	4.50E-05	1.06E-05			
r9	1.58E-04	4.08E-05			
r10	1.29E-04	2.26E+01			

TABLE 4.2 – Parameters calibrated for each cell line.

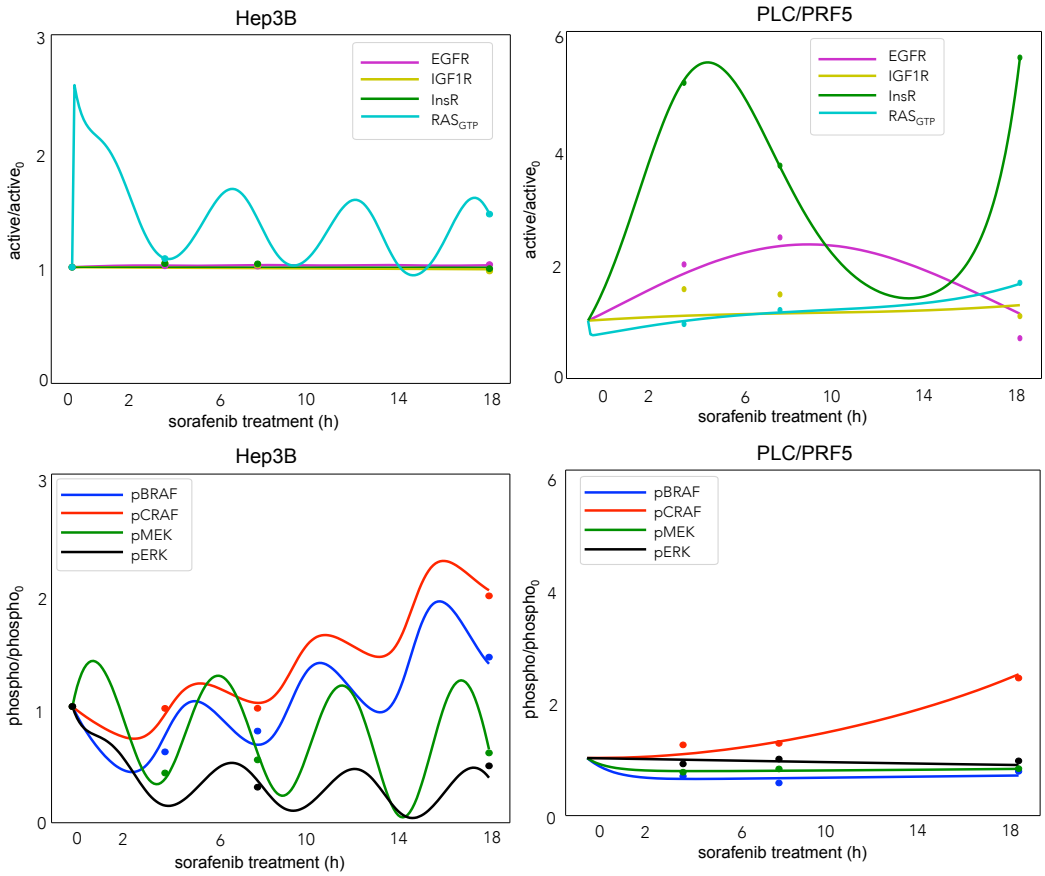

FIGURE 4.2 – Calibrated Hep3B and PLC cell lines solution. Experimental data are represented by the dots.

4.2.2 Global sensitivity analysis reveals different control mechanisms regulating the ERK phosphorylation between the PLC/PRF5 and Hep3b cell lines

Morris sensitivity analysis was applied to investigate the most influent parameters on the model output of interest, the phosphorylated ERK, after 18 hours of sorafenib treatment. As shown in Fig. 4.3, the analysis results highlight the ERK activation regarding the absolute mean tendency μ^* and the interaction effect σ. Concerning the PLC/PRF5 cell line, the pBRAF production parameter b_2, related to RAS activation, is the most influent on the ERK activity and interacts linearly with the ERK phosphorylation. The pERK dynamics is also driven by the nonlinear interactions of parameters $p_{e,1}$ and $p_{e,2}$, which govern the EGFR production and degradation respectively. Nevertheless, these effects are weak. About the Hep3b cell line, the pBRAF and pCRAF production parameters b_2 and c_2, related to the RAS activation, have the most impact and interact nonlinearly on the pERK evolution. Note that these parameters have a greater influence than in the PLC/PRF5 cell line. This study suggests that the ERK activity in the resistant cell line can be less controlled than the resilient cell line. This confirms the resistant profile of the PLC/PRF5 cell line to sorafenib and implies the existence of resistance mechanisms not explained by our modelling. However, we can expect a better understanding of the components involved in those processes.

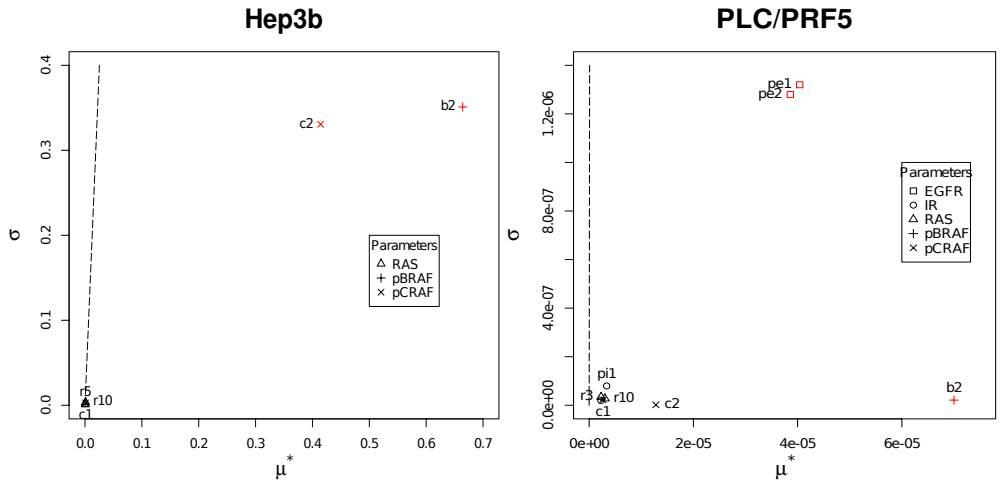

FIGURE 4.3 – Morris global sensitivity analysis expressed by the absolute mean tendency μ^* and the standard deviation σ. The first one provides a parameters ranking of their influence on the phosphorylated ERK amount after 18 hours of sorafenib exposure and the second one gives a quantification of the interactions and the nonlinear effects. The standard error of the mean of the elementary effects is illustrated by the dash line and gives a confidence interval for the parameters values.

Remark 4.1 *Sobol sensitivity analysis (Fig. 4.4) confirms the importance of pBRAF and pCRAF production parameters b_2 and c_2 related to the RAS activation for both cell lines. Two million sample were created.*

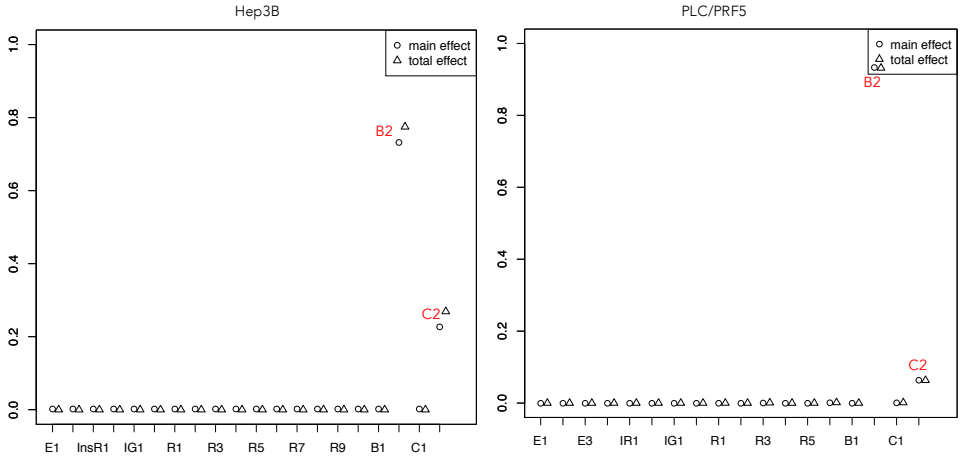

FIGURE 4.4 – Sobol sensitivity analysis expressed by the main and total effects.

4.2.3 Optimization results underlying the resistance mechanisms to sorafenib

In order to determine the best therapeutic strategy and to highlight possible mechanisms involved in the sorafenib resistance, we explored the possible inhibitions combinations inside the ERK pathway accounting for the EGFR, IFG1-R and IR. Optimal control achieved to find the best inhibition design to reduce the ERK activity (Table 4.3). The solution coming from the calibration of the *in vitro* experiments is used as the reference model. Figure 4 compares the phosphorylated ERK. To weaken the phosphorylated ERK concentration in the resistant cell lines PLC/PRF5, inhibition of pMEK is the only powerful lever. Nevertheless, the efficiency is quite relative, the normalized pERK concentration decreased from 0.876 to 0.764 (Fig. 4.5 and Table 4.3). Parameters $V_{M,1}$ and $V_{M,3}$ are related with the degradation and the dephosphorylation of MEK (Table 4.3). No effect on pBRAF and pCRAF are observed, which confirm resistant mechanisms to sorafenib. This suggests a use of trametinib which is an inhibitor of pERK. Regarding the resilient cell line Hep3b, the optimal control strategy is more efficient

regarding the phosphorylation of ERK. One notes that the phosphorylated ERK concentration declines from 0.390 to 0.006 (Fig. 4.5 and Table 4.3). The optimal control hints nonetheless that it is necessary to simultaneously bridle RAS_{GTP}, pBRAF and pMEK while EGFR is boosted. This advocates a combined use of sorafenib and trametinib.

Parameter	reference Hep3B	best inhibited Hep3B	reference PLC/PRF5	best inhibited PLC/PRF5
$p_{e,2}$ (EGFR)	-9.70E-05	-4.79E-06	-2.73E+00	-2.32E+00
$p_{i,1}$ (InsR)	6.49E-05	1.48E-04	1.90E-02	2.59E-02
$p_{j,1}$ (IGF1R)	7.13E-05	9.00E-04	7.11E-01	2.02E-01
r_{10} (RAS)	1.29E-04	**1.27E-02**	2.26E+01	5.47E+01
r_7 (RAS)	1.37E-04	3.42E-03	2.68E-05	9.00E-05
$V_{B,2}$ (BRAF)	9.93E-01	9.44E-01	3.84E+00	8.21E+00
b_1 (BRAF)	1.64E+00	**1.75E-01**	2.11E+00	6.44E+00
$V_{C,2}$ (CRAF)	5.43E-01	6.46E-01	3.33E-01	1.44E-01
c_1 (CRAF)	1.15E+00	**1.39E-01**	3.92E+00	6.30E+00
$V_{M,3}$ (MEK)	7.72E-01	**2.05E+00**	**1.02E+01**	**3.29E+02**
$V_{M,1}$ (MEK)	3.43E-01	7.71E-01	**2.99E+00**	**2.13E-06**
pERK after 18 hours	0.39	0.006	0.876	0.764

TABLE 4.3 – Comparison of parameter values between the reference solution and the optimal inhibition strategy for each cell line. The significant changes are highlighted in bold.

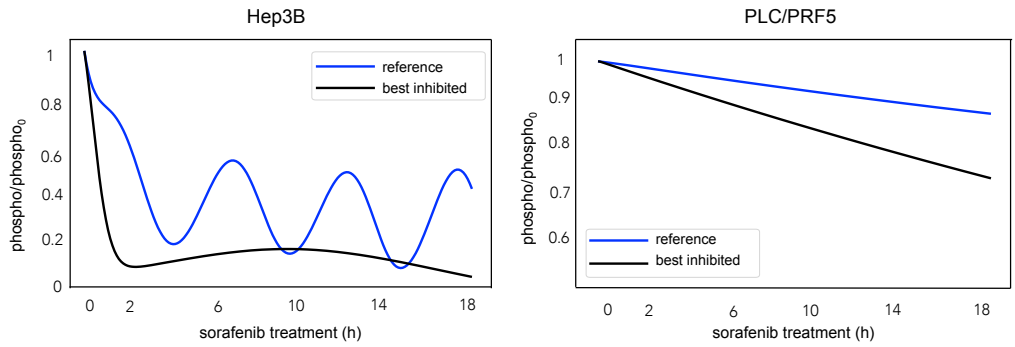

FIGURE 4.5 – Comparison of the pERK amount between the reference solution and the optimal design computed from the optimal control procedure.

4.3 Discussion

Therapeutic windows based on the dynamic resistances of the pERK regulation could be envisioned. To avoid an almost infinite number of available protocols, optimal control has been implemented. The results from this method were compared with *in vitro* experimentations thanks to four inhibitors of the ERK pathway : erlotinib as an inhibitor of EGFR, linsitinib for IGF1-R, sorafenib for the RAF kinases and trametinib for pMEK. Those inhibitors are estimated with respect to the phosphorylated ERK amount using assorted combinations for each cell line. As prescribed by the optimal control strategy, it can be observed that trametinib has a greater impact on the non phosphorylation of ERK than sorafenib for both cell lines (Fig. 4.6). Since the sorafenib makes a difference for the resilient cell line in early treatment, the pairing with trametinib is even more efficient. Furthermore, no visible effect of erlotinib is revealed relating to the pERK activation for both cell lines which is confirmed by [ZRea14]. This is underlined by the EGFR increasing provided by the optimal control. Those results indicate trametinib as a better therapeutic option in the HCC. This alternative therapy has been made in melanoma [SF13].

Our study clearly addressed a short part of the mechanisms leading to clinical failure. Nevertheless, combining the model with for example the pharmacokinetics and the pharmacodynamics of sorafenib and trametinib, could provide personalized mathematical models of tumours that could ultimately be helpful to instruct the therapeutic choices.
Our study unveils the rich array of the regulation and the versatility of the signal transduction. Because of the complexity, mathematical modelling was

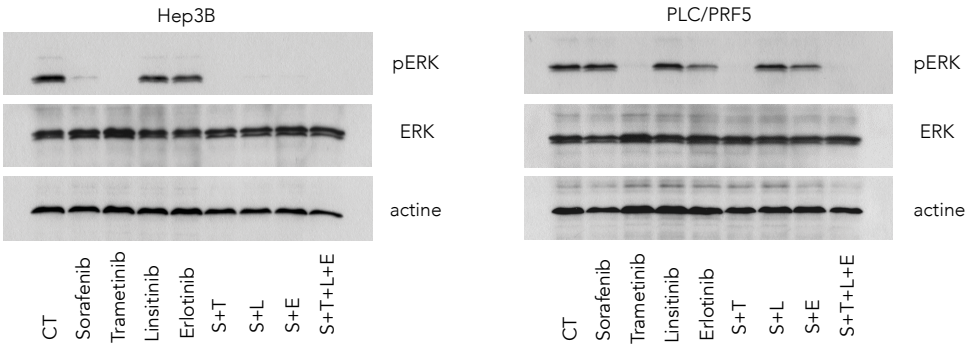

FIGURE 4.6 – Combinations of the pharmacological inhibitions to test the possible control of pERK.

the essential tool to exploit the temporal regulation of the oncogenic signalling in the resilient and the resistant cell lines (Hep3b and PLC/PRF5 respectively). According to the mathematical model, EGFR was activated as observed by [ELea12, NLea17]. Other synergies take place from simultaneous actions at different level of this cascade, which lead to the lack of the pERK inhibition [NLea17, ZZea17]. We noticed that the BRAF and MEK kinases are regulators of the sorafenib resistance for the resilient cell line, whereas MEK plays a major role in the resistance mechanisms for the resistant cell line.

References

[BGLS06] J.F. Bonnans, J.C. Gilbert, C. Lemaréchal, and C.A. Sagastizábal, *Numerical Optimization - Theoretical and Practical Aspects*, Berlin : Springer-Verlag, 2006.

[BMea14] C. Breunig, B.J. Mueller, and L. Umansky et al., *BRaf and MEK inhibitors differentially regulate cell fate and microenvironment in human hepatocellular carcinoma*, Clinical Cancer Research **20** (2014), 2410–2423.

[CCS07] F. Campolongo, J. Cariboni, and A. Saltelli, *An effective screening design for sensitivity analysis of large models*, Environmental Modelling and Software **22** (2007), 1509–1518.

[DMBea09] C. Desbois-Mouthon, A. Baron, and M.J. Blivet-Van Eggelpoël et al., *Insulin-like growth factor-1 receptor inhibition induces*

a resistance mechanism via the epidermal growth factor receptor/HER3/AKT signaling pathway : Rational basis for cotargeting insulin-like growth factor-1 receptor and epidermal growth factor receptor in hepatocellular carcinoma, Clinical Cancer Research **15** (2009), 5445–5456.

[ELea12] Z. Ezzoukhry, C. Louandre, and E. Trécherel et al., *EGFR activation is a potential determinant of primary resistance of hepatocellular carcinoma cells to sorafenib*, International Journal of Cancer **131** (2012), 2961–2969.

[GCB14] A. Galmiche, B. Chauffert, and J.-C. Barbare, *New biological perspectives for the improvement of the efficacy of sorafenib in hepatocellular carcinoma*, Cancer Letters **346** (2014), 159–162.

[GDea13] C. Godin, S. Dupont, and Z. Ezzoukhry et al., *Heterogeneous sensitivity of hepatocellular carcinoma to sorafenib revealed by the short-term culture of tumor fragments*, Anticancer Research **33** (2013), 1415–1420.

[KHGK15] W. Kolch, M. Halasz, M. Granovskaya, and B.N. Kholodenko, *The dynamic control of signal transduction networks in cancer cells*, Nature Reviews Cancer **15** (2015), 515–527.

[Mor91] M.D. Morris, *Factorial sampling plans for preliminary computational experiments*, Technometrics **33** (1991), 161–174.

[NLea17] L. Niu, L. Liu, and S. Yang et al., *New insights into sorafenib resistance in hepatocellular carcinoma : Responsible mechanisms and promising strategies*, Biochim Biophys Acta Rev Cancer **1868** (2017), 564–570.

[OSea05] R.J. Orton, O.E. Sturm, and V. Vyshemirsky et al., *Computational modelling of the receptor-tyrosine-kinase-activated MAPK pathway*, Biochemical Journal **392** (2005), 249–261.

[PNLDB06] P.R. Peres-Neto, P. Legendre, S. Dray, and D. Borcard, *Variation partitioning of species data matrices : Estimation and comparison of fractions*, Ecology **87** (2006), 2614–2625.

[Pow94] M.J.D. Powell, *A direct search optimization method that models the objective and constraint functions by linear interpolation.*, In Advances in Optimization and Numerical Analysis. Mathematics and Its Applications. Dordrecht : Springer Netherlands. (1994), 51–67.

[RDea14] R. Rudalska, D. Dauch, and T. Longerich et al., *In vivo RNAi screening identifies a mechanism of sorafenib resistance in liver cancer*, Nature Medicine **20** (2014), 1138–1146.

[RPM+00] F.L. Roudabush, K.L. Pierce, S. Maudsley, K.D. Khan, and L.M. Luttrell, *Transactivation of the EGF receptor mediates IGF-1-stimulated Shc phosphorylation and ERK1/2 activation in COS-7 cells*, Journal of Biological Chemistry **275** (2000), 22583–22589.

[SEJGM02] B. Schoeberl, C. Eichler-Jonsson, E.D. Gilles, and G. MÃ¼ller, *Computational modeling of the dynamics of the MAP kinase cascade activated by surface and internalized EGF receptors*, Nature Biotechnology **20** (2002), 370–375.

[SF13] R.J. Sullivan and K.T. Flaherty, *Resistance to BRAF-targeted therapy in melanoma*, Eur. J. Cancer **49** (2013), 1297–1304.

[SGea17] Z. Saidak, A.-S. Giacobbi, and C. Louandre et al., *Mathematical modelling unveils the essential role of cellular phosphatases in the inhibition of RAF-MEK-ERK signalling by sorafenib in hepatocellular carcinoma cells*, Cancer Letters **392** (2017), 1–8.

[SHea02] S.Y. Shvartsman, M. P. Hagan, and A. Yacoub et al., *Autocrine loops with positive feedback enable context-dependent cell signaling*, American Journal of Physiology-Cell Physiology **282** (2002), 545–559.

[SRea09] S.Y. Shin, O. Rath, and S.M. Choo et al., *Positive- and negative-feedback regulations coordinate the dynamic behavior of the Ras-Raf-MEK-ERK signal transduction pathway*, Journal of Cell Science **122** (2009), 425–435.

[VVH11] J. Villanueva, A. Vultur, and M. Herlyn, *Resistance to BRAF inhibitors : unraveling mechanisms and future treatment options*, Cancer Res. **71** (2011), 7137–7140.

[WCea04] S.M. Wilhelm, C. Carter, and L. Tang et al., *Bay 43-9006 exhibits broad spectrum oral antitumor activity and targets the RAF/MEK/ERK pathway and receptor tyrosine kinases involved in tumor progression and angiogenesis*, Cancer Research **64** (2004), 7099–7109.

[WFJ+12] H.M. Wainwright, S. Finsterle, Y. Jung, Q. Zhou, and J.T. Birkholzer, *Making sense of global sensitivity analyses*, Computers and Geosciences **65** (2012), 84–94.

[ZRea14] A.X. Zhu, O. Rosmorduc, and T.R. Jeffry Evans et al., *A phase III, randomized, double-blind, placebo-controlled trial of sorafenib plus erlotinib in patients with advanced hepatocellular carcinoma*, Journal of Clinical Oncology **33** (2014), 559–566.

[ZZea17] Y-J. Zhu, B. Zheng, and H-Y Wang et al., *New knowledge of the mechanisms of sorafenib resistance in liver cancer*, Acta Pharmacologica Sinica **38** (2017), 614–622.

Chapitre 5

Comportement asymptotique de la signalisation cellulaire sous diffusion spatiale

Asymptotic behavior of cellular signalling under spatial diffusion

This chapter is devoted to the theoretical aspects. The 3 different behaviors of the cell lines observed inside the Raf-MEK-ERK pathway exposed to sorafenib, namely sensitive, resistant and resilient, are investigated with respect to the convergence to the equilibrium (Fig. 5.1). This convergence is observed as a function of the dephosphorylation parameters $V_{u,2}$ and $V_{v,2}$.

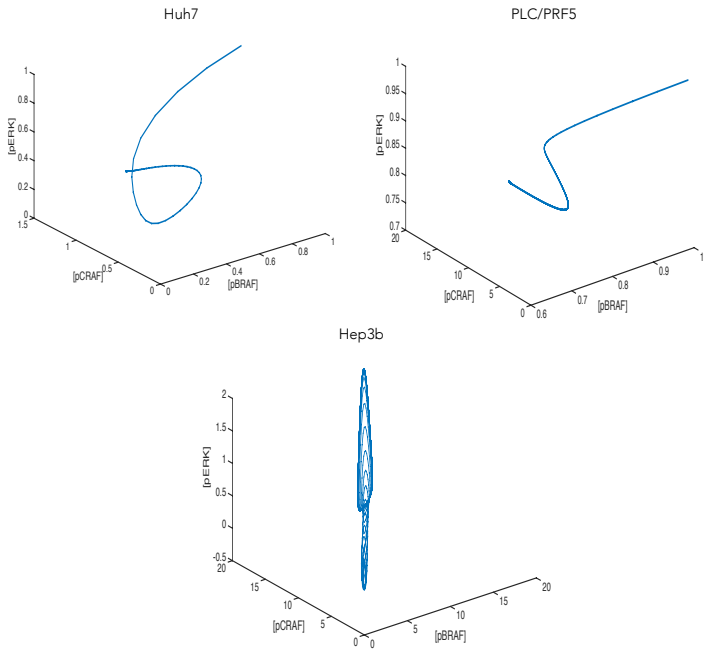

Figure 5.1 – Dynamic of pERK in long-time regarding pBRAF and pCRAF rates in Huh7, Hep3b and PLC/PRF5 cell lines.

A simplified model accounting for two activated proteins is considered. The first component (u) can activate the second one (v), which balances the dynamic with a negative feedback regulation (Fig. 5.2).

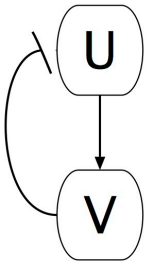

FIGURE 5.2 – Schematic representation of the pathway with feedback.

Let $0 < \tau \ll 1$ a given tolerance. The behavior of the cell lines can be translated as follows.

- The cell line is sensitive to sorafenib if the solution is decreasing to a positive asymptotically stable equilibrium (u^*, v^*) with $|v^*| \leq \tau$.
- The cell line is resistant to sorafenib if the solution converges to a positive asymptotically stable equilibrium (u^*, v^*) with $v^* > \tau$.
- The cell line is resilient if there exists a time t^* when the solution (u, v) verifies $v(t^*) \leq \tau$ but goes to a positive equilibrium (u^*, v^*) with $v^* > \tau$.

The chapter is organized as follows. In Section 1, the asymptotic stability of solution is proved. Section 2 deals with spatiotemporal model described by two reaction-diffusion equations. One notes that the asymptotic behavior of the solution is preserved.

5.1 Stability of equilibrium without diffusion

Consider the initial value problem

$$u'(t) = \frac{V_{u,1}(\overline{u} - u(t))}{K_{u,1} + \overline{u} - u(t)} \left(1 + \frac{v(t)}{K_{u,3}}\right)^{-\alpha} - \frac{V_{u,2}u(t)}{K_{u,2} + u(t)} \tag{5.1}$$

$$v'(t) = \frac{V_{v,1}u(t)(\overline{v} - v(t))}{K_{v,1} + \overline{v} - v(t)} - \frac{V_{v,2}v(t)}{K_{v,2} + v(t)} \tag{5.2}$$

$$u(0) = u_0,\ v(0) = v_0. \tag{5.3}$$

We assume that kinetic parameters $V_{u,i}, K_{u,j}, V_{v,i}$ and $K_{v,i}$ and α are positive for $i = \{1, 2\}$ and $j = \{1, 2, 3\}$.

Theorem 5.1 *Let $0 \leq u_0 \leq \overline{u}$ and $0 \leq v_0 \leq \overline{v}$. Then there exists a unique solution $(u, v) \in \mathcal{C}(\mathbb{R}_+, \mathbb{R}_+) \times \mathcal{C}(\mathbb{R}_+, \mathbb{R}_+)$ of the Cauchy problem (5.1)-(5.2)-(5.3). Moreover, for all time $t \in \mathbb{R}_+$,*

$$0 \leq u(t) \leq \overline{u},\ 0 \leq v(t) \leq \overline{v}.$$

Proof. The Cauchy problem can be rewritten as

$$\begin{aligned} w'(t) &= F(w) && (5.4)\\ w(0) &= w_0, && (5.5) \end{aligned}$$

where $w(t) = \Big(u(t), v(t)\Big)$, $w_0 = \Big(u_0, v_0\Big)$ and $F(w) = \Big(f(u, v), g(u, v)\Big)$ with

$$\begin{aligned} u' &= f(u, v) && (5.6)\\ v' &= g(u, v). && (5.7) \end{aligned}$$

The function F is locally Lipschitz and the Cauchy-Lipschitz theorem provides local well-posedness of the initial value problem (5.1)-(5.2)-(5.3). Moreover, the domain $D = \{(u, v) \in \mathbb{R}^2, 0 \leq u \leq \overline{u},\ 0 \leq v \leq \overline{v}\}$ is positively invariant. Indeed, the right-hand-side verifies, for $(u, v) \in D$,

$$\begin{aligned} f(0, v) &= \frac{V_{u,1}\overline{u}}{K_{u,1} + \overline{u}} \left(1 + \frac{v}{K_{u,3}}\right)^{-\alpha} \geq 0,\\ f(\overline{u}, 0) &= -\frac{V_{u,2}\overline{u}}{K_{u,2} + \overline{u}} \leq 0,\\ g(u, 0) &= \frac{V_{v,1}u\overline{v}}{K_{v,1} + \overline{v}} \geq 0,\\ g(u, \overline{v}) &= -\frac{V_{v,2}\overline{v}}{K_{v,2} + \overline{v}} \leq 0. \end{aligned}$$

□

Theorem 5.2 *The equilibrium (u*, v*) is globally asymptotically stable.*

Proof. Let first consider (u^*, v^*) the non-negative equilibrium solution of

$$\begin{aligned} \frac{V_{u,1}(\overline{u}-u^*)}{K_{u,1}+\overline{u}-u^*}\left(1+\frac{v^*}{K_{u,3}}\right)^{-\alpha} - \frac{V_{u,2}u^*}{K_{u,2}+u^*} &= 0 \\ \frac{V_{v,1}u^*(\overline{v}-v^*)}{K_{v,1}+\overline{v}-v^*} - \frac{V_{v,2}v^*}{K_{v,2}+v^*} &= 0. \end{aligned}$$

The Jacobian matrix is written

$$J = \begin{pmatrix} -\frac{V_{u,1}K_{u,1}}{(K_{u,1}+\overline{u}-u^*)^2}\left(1+\frac{v^*}{K_{u,3}}\right)^{-\alpha} - \frac{V_{u,2}K_{u,2}}{(K_{u,2}+u^*)^2} & -\frac{\alpha V_{u,1}(\overline{u}-u^*)}{K_{u,3}(K_{u,1}+\overline{u}-u^*)}\left(1+\frac{v^*}{K_{u,3}}\right)^{-(\alpha+1)} \\ \frac{V_{v,1}(\overline{v}-v^*)}{K_{v,1}+\overline{v}-v^*} & -\frac{V_{v,1}K_{v,1}u^*}{(K_{v,1}+\overline{v}-v^*)^2} - \frac{V_{v,2}K_{v,2}}{(K_{v,2}+v^*)^2} \end{pmatrix}.$$

Since (u^*, v^*) is the positive equilibrium, we get

$$f_u, f_v, g_v \leq 0, g_u \geq 0.$$

We deduce that

$$\det(J) \geq 0 \text{ and } \mathrm{tr}(J) \leq 0,$$

and (u^*, v^*) is locally asymptotically stable.
Moreover, since D is positively invariant and $Tr(J) < 0$, the equilibrium is globally asymptotically stable thanks to Bendixson's condition. □

To illustrate the cell lines differences, parameters are set to $\alpha = 3.5, V_{u,1} = K_{u,1} = V_{u,2} = K_{u,2} = K_{u,3} = 1, \overline{u} = 2$ and $V_{v,1} = K_{v,1} = K_{v,2} = 1, \overline{v} = 2$ with respect to [SGea17,KHGK15]. Parameters $V_{v,2}$, related to dephosphorylation of v, varies between 0.1 and 10. The numerical simulations with respect to time are represented in the figure below. For this choice of parameters and $V_{v,2} = 10$, the equilibrium is equal to

$$v^* = 0.05659973.$$

For the sensitive cell line (Fig. 5.3), the solution (u, v) is quickly decreasing and reaches the stable state over the time. This behavior is in agreement with the previous study in which the cell signaling is turned off by inhibiting the RAF activation via sorafenib. The phase portrait describes a faster decrease of v from 1 to 0.05659973, while u decreases from 1 to 0.8. Concerning the resilient cell line, the solution (u, v) first decreases and then increases before 10 hours, which well describes the resilient response to sorafenib (Fig. 5.4). The solution gets to a stationary point $(u^*, v^*) = (0.35028511, 0.284245)$ over time and the equilibrium u^* is less than the sensitivity cell line. The displayed trajectory well illustrates the resilient behaviour as it tends to decrease before reaching the stable state. In the context of the resistant cell

line, the solutions u and v have an opposite behavior : v increases until 1.45 whereas u increases to 0.04 during a time period of approximatively 5 hours after sorafenib treatment (Fig. 5.5). Then, v decreases whereas u increases and the solutions (u, v) tends to stabilize over time but the stable state is not reached. The amount of v is always greater than 0.8378 which characterizes the cell resistant response to the targeted therapy.

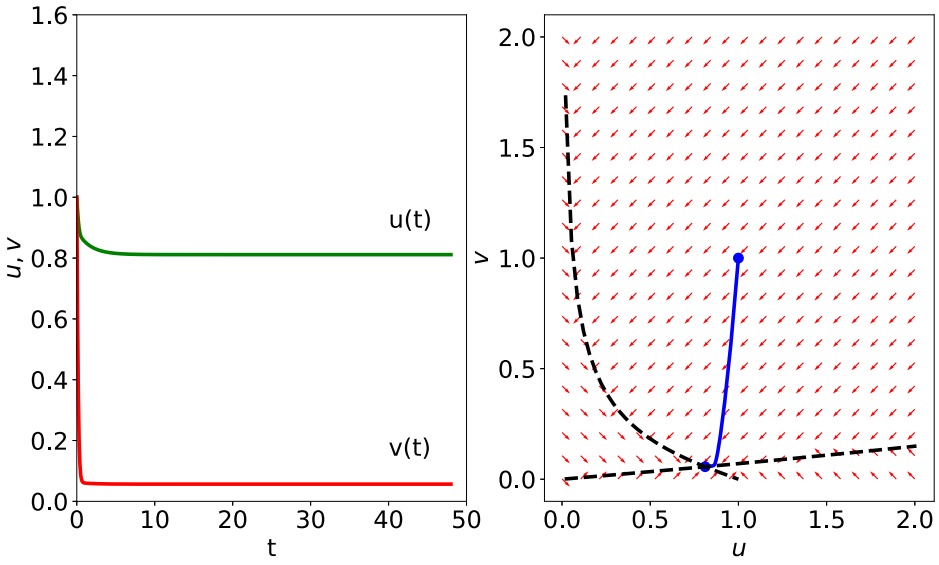

FIGURE 5.3 – Spatiotemporal evolution of the solution for the sensitive cell line ($V_{v,2} = 10$). The solution v is decreasing to 0.05659973.

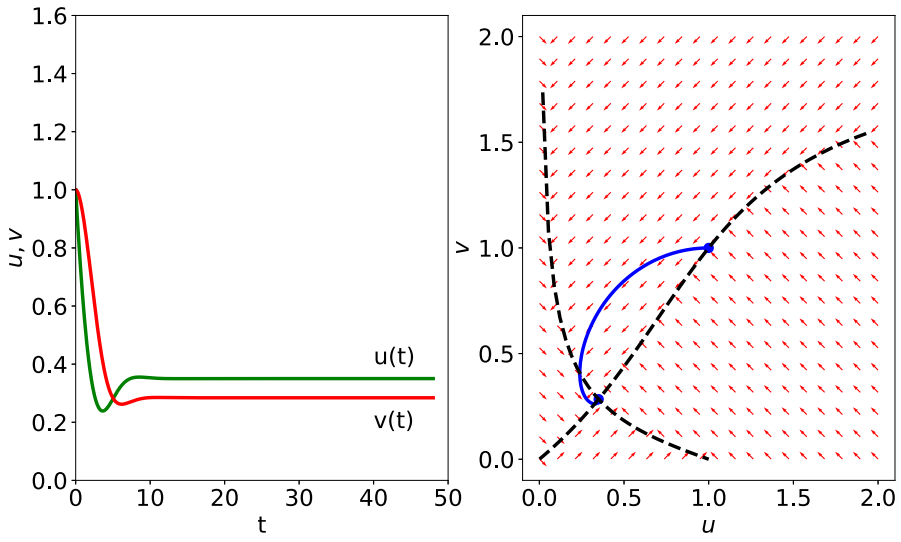

FIGURE 5.4 – Spatiotemporal evolution of the solution for the resilient cell line ($V_{v,2} = 1$). The solution v is decreasing then increasing to 0.284245.

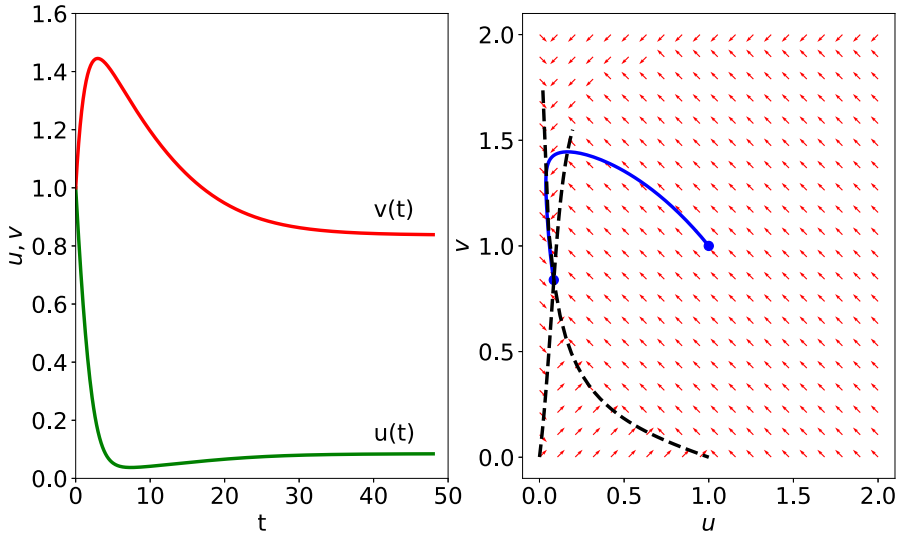

FIGURE 5.5 – Spatiotemporal evolution of the solution for the resitant cell line ($V_{v,2} = 0.1$). The solution v is increasing then decreasing to 0.8378.

The equilibrium (u^*, v^*) as function of $V_{v,2}$ is represented in Figure 5.6. We notice that the maximum value of v^* closed to 1 is reached when $V_{v,2}$ is small (resistant case), while v^* goes to zero when $V_{v,2}$ is large (sensitive case). In the resistant and resilient cases, the stationary point v^* satisfies $v^* > \tau$, with $\tau = 0.13617414727374951 84$, which is related to a value of $V_{v,2} < 1$. In the sensitive case, $v^* \leq \tau$ and $V_{v,2} \geq 1$. Regarding the point u^* with respect to $V_{v,2}$, its behavior is on the contrary described by an upward curve. Similar behavior according to the desactivation of u, i.e $V_{u,2}$, is observed in Figure 5.7.

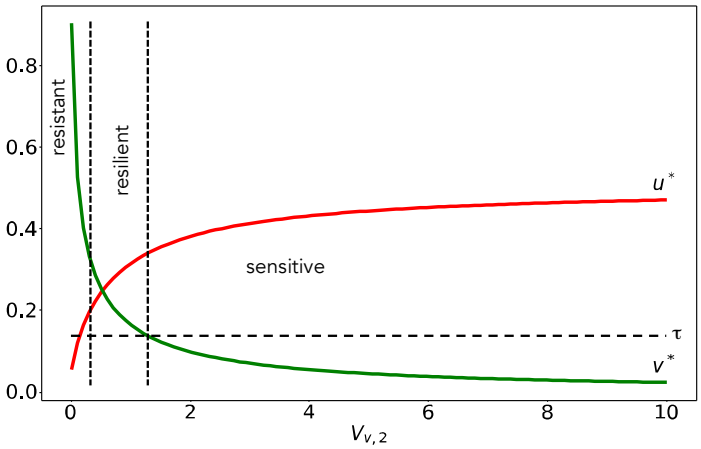

FIGURE 5.6 – The evolution of the stationary point (u^*, v^*) regarding the parameter $V_{v,2}$.

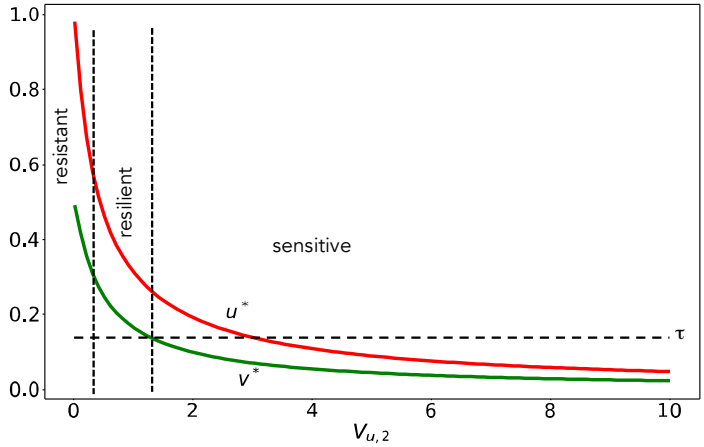

FIGURE 5.7 – The evolution of the stationary point (u^*, v^*) regarding the parameter $V_{u,2}$.

5.2 Asymptotic behavior of solution with diffusion

We consider in this part the spatial effect of a single cell on the chemical reactions. The dynamic of each protein is now driven by a diffusion term $D_u \Delta u$, where u is the protein amount, Δu is the Laplacian operator and the constant coefficient D_u is the diffusion. We denote by $\mathcal{Q}$ the regular domain describing the geometry of a cell. Here, the different compartments of a cell such as the cytoplasm or the nucleus are not taken into account, and we assume that the chemical reactions occur in the whole cell. Furthermore, zero-flux boundary conditions are supposed which means that the proteins remain inside the domain. This assumption leads to homogeneous Neumann boundary conditions. Then, we consider the initial boundary value problem for $t \geq 0$ and $x \in \mathcal{Q}$,

$$\frac{\partial u}{\partial t} = D_1 \Delta u + \frac{V_{u,1}(\overline{u} - u)}{K_{u,1} + \overline{u} - u} \left(1 + \frac{v}{K_{u,3}}\right)^{-\alpha} - \frac{V_{u,2} u}{K_{u,2} + u} \tag{5.8}$$

$$\frac{\partial v}{\partial t} = D_2 \Delta v + \frac{V_{v,1} u(\overline{v} - v)}{K_{v,1} + \overline{v} - v} - \frac{V_{v,2} v}{K_{v,2} + v} \tag{5.9}$$

$$\frac{\partial u}{\partial n} = \frac{\partial v}{\partial n} = 0 \tag{5.10}$$

$$u(0, x) = u_0(x),\ v(0, x) = v_0(x). \tag{5.11}$$

5.2.1 Well-posedness of the system

Theorem 5.3 *Let $0 \leq u_0 \leq \overline{u}$ and $0 \leq v_0 \leq \overline{v}$. Then there exists a unique weak solution $(u, v) \in L^\infty(\mathbb{R}_+, L^\infty(\mathcal{Q})) \times L^\infty(\mathbb{R}_+, L^\infty(\mathcal{Q}))$ of the Cauchy problem (5.8)-(5.9)-(5.10)-(5.11). Moreover, for all time $t \in \mathbb{R}_+$, and $x \in \mathcal{Q}$*

$$0 \leq u(t,x) \leq \overline{u},\ 0 \leq v(t,x) \leq \overline{v}.$$

Proof. Let $M > 0$ and $T > 0$ that will be chosen later. We define the closed ball B_T as

$$B_T = \{(u,v) \in L^\infty([0,T], L^\infty(\mathcal{Q}))^2,\ \sup_{t\in[0,T]} ||(u,v)(t,.) - (u_0,v_0)||_{L^\infty(\mathcal{Q})} \leq M\}.$$

We look after a fixed point of the Duhamel formulation given by the following map for all $(u, v) \in B_T$

$$\Phi(u,v)(t) := \Bigg(K_1 * u_0(t) + \int_0^T K_1(t-s) * f(u,v)(s)\,\mathrm{d}s,$$
$$K_2 * v_0(t) + \int_0^T K_2(t-s) * g(u,v)(s)\,\mathrm{d}s \Bigg).$$

For $i = \{1, 2\}$, K_i is here the heat kernel defined as the solution of the following diffusion equation with the homogeneous Neumann boundary conditions

$$\begin{aligned} \frac{\partial K_i}{\partial t} - D_i \Delta K_i &= 0 && \text{for } x \in Q,\ t \geq 0 \\ \frac{\partial K_i}{\partial n} &= 0 && \text{on } \partial\mathcal{Q}. \end{aligned}$$

with $\int_{\mathcal{Q}} K_i(t,x)\mathrm{d}x = 1$.

According to [Ouh05], there exists a constant $C_{\mathcal{Q}} > 0$, depending only on $\mathcal{Q}$, such that the kernel satisfies

$$||K_i(t,.)||_{L^1(\mathcal{Q})} \leq C_{\mathcal{Q}}$$

Let $(u,v) \in B_T$, we have

$$\begin{aligned}
|\Phi(u,v)(t,x) - (u_0,v_0)(x)| \;\leq\; & \int_Q K_1(t,x-y)|u_0(y)-u_0(x)|\,\mathrm{d}y \\
& + \int_0^T \int_Q K_1(t-s,x-y)|f(u,v)(s,x)|\,\mathrm{d}y\,\mathrm{d}s \\
& + \int_Q K_2(t,x-y)|v_0(y)-v_0(x)|\,\mathrm{d}y \\
& + \int_0^T \int_Q K_2(t-s,x-y)|g(u,v)(s,x)|\,\mathrm{d}y\,\mathrm{d}s
\end{aligned}$$

and

$$\begin{aligned}
||\Phi(u,v)(t,.) - (u_0,v_0)||_{L^\infty(\mathcal{Q})} \;\leq\; & 2C_{\mathcal{Q}}\left(||u_0(.)||_{L^\infty(\mathcal{Q})} + ||v_0(.)||_{L^\infty(\mathcal{Q})}\right) \\
& + C_{\mathcal{Q}}T\left(\sup_{t\in[0,T]} ||f(u,v)(t,.)||_{L^\infty(\mathcal{Q})} + \sup_{t\in[0,T]} ||g(u,v)(t,.)||_{L^\infty(\mathcal{Q})}\right) \\
\leq\; & 2C_{\mathcal{Q}}\left(||u_0(.)||_{L^\infty(\mathcal{Q})} + ||v_0(.)||_{L^\infty(\mathcal{Q})}\right) + 2C_{\mathcal{Q}}LT,
\end{aligned}$$

where L is the maximum of the Lipschitz constant of f and g.

Then, choosing $T > 0$ such that

$$2C_{\mathcal{Q}}\left(||u_0(.)||_{L^\infty(\mathcal{Q})} + ||v_0(.)||_{L^\infty(\mathcal{Q})}\right) + 2C_{\mathcal{Q}}LT \leq M := 4C_{\mathcal{Q}}\left(||u_0(.)||_{L^\infty(\mathcal{Q})} + ||v_0(.)||_{L^\infty(\mathcal{Q})}\right),$$

i.e.

$$T \leq \frac{\left(||u_0(.)||_{L^\infty(\mathcal{Q})} + ||v_0(.)||_{L^\infty(\mathcal{Q})}\right)}{L},$$

implies that $\Phi(B_T) \subset B_T$.

Let now (u,v) and $(\widetilde{u},\widetilde{v})$ be in B_T. Then, we have

$$\begin{aligned}
&\Phi(u,v)(t) - \Phi(\widetilde{u},\widetilde{v})(t) \\
&\quad = \left(\int_0^T \int_Q \Big(K_1(t-s,x-y)f(u,v)(s,y) - K_1(t-s,x-y)f(\widetilde{u},\widetilde{v})(s,y)\Big)\,\mathrm{d}y\,\mathrm{d}s,\right. \\
&\qquad \left.\int_0^T \int_Q \Big(K_2(t-s,x-y)g(u,v)(s,y) - K_2(t-s,x-y)g(\widetilde{u},\widetilde{v})(s,y)\Big)\,\mathrm{d}y\,\mathrm{d}s\right).
\end{aligned}$$

Then,

$$\begin{aligned}
\sup_{t\in[0,T]} ||\,\Phi(u,v) - \Phi\,(\widetilde{u},\widetilde{v})\,||_{L^\infty(\mathcal{Q})} &\leq C_{\mathcal{Q}}T \sup_{t\in[0,T]} ||\,f(u,v)(t,.) - f(\widetilde{u},\widetilde{v})(t,.)\,||_{L^\infty(\mathcal{Q})} \\
&\quad + C_{\mathcal{Q}}T \sup_{t\in[0,T]} ||\,g(u,v)(t,.) - g(\widetilde{u},\widetilde{v})(t,.)\,||_{L^\infty(\mathcal{Q})} \\
&\leq 2C_{\mathcal{Q}}LT \sup_{t\in[0,T]} ||\,(u,v)(t,.) - (\widetilde{u},\widetilde{v})(t,.)\,||_{L^\infty(\mathcal{Q})}\,.
\end{aligned}$$

Choosing $T < \frac{1}{2C_{\mathcal{Q}}L}$ provides an unique fixed point in B_T using the Picard fixed point theorem [Hen81].

The positivity is ensured by the quasi-positivity of the right-hand-side of equation which is similar to the problem without space [Fri83]. The upper bound is deduced from the maximum principle that implies $0 \leq u(t,.) \leq a(t)$ and $0 \leq v(t,.) \leq b(t)$ where (a,b) is the solution of the ordinary differential system

$$\begin{aligned} a'(t) &= \frac{V_{u,1}(\overline{u}-a(t))}{K_{u,1}+\overline{u}-a(t)}\left(1+\frac{a(t)}{K_{u,3}}\right)^{-\alpha} - \frac{V_{u,2}a(t)}{K_{u,2}+a(t)} \\ b'(t) &= \frac{V_{v,1}a(t)(\overline{v}-b(t))}{K_{v,1}+\overline{v}-b(t)} - \frac{V_{v,2}b(t)}{K_{v,2}+b(t)}. \end{aligned}$$

According to Theorem (5.1), the solution (a,b) is bounded by $(\overline{u},\overline{v})$ for all time. We deduce that for all $t \in \mathbb{R}_+$

$$|| \, u(t,.) \, ||_{L^\infty(\mathcal{Q})} \leq \overline{u} \text{ and } || \, v(t,.) \, ||_{L^\infty(\mathcal{Q})} \leq \overline{v}.$$

□

5.2.2 Stability preservation

The asymptotic behavior of the reaction-diffusion equations is preserved.

Theorem 5.4 *Let (u^*,v^*) be the equilibrium of the ordinary differential system. Then the solution of the initial value boundary problem (5.8) – (5.9) – (5.10) – (5.11) remains locally asymptotically stable.*

Proof. Let be $w = \begin{pmatrix} u \\ v \end{pmatrix}$. The linearization around (u^*,v^*) gives the system

$$\frac{\partial}{\partial t}w = \begin{pmatrix} D_1\Delta & 0 \\ 0 & D_2\Delta \end{pmatrix} w + Jw$$

The Laplace operator with the Neumann boundary condition (5.10) admits an orthonormal basis of eigenfunctions $(w_k)_{k\geq 1}$ such as

$$-\Delta w_k = k^2 w_k$$

with k^2 the associated positive eigenvalues.
For $k=0$, we have the problem without diffusion and the solution is asymptotically stable (Theorem 5.2). Using this basis, we can rewrite the solution of the system for all $k \neq 0$

$$u(t,x) = \sum_{k=1}^{\infty} a_k(t) w_k(x),\ v(t,x) = \sum_{k=1}^{\infty} b_k(t) w_k(x).$$

Then, the system becomes

$$\frac{\partial}{\partial t}\begin{pmatrix} a_k(t) \\ b_k(t) \end{pmatrix} = -k^2 \begin{pmatrix} D_1 & 0 \\ 0 & D_2 \end{pmatrix} \begin{pmatrix} a_k(t) \\ b_k(t) \end{pmatrix} + J \begin{pmatrix} a_k(t) \\ b_k(t) \end{pmatrix}$$

Since we consider the solutions with exponential growth, we have

$$a_k(t) = \alpha_k e^{\lambda_k t} \text{ and } b_k(t) = \beta_k e^{\lambda_k t}$$

which reduces the system as follows

$$\lambda_k \begin{pmatrix} \alpha_k \\ \beta_k \end{pmatrix} = (-Dk^2 + J) \begin{pmatrix} \alpha_k \\ \beta_k \end{pmatrix}.$$

This equality shows that λ_k are the eigenvalues of the matrix $-Dk^2 + J$. The characteristic polynomial related to this matrix is

$$P(\lambda_k) = \lambda_k^2 - \lambda_k\Big(tr(J) - k^2(D_1 + D_2)\Big) + D_1 D_2 k^4 - k^2(D_2 f_u + D_1 g_v) + det(J).$$

The roots of P are given by

$$\lambda_k = \frac{1}{2}\Big(\mathcal{H}_k \pm \sqrt{\mathcal{H}_k^2 - 4g(k)}\Big)$$

with

$$\mathcal{H}_k = tr(J) - k^2(D_1 + D_2)$$

and

$$g(k^2) = D_1 D_2 k^4 - k^2(D_1 f_u + D_2 g_v) + det(J).$$

To have the stability of the system around (u^*, v^*), the real part of λ_k must be negative for all $k \neq 0$. It requires $\mathcal{H}_k < 0$ and $\sqrt{\mathcal{H}_k^2 - 4g(k)} < -\mathcal{H}_k$. Because $tr(J) \leq 0$, $D_1 > 0$ and $D_2 > 0$, the first condition is satisfied. The last condition implies that the parabolic function g in k^2 must be positive. We have

$$D_1 > 0, D_2 > 0, f_u \leq 0, g_v \leq 0 \text{ and } det(J) > 0.$$

Then, $g(k^2) > 0$ and $Re(\lambda_k) > 0$ for all $k \neq 0$. □

For large enough diffusion coefficients, which is not the case for cell signalling, the asymptotic stability is exponential.

Theorem 5.5 *Let* $D = \min(D_1, D_2)$, $L = \max(V_{u,1}, V_{u,2}, \overline{u}V_{v,1}, , \overline{v}V_{v,1}, V_{v,2})$. *Assume that*

$$\delta = D\lambda_2 - L > 0,$$

where λ_2 *is the second eigenvalue of the Laplace operator with Neumann boundary condition. Then*

$$\int_{\mathcal{Q}} (u(t,x) - \overline{u}(t))^2 \, dx + \int_{\mathcal{Q}} (v(t,x) - \overline{v}(t))^2 \, dx \quad \leq \quad \mathrm{e}^{-2\delta t} \int_{\mathcal{Q}} (u_0(x) - \overline{u_0})^2 \, dx$$

with $\overline{u}(t) = \int_{\mathcal{Q}} u(t,x)dx, \overline{v}(t) = \int_{\mathcal{Q}} v(t,x)dx$.

Proof. The proof follows [Per15]. Integrating over space provides

$$\begin{aligned} \frac{d}{dt}\int_{\mathcal{Q}} u &= \int_{\mathcal{Q}} \frac{V_{u,1}(\overline{u}-u)}{K_{u,1}+\overline{u}-u}\left(1+\frac{v}{K_{u,3}}\right)^{-\alpha} - \frac{V_{u,2}u}{K_{u,2}+u} \\ \frac{d}{dt}\int_{\mathcal{Q}} v &= \int_{\mathcal{Q}} \frac{V_{v,1}u(\overline{v}-v)}{K_{v,1}+\overline{v}-v} - \frac{V_{v,2}v}{K_{v,2}+v}, \end{aligned}$$

or shortly

$$\begin{aligned} \frac{d}{dt}\overline{u}(t) &= \overline{f}(t) \\ \frac{d}{dt}\overline{v}(t) &= \overline{g}(t). \end{aligned}$$

We deduce

$$\begin{aligned} \frac{\partial}{\partial t}(u-\overline{u}) &= D_1\Delta u + (f-\overline{f}) \\ \frac{\partial}{\partial t}(v-\overline{v}) &= D_2\Delta v + (g-\overline{g}). \end{aligned}$$

Multiplying these equations by $(u-\overline{u})$ and $(v-\overline{v})$ respectively, one gets

$$\begin{aligned} \frac{1}{2}\frac{d}{dt}\int_{\mathcal{Q}}(u-\overline{u})^2 + D_1\int_{\mathcal{Q}}(\nabla u)^2 &= \int_{\mathcal{Q}}(f-\overline{f})(u-\overline{u}) \\ \frac{1}{2}\frac{d}{dt}\int_{\mathcal{Q}}(v-\overline{v})^2 + D_2\int_{\mathcal{Q}}(\nabla v)^2 &= \int_{\mathcal{Q}}(g-\overline{g})(v-\overline{v}). \end{aligned}$$

Since for all $0 \leq u \leq \overline{u}$ and $0 \leq v \leq \overline{v}$,

$$(f(u,v)-\overline{f(u,v)})(u-\overline{u})+(g(u,v)-\overline{g(u,v)})(v-\overline{v}) \leq L\left((u-\overline{u})^2+(v-\overline{v})^2\right),$$

and according to the Poincaré-Wirtinger inequality

$$\int_{\mathcal{Q}}(\nabla u)^2 \geq \lambda_2 \int_{\mathcal{Q}}(u-\overline{u})^2,$$

we finally obtain

$$\frac{d}{dt}\int_{\mathcal{Q}}(u-\overline{u})^2+\frac{d}{dt}\int_{\mathcal{Q}}(v-\overline{v})^2\leq -2\delta\left(\int_{\mathcal{Q}}(u-\overline{u})^2+\int_{\mathcal{Q}}(v-\overline{v})^2\right).$$

□

5.3 Numerical illustrations

5.3.1 Space and time discretization

Finite elements are used to illustrate the asymptotic behavior of the solution according to the sensitive, resistant and resilient cell lines. Let φ_1, φ_2 be test functions, with $\varphi_i, \nabla\varphi_i$ in L^2, for $1 \leq i \leq 2$. Finite elements method in space is used, while the time discretization is obtained with a semi-implicit scheme.

Algorithm 4 Semi-implicit scheme

Given u_0, v_0 and $N \in \mathbb{N}^*$.
for $n = 1$ to N **do**

$$\begin{aligned}
\langle\frac{u^{n+1}-u^n}{\Delta t},\varphi_1\rangle+\langle D_1\nabla u^{n+1},\nabla\varphi_1\rangle &= \langle\frac{V_{u,1}(\overline{u}-u^n)}{K_{u,1}+\overline{u}-u^n}\left(1+\frac{v^n}{K_{u,3}}\right)^{-\alpha} \\
&\quad -\frac{V_{u,2}u^n}{K_{u,2}+u^n},\varphi_1\rangle \\
\langle\frac{v^{n+1}-v^n}{\Delta t},\varphi_2\rangle+\langle D_2\nabla v^{n+1},\nabla\varphi_1\rangle &= \langle\frac{V_{v,1}u^n(\overline{v}-v^n)}{K_{v,1}+\overline{v}-v^n}-\frac{V_{v,2}v^n}{K_{v,2}+v^n},\varphi_2\rangle
\end{aligned}$$

5.3.2 $(2+1)-$d simulations

We consider a sample of diameter $1.5cm$ where diffusion coefficients are equal to $100\mu m^2/s$ [MS11]. Initial datum follow a random distribution valued in $[0,1]$.
As above, the cell lines differences are illustrated by choosing parameters as $\alpha = 3.5, V_{u,1} = K_{u,1} = V_{u,2} = K_{u,2} = K_{u,3} = 1, \overline{u} = 2$ and $V_{v,1} = K_{v,1} = K_{v,2} = 1, \overline{v} = 2$. The parameter $V_{v,2}$, related to dephosphorylation of v, varies between 0.1 and 10. Figures 5.8-5.9-5.10 present the spatiotemporal evolution of the solution. We note that v reaches the stable state at $t = 48$

as the distribution of v is homogeneous in the domain when $V_{v,2} = 10$ (Fig. 5.8) and $V_{v,2} = 1$ (Fig. 5.9). The value of the stable state gets to almost zero for the sensitive cell line whereas it is higher for the resilient cell line as observed before. For the resistant context, when $V_{v,2}$ is set to 0.1 (Fig. 5.10), the distribution of v tends to stabilize over the time but small variabilities are still observed at the end time point $t = 48$.

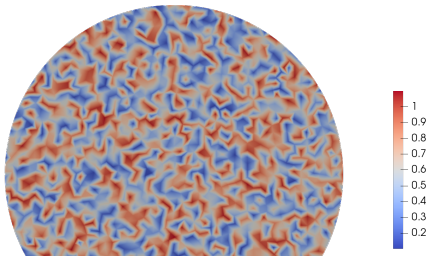

(a) $t = 0$.

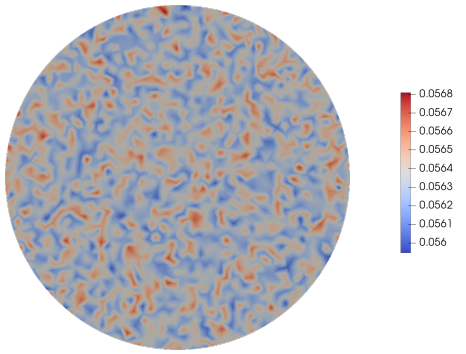

(b) $t = 8$.

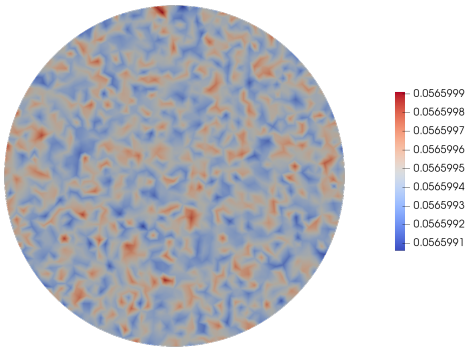

(c) $t = 18$.

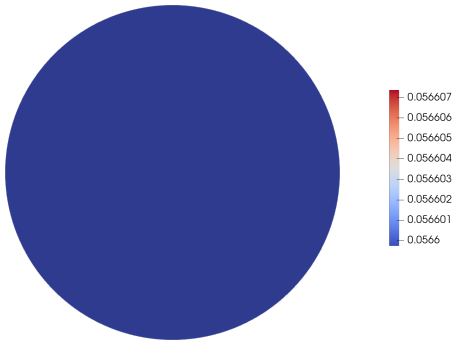

(d) $t = 48$.

FIGURE 5.8 – Spatiotemporal evolution of the solution for the sensitive cell line ($V_{v,2} = 10$). The solution v is decreasing to 0.05656.

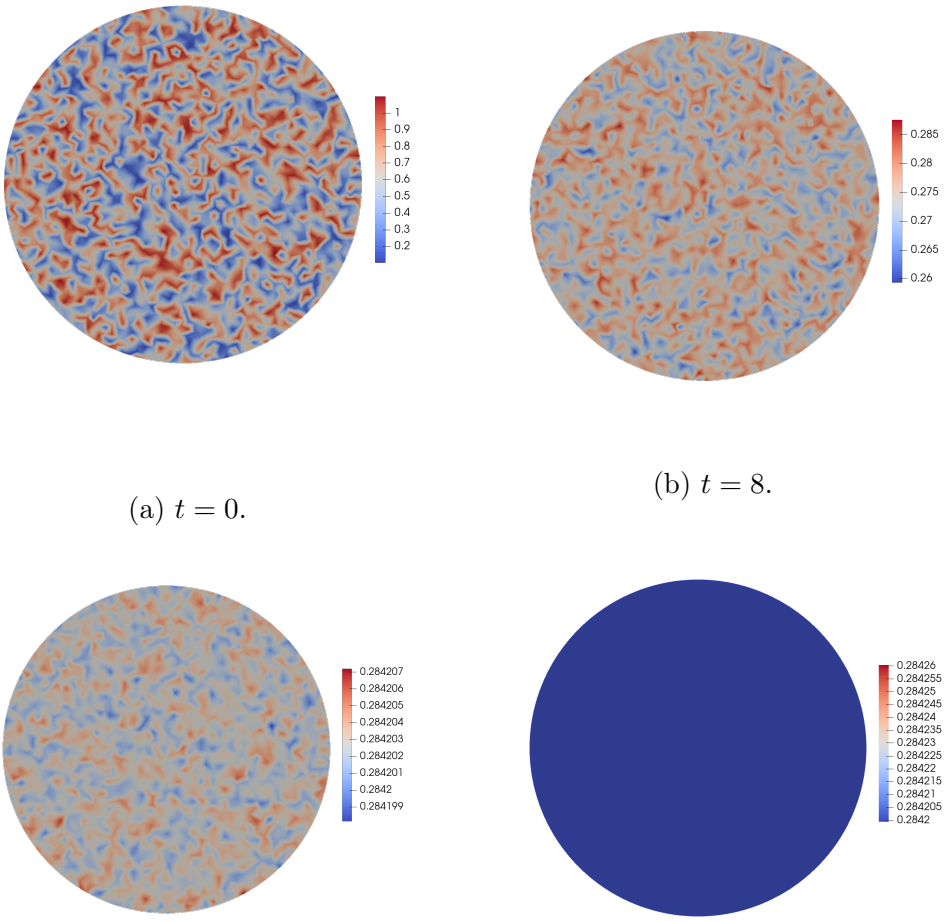

(a) $t = 0$.

(b) $t = 8$.

(c) $t = 18$.

(d) $t = 48$.

FIGURE 5.9 – Spatiotemporal evolution of the solution for the resilient cell line ($V_{v,2} = 1$). The solution v is decreasing then increasing to 0.2842.

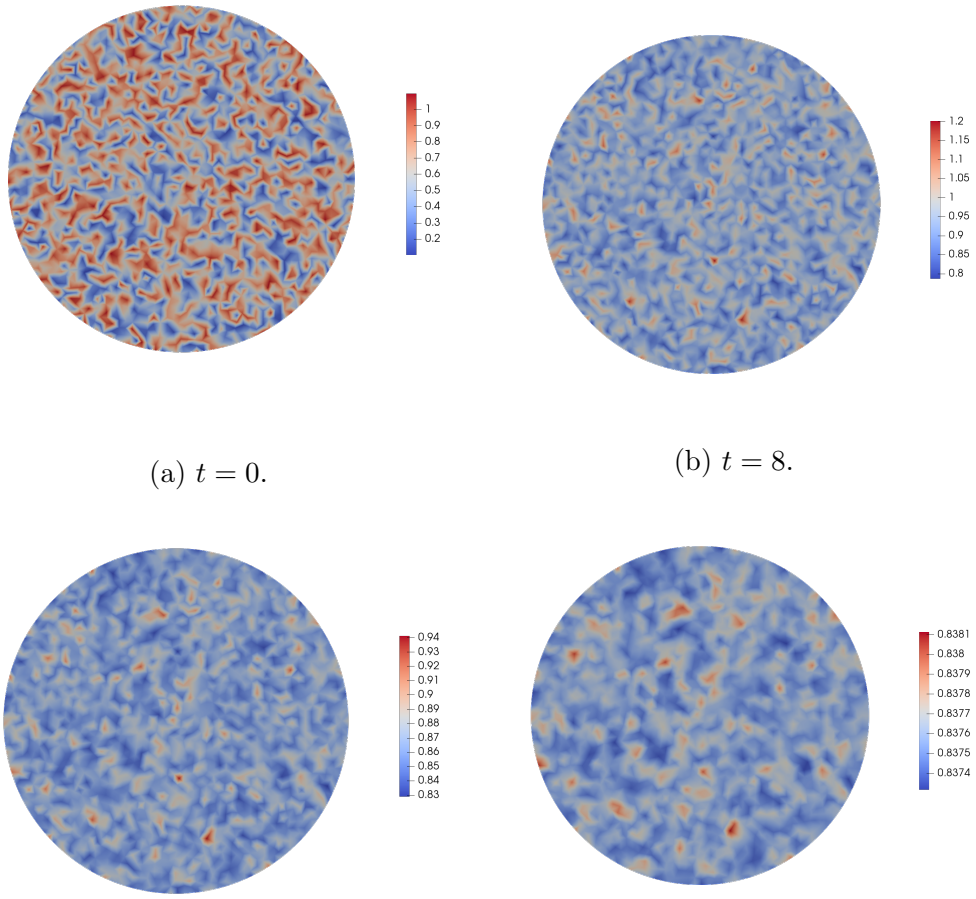

(a) $t = 0$.

(b) $t = 8$.

(c) $t = 18$.

(d) $t = 48$.

FIGURE 5.10 – Spatiotemporal evolution of the solution for the resistant cell line ($V_{v,2} = 0.1$). The solution v is increasing then decreasing to 0.8378.

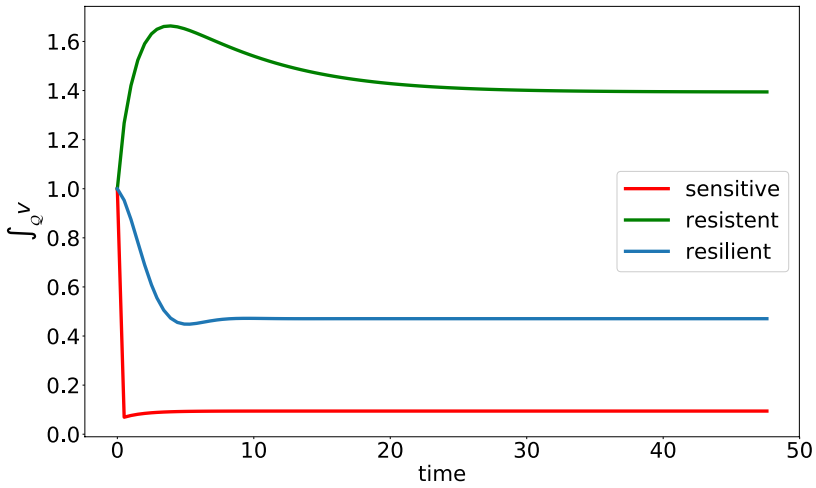

FIGURE 5.11 – The time evolution of the spatial mean $\int_{\mathcal{Q}} v(t,x)dx$.

Computing the spatial mean evolution over time (Fig. 5.11), the diffusion does not affect the asymptotic behavior of solutions.

5.3.3 Influence of 2−d cells shape

We explore the influence of the shape on the signalling pathway, which can be of importance [Fri15, LKea10]. We extract from [LKea10] the cellular shapes of a resistant cell line (PLC) and a highly sensitive cell line (HepG2) to perform the simulations. Here, the cells are cultivated on 2D tissue culture plates and take a specific morphology due to the adaptation to the culture constraints. The scale is now of order $10\mu m$.

The simulations are presented in Figures 5.12-5.13. It starts from a random distribution valued in $[0,1]$. The solutions tend to a stable state at an earlier time ($t = 5$). Nevertheless, the behaviour of solutions is similar to the previous one.

Computing the spatial mean evolution over time (Fig. 5.14), the shape does not affect the asymptotic behavior of solutions.

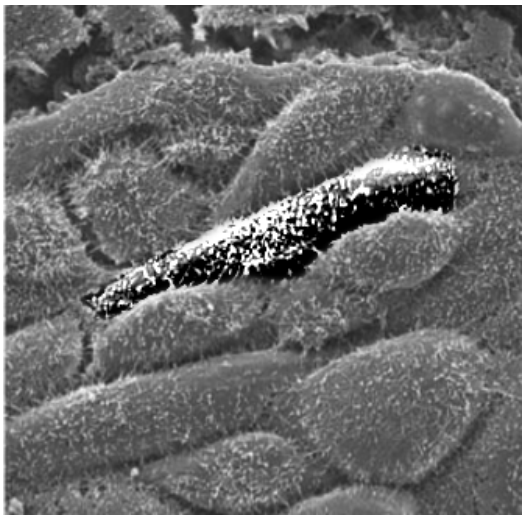

(a) PLC cells cultured on 2D plates from [LKea10].

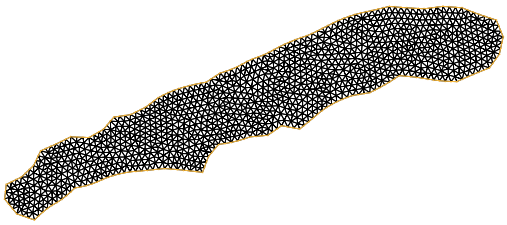

(b) Finite elements mesh on the shape of PLC cells extract from (a).

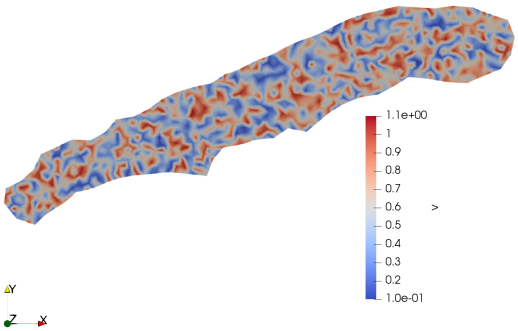

(c) $t = 0$.

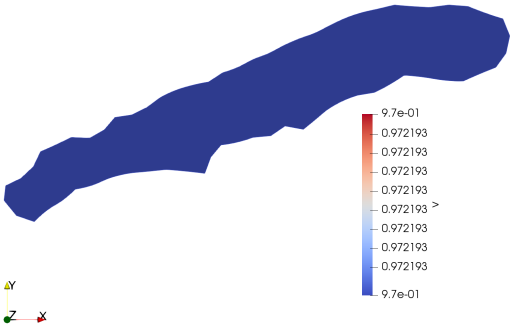

(d) $t = 5$.

FIGURE 5.12 – (a)-(b) preprocessing to extract PLC 2D shape and to create the finite elements mesh. (c)-(d) present the spatiotemporal evolution of the solution for the PLC cell line at $t = 0$ and $t = 5$ respectively. The solution v is decreasing to 0.972.

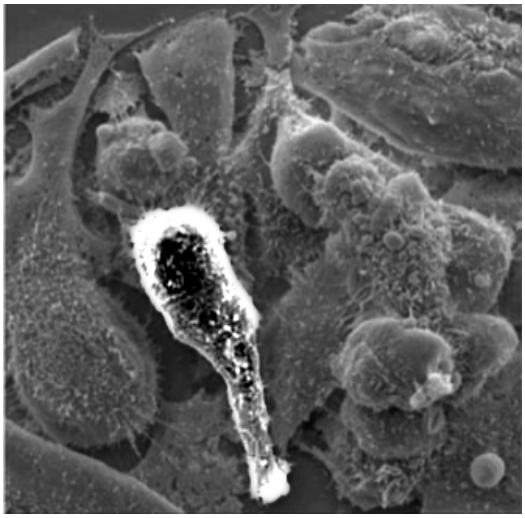

(a) HEPG2 cells cultured on 2D plates from [LKea10].

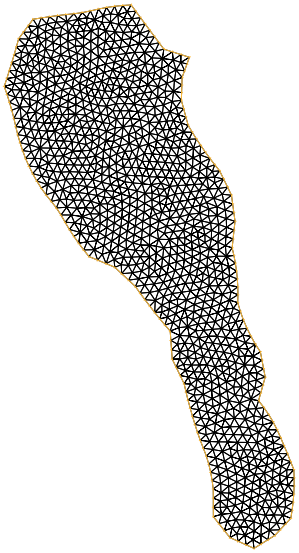

(b) Finite elements mesh.

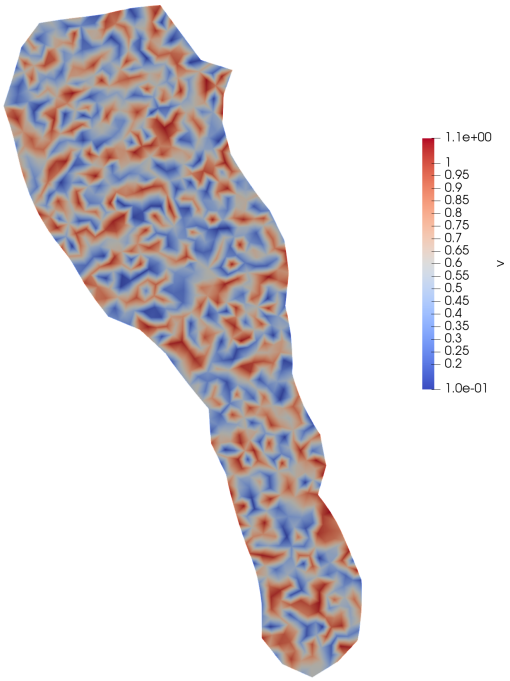

(c) $t = 0$.

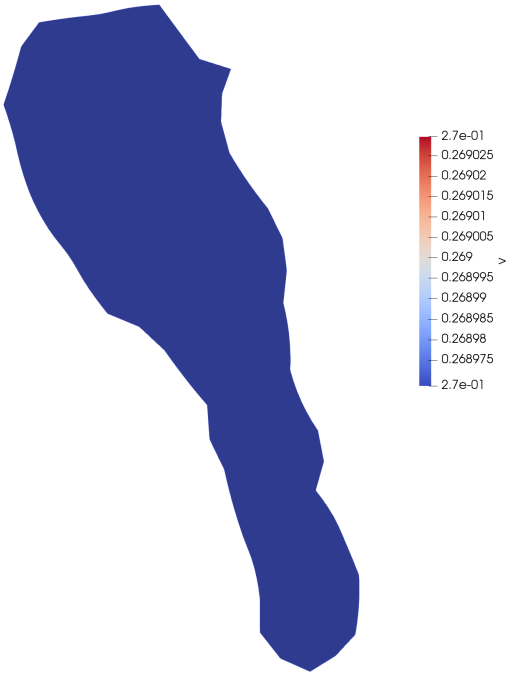

(d) $t = 5$.

FIGURE 5.13 – (a)-(b) preprocessing to extract HEPG2 2D shape and to create the finite elements mesh. (c)-(d) present the spatiotemporal evolution of the solution for the HEPG2 cell line at $t = 0$ and $t = 5$ respectively. The solution v is decreasing to 0.269.

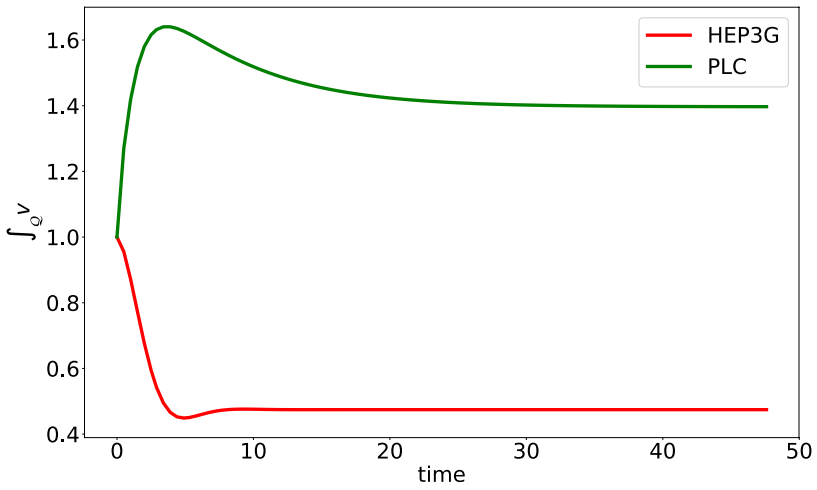

FIGURE 5.14 – The time evolution of the spatial mean $\int_{\mathcal{Q}} v(t,x)dx$.

5.3.4 $(3+1)-$d simulations

3D cells cultures give new informations about the cells behaviour. Growth, metabolism, cell-cell interactions, drugs efficacy and toxicity seems to be different in this environnemental context in comparison with 2D cultures [LKea10, KPea18, BO16]. Regarding the cells morphology on 3D tissue, Hep cells are spherical, Huh7 cells are ellipsoidal and PLC cells are conical. We build 3D finite element mesh with Freefem++ [Hec12] to simulate the model solution in each sensitivity case in order to evaluate the impact of the cell shape on the cellular signalling.

For each cell line, the distribution of solution v becomes homogeneous in the domain (Figures 5.15-5.16-5.17). We observe this behavior at a later time ($t = 10$) compared to the 2D shape simulations ($t = 5$) but at an earlier time when the domain is a disk ($t = 48$). Nevertheless, the asymptotic dynamic of the solution seems to be not altered by the cell morphology when we look at the solution spatial mean (Fig. 5.18).

(a) Huh7 cells cultured in 3D Scaffold from [KPea18].

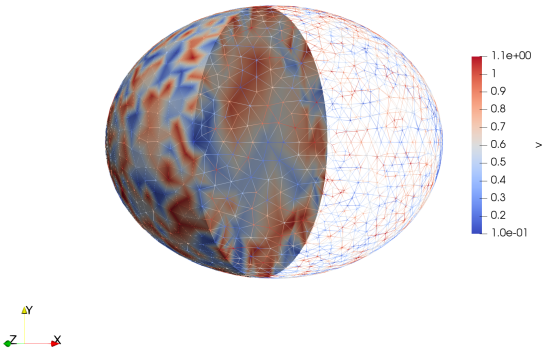

(b) $t = 0$.

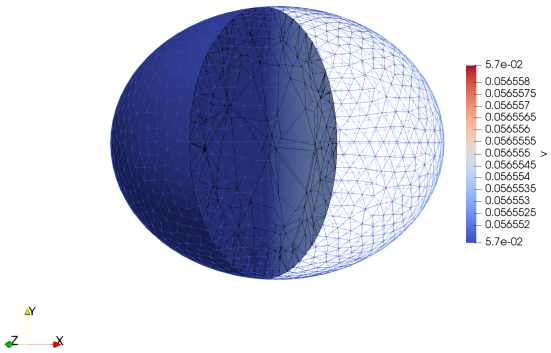

(c) $t = 10$.

FIGURE 5.15 – Spatiotemporal evolution of the solution for the Huh7 (sensitive) cell line. The solution v is decreasing to 0.056.

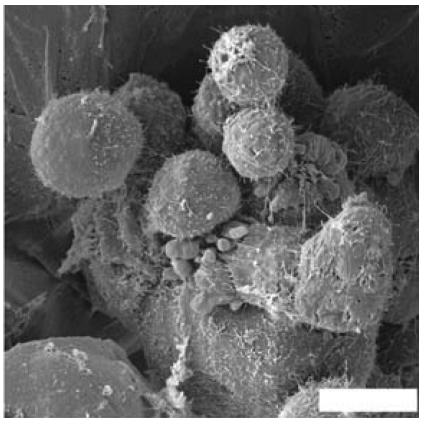

(a) HEP cells cultured in 3D Scaffold from [LKea10].

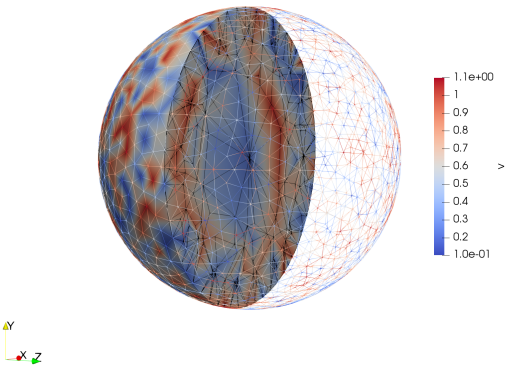

(b) $t = 0$.

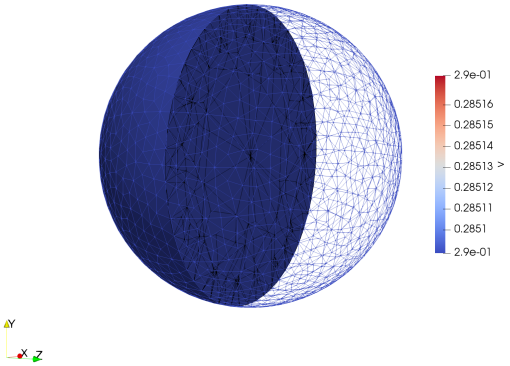

(c) $t = 10$.

FIGURE 5.16 – Spatiotemporal evolution of the solution for the Hep (resilient) cell line. The solution v is decreasing to 0.285.

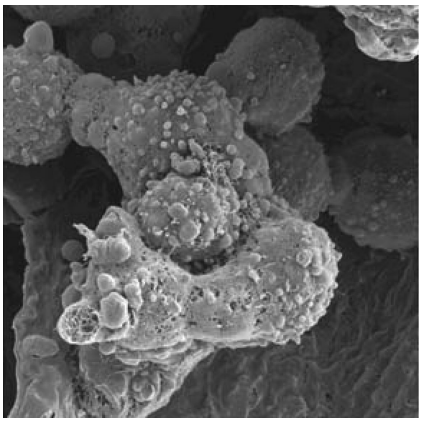

(a) HEP cells cultured in 3D Scaffold from [LKea10].

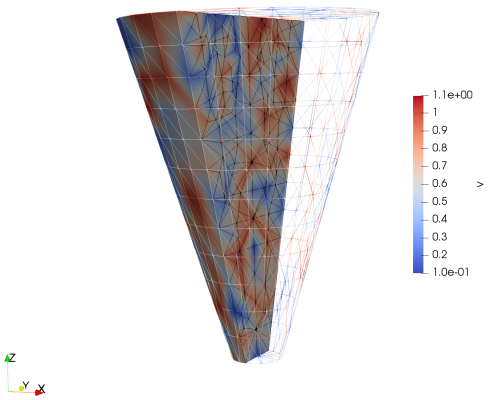

(b) $t = 0$.

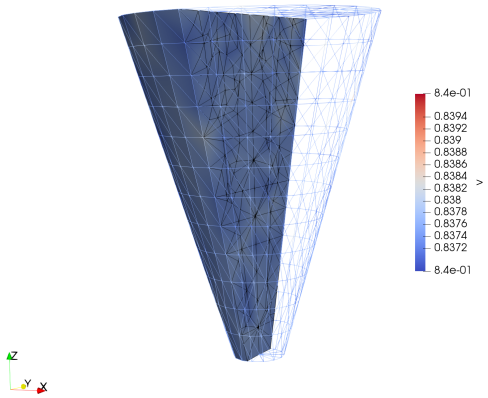

(c) $t = 10$.

FIGURE 5.17 – Spatiotemporal evolution of the solution for the PLC (resistant) cell line. The solution v is decreasing to 0.839.

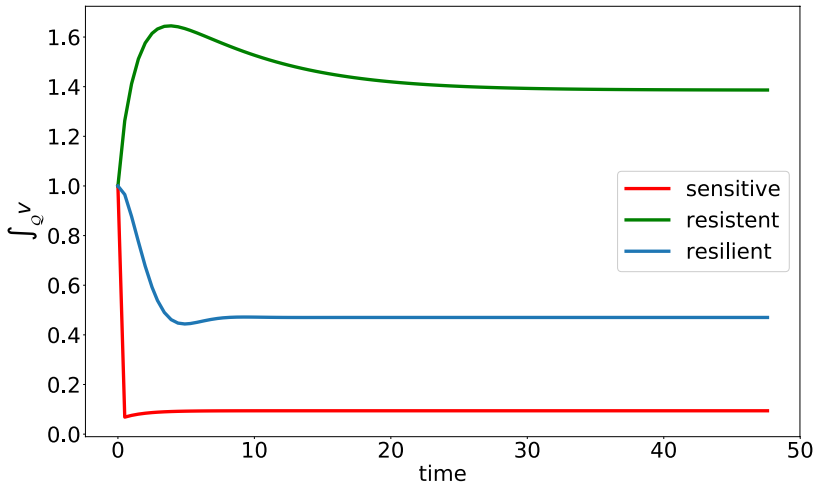

FIGURE 5.18 – The time evolution of the spatial mean $\int_{\mathcal{Q}} v(t,x)dx$. The shape does not affect the asymptotic behavior of solutions.

References

[BO16] S. Breslin and L. O'Driscoll, *The relevance of using 3D cell cultures, in addition to 2D monolayer cultures, when evaluating breast cancer drug sensitivity and resistance*, Oncotarget **7** (2016), 45745–45756.

[Fri83] A. Friedman, *Partial Differential Equations of Parabolic Type*, Englewood Cliffs, N.J. Prentice Hall, 1983.

[Fri15] E. Friedmann, *PDE/ODE modeling and simulation to determine the role of diffusion in long-term and -range cellular signaling*, BMC Biophysics **8** (2015), 1–16.

[Hec12] F. Hecht, *New development in freefem++*, Journal of numerical mathematics **20** (2012), 251–266.

[Hen81] D. Henry, *Geometric theory of semilinear parabolic equations*, Springer, 1981.

[KHGK15] W. Kolch, M. Halasz, M. Granovskaya, and B.N. Kholodenko, *The dynamic control of signal transduction networks in cancer cells*, Nature Reviews Cancer **15** (2015), 515–527.

[KPea18] I.A. Khawar, J.K. Park, and E.S. Jung et al., *Three dimensional mixed-cell spheroids mimic stroma-mediated chemoresistance and invasive migration in hepatocellular carcinoma*, Neopplasia **20** (2018), 800–812.

[LKea10] M. Leung, F.M. Kievit, and S.J. Florczyk et al., *Chitosan-alginate scaffold culture system for hepatocellular carcinoma increases malignancy and drug resistance*, Pharm Res. **27** (2010), 1939–1948.

[MS11] P. Müller and A. F. Schier, *Extracellular movement of signaling molecules*, Dev Cell. **21** (2011), 145–158.

[Ouh05] E. M. Ouhabaz, *Analysis of Heat Equations on Domains*, London Math. Soc. Monographs Series, Princeton University Press, 2005.

[Per15] B. Perthame, *Parabolic equations in biology*, Lecture Notes on Mathematical Modelling in the Life Sciences, Springer, 2015.

[SGea17] Z. Saidak, A.-S. Giacobbi, and C. Louandre et al., *Mathematical modelling unveils the essential role of cellular phosphatases in the inhibition of RAF-MEK-ERK signalling by sorafenib in hepatocellular carcinoma cells*, Cancer Letters **392** (2017), 1–8.

Chapitre 6

Conclusion et Perspectives

6.1 Conclusion à propos du CHC

La modélisation dynamique de la voie Raf-MEK-ERK dans les cellules du carcinome hépatocellulaire exposées au sorafénib a permis de mettre en évidence les mécanismes d'action du sorafénib. Bien que ce traitement ait été prescrit comme un inhibiteur des kinases Raf, son efficacité repose sur l'activation des phosphatases liées à la déphosphorylation de la protéine ERK. De plus, les acteurs de la régulation de cette voie de signalisation sont différents chez les patients suivant leur profil de sensibilité. Cela suggère la mise en place d'une thérapie ciblée en fonction du profil biologique de chaque patient. Notre étude participe ainsi à l'émergence du nouveau concept de la médecine de demain : la médecine personnalisée.
L'étude du modèle de la voie étendu à la protéine RAS et aux trois récepteurs RTKs sélectionnés (l'EGFR, l'IR et l'IGF1-R) apporte des éléments de réponse concernant la résistance de la cellule au sorafénib. Il semblerait que les cellules résilientes au sorafénib ne répondent pas de façon optimale à la thérapie ciblée par le biais de mécanismes de résistance liés à l'EGFR et aux protéines Ras, B-Raf et MEK. Quant aux cellules résistantes, des processus biologiques liés à la protéine MEK seraient en cause. Une meilleure stratégie thérapeutique pour ces patients serait alors d'établir un plan thérapeutique incluant le sorafénib et un inhibiteur de MEK, le tramétinib.
Enfin, l'étude théorique du modèle a montré que la prise en compte de la dimension spatiale de la cellule dans le modèle ne perturbait pas la dynamique intracellulaire par rapport au modèle sans diffusion. De plus, ce résultat a été observé sur différentes morphologies de cellule en 2D et en 3D. De nouvelles perspectives mathématiques sont apportées dans le paragraphe suivant afin d'approfondir nos recherches sur les possibles instabilités moléculaires qui pourraient survenir dans la cellule.

6.2 Perspectives mathématiques

Nous présentons ici quelques points qui n'ont pas été considérés dans le modèle de la voie ERK. Avec une meilleure prise en compte de ceux-ci, nous pourrions affiner nos résultats concernant la régulation et les mécanismes de résistance de la signalisation cellulaire.

Tout d'abord, le sorafénib ou tout autre thérapie ciblant la voie pourrait être intégré à travers une étude PK/PD (pharmacokinetic/pharmacodynamic) ce qui permettrait d'étudier de façon quantitative la relation dose-concentration-effet du traitement sur la voie ERK. D'un point de vue mathématique, cela consisterait à ajouter au modèle d'autres EDO non-linéaires en fonction du mode d'administration (oral ou intra-veineuse).

Suite aux simulations numériques en 2D et en 3D du quatrième chapitre, nous avons observé que les solutions du modèle n'étaient pas perturbées par la morphologie cellulaire et le terme de diffusion. Une meilleure prise en compte de ces caractéristiques est essentielle afin de s'assurer du comportement de la voie ERK *in vivo*. Pour cela, nous pourrions considérer les différentes structures de la cellule comme la membrane, le cytoplasme, le noyau ou encore la matrice extra-cellulaire. Aussi, le coefficient de diffusion est calculé à partir de la relation de Stokes-Einstein $D = \frac{kT}{6\pi\mu r}$ où k la constante de Boltzmann, T la température, μ la viscosité dynamique du fluide et r le rayon de la cellule. Une alternative interessante serait de tenir compte de la porosité P et de la tortuosité τ du milieu avec la relation $D \simeq \frac{P}{\tau}$.

Nous introduisons ici une nouvelle perspective de modélisation de la voie ERK. Les voies de signalisation sont connues pour avoir un fonctionnement très complexe qui reste difficile à appréhender. Des processus biologiques inconnus et extérieurs à la voie ERK contribuent à sa régulation. Pour cette raison, nous proposons un modèle incluant une partie stochastique décrivant cette contribution. On considère alors le système d'équations différentielles stochastiques suivant

$$
\begin{aligned}
du(t) &= \left(\frac{V_{u,0} + V_{u,1}(\overline{u} - u(t))}{K_{u,1} + \overline{u} - u(t)} \left(1 + \frac{v(t)}{K_{u,3}}\right)^{-\alpha} - \frac{V_{u,2} u(t)}{K_{u,2} + u(t)} \right) dt && (6.1)\\
&\quad + \sigma_{u,1} u(t) dW_{u,1} + \sigma_{u,2} v(t) dW_{u,2} && (6.2)\\
dv(t) &= \left(\frac{V_{v,0} + V_{v,1} u(t)(\overline{v} - v(t))}{K_{v,1} + \overline{v} - v(t)} - \frac{V_{v,2} v(t)}{K_{v,2} + v(t)} \right) dt && (6.3)\\
&\quad + \sigma_{v,1} u(t) dW_{v,1} + \sigma_{v,2} v(t) dW_{v,2}. && (6.4)
\end{aligned}
$$

Théorème 5.1 [Oks95] Soient u_0 and v_0 deux variables aléatoires non nulles dans $L^2(\Omega)$. Alors il existe une unique solution (u, v) dans $L^2(0,T) \times L^2(0,T)$ pour le problème différentiel stochastique (6.1)-(6.3).

Contrairement au modèle en espace, on peut montrer que ce système peut-être déstabilisé dès lors que la dérive stochastique est élevée [MAR08].

Les simulations *in silico* du modèle ont été réalisées à l'aide du schéma d'Euler-Muryama (Algorithm 5) pour chaque lignée cellulaire. Elles sont présentées dans les figures 6.1-6.2. Le choix du nombre de simulations des processus stochastiques u et v a été fixé à 1000 afin de pouvoir obtenir une bonne approximation de la probabilité que la solution du système tende vers un état d'équilibre. Concernant les paramètres du système, le choix a été fait comme précédemment : $\alpha = 3.5, V_{u,0} = 0, V_{u,1} = K_{u,1} = V_{u,2} = K_{u,2} = K_{u,3} = 1, \overline{u} = 2$, $V_{v,0} = 0, V_{v,1} = K_{v,1} = K_{v,2} = 1, \overline{v} = 2$ et la valeur du paramètre $V_{v,2}$ a été fixée à 1 pour la lignée résiliente.

On note que lorsque la dérive stochastique est grande ($5Id$), le comportement des cellules résilientes est proche du comportement de la lignée sensible puisque l'espérance de v est proche de 0 sauf en certains points, où les cellules présentent une dynamique caractéristique des lignées résistantes (Fig. 6.2). En effet, on observe des pics allant jusqu'à plus de 1. Lorsque la dérive stochastique est petite, le comportement des cellules peut être différent des cellules résilientes dans le cas déterministe. Néanmoins, le comportement reste en moyenne assez proche du cas déterministe.

Algorithm 5 Euler-Muryama

Given u_0, v_0 and $N \in \mathbb{N}^*$.
for $n = 1$ to N **do**
$\Delta W^n_{u,1}, \Delta W^n_{u,2}, \Delta W^n_{v,1}, \Delta W^n_{v,2} \sim \mathcal{N}(0,1)\sqrt{\Delta t}$

$$\begin{aligned} u^{n+1} &= u^n + \Delta t \left(\frac{V_{u,0} + V_{u,1}(\overline{u} - u^n)}{K_{u,1} + \overline{u} - u^n} \left(1 + \frac{v^n}{K_{u,3}}\right)^{-\alpha} - \frac{V_{u,2} u^n}{K_{u,2} + u^n} \right) \\ &\quad + \sigma_{u,1} u^n \Delta W^n_{u,1} + \sigma_{u,2} v^n \Delta W^n_{u,2} \\ v^{n+1} &= v^n + \Delta t \left(\frac{V_{v,0} + V_{v,1} u^n (\overline{v} - v^n)}{K_{v,1} + \overline{v} - v^n} - \frac{V_{v,2} v^n}{K_{v,2} + v^n} \right) \\ &\quad + \sigma_{v,1} u^n \Delta W^n_{v,1} + \sigma_{v,2} v^n \Delta W^n_{v,2} \end{aligned}$$

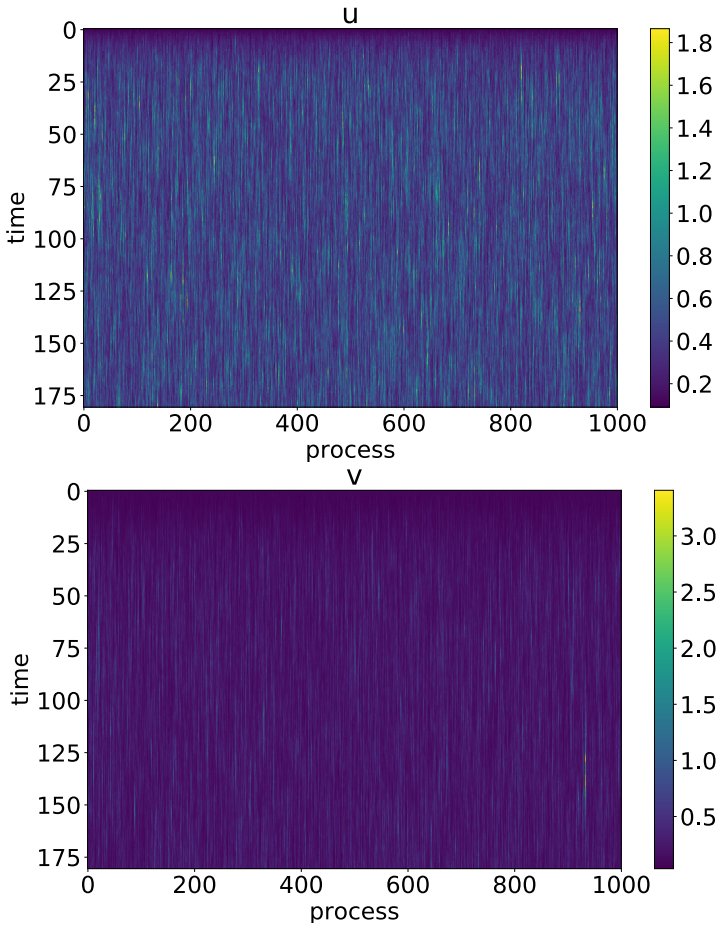

FIGURE 6.1 – Evolution en temps des solutions pour la lignée cellulaire résiliente ($V_{v,2} = 1$) en fonction du processus de Wiener.

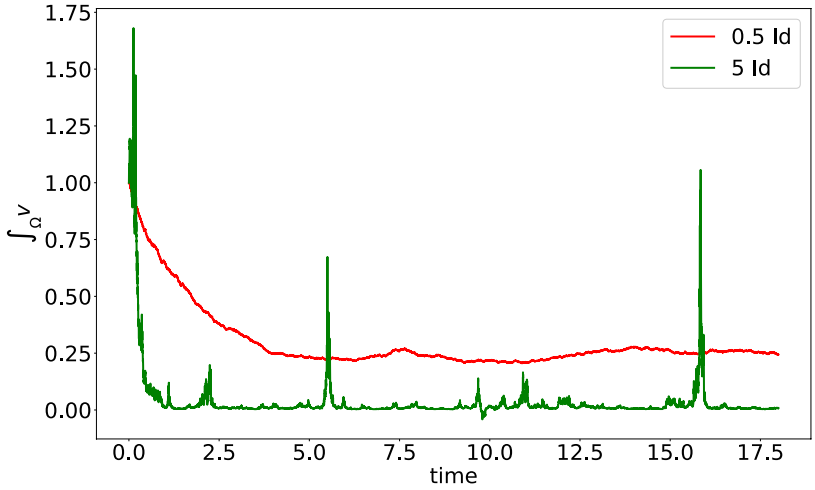

FIGURE 6.2 – Evolution en temps de l'espérance de v pour la lignée cellulaire résiliente ($V_{v,2} = 1$) avec $0.5Id$ et $5Id$ pour la dérive stochastique.

6.3 Perspectives cliniques

Actuellement, la place du sorafénib dans le traitement du carcinome hépatocellulaire à un stade avancé est remise en cause [KFea18, BBea17]. Une étude clinique récente de phase III rapporte que les patients sous lenvatinib ont eu une survie sans progression tumorale supérieure à celle du sorafénib (7,4 vs 3,7 mois). Le lenvatinib est un inhibiteur de plusieurs récepteurs RTKs, en particulier des récepteurs des facteurs de croissance dérivé des plaquettes (PDGF), de l'endothélium vasculaire (VEGF) et des fibroblastes (FGF). Il serait intéressant de pouvoir proposer à l'aide de la modélisation mathématique un protocole optimal de traitement de première ligne incluant le lenvatinib et le tramétinib en recherchant l'administration optimale de ces deux inhibiteurs.
Par ailleurs, notre modèle reste limité à la voie de signalisation Ras-Raf-MEK-ERK. On sait que le carcinome hépatocellulaire survient majoritairement après une cirrhose du foie (75 à 80% des cas) mais cette information n'a pas été prise en compte dans le modèle. D'autres voies de transduction du signal en interaction avec la voie Ras-Raf-MEK-ERK et sur lesquelles on aurait un contrôle par le biais d'un traitement pourraient être aussi incluses dans le modèle. Par exemple, on pourrait inclure la voie de signalisation PI3K/AKT qui est connue pour contribuer à la résistance des cellules au sorafénib [NLea17, ZZea17]. Pour cela, des données relatives à cette voie seraient nécessaires.

Notre modèle pourrait être couplé à d'autres types de thérapies (radiothérapie et/ou immunothérapie) afin d'évaluer l'efficacité de multithérapie sur le CHC. Des travaux sur l'intérêt de l'immunothérapie dans le contexte du CHC offre une nouvelle piste thérapeutique prometteuse. Le modèle que nous avons construit pourrait être également appliqué dans d'autres types de tumeurs afin d'améliorer la compréhension de leur formation et leur prise en charge thérapeutique. Par exemple, dans le cas du glioblastome (un type de tumeur cérébrale), le couplage de notre modèle de la voie Ras-Raf-MEK-ERK avec le facteur de transcription tumoral p53 pourrait apporter une nouvelle piste thérapeutique pour contrôler la tumeur.

Les études que nous relatons apportent la preuve de principe que la modélisation mathématique permet d'étudier le fonctionnement dynamique des voies de transduction oncogéniques, et que cette information est utile afin d'identifier des modalités de ciblage thérapeutique qui soient optimisées. Désormais, un objectif essentiel de la modélisation mathématique consiste en la conception d'outils qui permettront d'apprécier, pour chaque patient, cette organisation dynamique et de reconstruire in silico le réseau de transduction oncogénique qui lui est propre, ceci dans l'optique du développement d'une médecine personnalisée et prédictive [YQER15]. Il est donc important, après l'étape préclinique, d'envisager désormais des études clinico-biologiques. Ceci suppose d'appliquer la modélisation établie dans les lignées de cellules, aux réseaux de transduction du signal présents dans les tumeurs des patients, à partir des données biologiques accessibles dans le contexte clinique. Ces données sont souvent limitées, notamment parce qu'elles nécessitent la réalisation de biopsies. Les mathématiques offrent des solutions pratiques à cette limitation. Une étude récente montre comment il est possible de tirer parti des stratégies mathématiques d'optimisation combinatoire pour exploiter les données de phospho-protéomique obtenues à partir de biopsies de glioblastomes [TMPea16] : associée aux connaissances préexistantes des réseaux d'interaction entre protéines, et avec un nombre limité de marqueurs analysés, la modélisation a permis de reconstruire in silico les voies de transduction activées dans ces tumeurs [TMPea16]. Un deuxième objectif essentiel consistera à valider le caractère prédictif des modèles mathématiques, en les comparant notamment aux analyses « classiques », centrées sur les éléments isolés constituant les réseaux modélisés [FHea15]. A long terme, modéliser en clinique les voies de transduction oncogénique devrait contribuer à favoriser l'émergence de l'oncologie prédictive [YQER15]. L'utilisation des modèles mathématiques permet l'intégration de données obtenues à différents niveaux. L'oncologie prédictive repose ainsi sur la conception de larges modèles multi-échelle, qui combinent la modélisation mathéma-

tique des voies oncogéniques, et celle décrivant les interactions entre clones cellulaires [MTAea14, ACRea14, CLLea15, BRRea15], avec des aspects spécifiques, comme la pharmacocinétique/pharmacodynamique des médicaments [BCLea16]. Au final, la modélisation mathématique constitue une piste prometteuse pour optimiser les recherches biologiques et faciliter la transposition en clinique des connaissances qui en sont issues.

References

[ACRea14] V. Almendro, Y-K. Cheng, A. Randles, and S. Itzkovitz et al., *Inference of tumor evolution during chemotherapy by computational modeling and in situ analysis of genetic and phenotypic cellular diversity*, Cell Reports **6** (2014), 514–527.

[BBea17] J.F. Blanc, J.C. Barbare, and A.S. Baumann et al., *Carcinome hépatocellulaire (cancer primitif du foie)*, Tech. report, Société Nationale Française de Gastro-entérologie, 2017.

[BCLea16] D. Barbolosi, J. Ciccolini, B. Lacarelle, and F. Barlési et al., *Computational oncology -mathematical modelling of drug regimens for precision medicine*, Nature Reviews Clinical Oncology **13** (2016), 242–254.

[BRRea15] H.C. Bhang, D.A. Ruddy, V. Krishnamurthy Radhakrishna, and J.X. Caushi et al., *Studying clonal dynamics in response to cancer therapy using high-complexity barcoding*, Nature Medicine **21** (2015), 440–448.

[CLLea15] R.H. Chisholm, T. Lorenzi, A. Lorz, and A.K. Larsen et al., *Emergence of drug tolerance in cancer cell populations : an evolutionary outcome of selection, nongenetic instability, and stress-induced adaptation*, Cancer Research **75** (2015), 930–939.

[FHea15] D. Fey, M. Halasz, and D. Dreidax et al., *Signaling pathway models as biomarkers : Patient-specific simulations of JNK activity predict the survival of neuroblastoma patients*, Science Signaling **8** (2015).

[KFea18] M. Kudo, R.S. Finn, and S. Qin et al., *Lenvatinib versus sorafenib in first-line treatment of patients with unresectable hepatocellular carcinoma : a randomised phase 3 non-inferiority trial*, Lancet **391** (2018), 1163–1173.

[LRea08] J.M. Llovet, S. Ricci, and V. Mazzaferro et al., *Sorafenib in advanced hepatocellular carcinoma*, N. Engl. J. Med. **359** (2008), 378–90.

[MAR08] X. Mao, J.A. Appleby, and A. Rodkina, *Stabilization and destabilization of nonlinear differential equations by noise*, IEEE Trans. Autom. Control **53** (2008), 683–691.

[MTAea14] A. Marusyk, D.P. Tabassum, P.M. Altrock, and V. Almendro et al., *Non-cell-autonomous driving of tumour growth supports sub-clonal heterogeneity*, Nature **514** (2014), 54–58.

[NLea17] L. Niu, L. Liu, and S. Yang et al., *New insights into sorafenib resistance in hepatocellular carcinoma : Responsible mechanisms and promising strategies*, Biochim Biophys Acta Rev Cancer **1868** (2017), 564–570.

[Oks95] B. Oksendal, *Stochastic Differential Equations : An introduction with applications*, 5th Ed., Springer, 1995.

[TMPea16] N. Tuncbag, P. Milani, J.L. Pokorny, and et al., *Network modeling identifies patient-specific pathways in glioblastoma*, Sci Rep **6** (2016), 28668.

[YQER15] T.E. Yankeelov, V. Quaranta, K.J. Evans, and E.C. Rericha, *Toward a science of tumor forecasting for clinical oncology*, Cancer Res **75** (2015), 918–23.

[ZZea17] YJ. Zhu, B. Zheng, and HY. Wang et al., *New knowledge of the mechanisms of sorafenib resistance in liver cancer*, Acta Pharmacologica Sinica **38** (2017), 614–622.

Notations

Liste des abbréviations

DUSP : Dual-specificity phosphatases
EGFR : Epidermal Growth Factor Receptor
ERK1/2 : Extracellular signal-Regulated Kinase 1/2
HCC : Hepatocellular carcinoma
IGF1-R : Insulin-like Growth Factor 1 Receptor
IR : Insulin Receptor
MEK : derived from MAPK-ERK Kinase
ODE : Ordinary Differential Equations
PP2A : Protein Phosphatase 2A
RTK : Receptor Tyrosine Kinase
VEGF : Vascular Endothelial Growth Factor

Table des figures

Modélisation dynamique de la voie RAS-RAF-MEK-ERK dans les cellules du carcinome hépatocellulaire exposées au sorafénib

Le carcinome hépatocellulaire (CHC) est la forme la plus fréquente du cancer primitif du foie. Il apparaît majoritairement comme une complication de la cirrhose du foie chez les patients exposés à des agents toxiques (alcool, virus hépatiques).

L'étude du ciblage thérapeutique des voies oncogéniques apporte de nouvelles perspectives sur des traitements anticancéreux, plus efficaces et mieux tolérés par les patients. Une voie oncogénique est retrouvée activée dans presque tous les types de tumeurs. Il s'agit de la voie RAS-RAF-MEK-ERK. La compréhension de sa régulation reste encore mal connue à ce jour. Le sorafénib est prescrit comme un inhibiteur des kinases RAF dans les stades avancés du carcinome hépatocellulaire. Son efficacité est relative puisqu'il prolonge la survie de certains patients de quelques mois. De plus, il semblerait qu'il n'apporte pas le même bénéfice clinique chez tous les patients. Aucun biomarqueur prédictif de son efficacité n'a été mis en évidence à ce jour, ce qui rend la personnalisation de sa prescription impossible.

Cette thèse fournit une étude des modalités de régulation de la voie RAS-RAF-MEK-ERK dans le CHC à travers la modélisation mathématique. Cette approche novatrice permet d'améliorer la compréhension du comportement de réseaux biologiques sans approche réductionniste. Elle est également un outil d'exploration non invasive *in silico* pour ainsi éclairer la recherche pharmacologique et la personnalisation médicale.

L'objectif est de construire des modèles mathématiques en vue de mieux comprendre l'action du traitement anticancéreux sur les réseaux de transduction du signal de la voie RAS-RAF-MEK-ERK, et d'apporter de nouvelles perspectives sur le ciblage thérapeutique. Les grandes étapes du travail consistent à :

- Créer des modèles mathématiques, basés sur des équations différentielles décrivant la cinétique de Michaelis-Menten et la loi d'action de masse.
- Développer des codes numériques en python pour la simulation numérique de ces modèles.
- Explorer différents scénarios *in silico* de perturbations de la voie et de personnalisation des traitements.
- Proposer et mettre en place des leviers d'action *in vivo*.

Mots-clés : *voie RAS-RAF-MEK-ERK, cancer primitif du foie, modélisation dynamique, équations différentielles, estimation de paramètres, stratégie thérapeutique.*

Dynamical modelling of the RAS-RAF-MEK-ERK pathway in the hepatatocellular carcinoma cells exposed to sorafenib

Hepatocellular carcinoma (HCC) is the most common form of primary liver cancer. It appears mainly as a complication of cirrhosis of the liver in patients exposed to toxic agents (alcohol, hepatic viruses).

The study of therapeutic targeting of oncogenic pathways brings new perspectives on cancer treatments that are more effective and better tolerated by patients. An oncogenic pathway is found to be activated in almost all types of tumors. This is the RAS-RAF-MEK-ERK path. The understanding of its regulation is still poorly known today. Sorafenib is prescribed as an inhibitor of RAF kinases in the advanced stages of hepatocellular carcinoma. Its effectiveness is relative since it prolongs the survival of certain patients by a few months. Moreover, it seems that it does not bring the same clinical benefit to all patients. No biomarker predictive of its effectiveness has been highlighted to date, which makes the customization of its prescription impossible.

This thesis provides a study of the modalities of regulation of the RAS-RAF-MEK-ERK pathway in HCC through mathematical modelling. This innovative approach improves the understanding of the behavior of biological networks without a reductionist approach. It is also a non-invasive *in silico* exploration tool to inform pharmacological research and medical personalization. The aim is to build mathematical models to better understand the action of cancer therapy on RAS-RAF-MEK-ERK signal transduction networks, and to bring new perspectives on targeting therapeutic.

The main stages of the work consist in :

- Creating mathematical models, based on differential equations describing the kinetics of Michaelis-Menten and the mass action law.
- Developing numeric codes in python for the numerical simulation of these models.
- Exploring different *in silico* scenarios of channel disruption and customization of treatments.
- Proposing and implementing *in vivo* levers of action.

Keywords : *the RAS-RAF-MEK-ERK pathway, primary liver cancer, dynamic modelling, differential equations, parameter estimation, therapeutic strategy.*